Structural and functional investigation of tRNA guanine transglycosylase

Dissertation

for the award of the degree

Doctor rerum naturalium

by the Georg-August-University Göttingen

within the graduate program

"Biomolecules: Structure-Function-Dynamics"

of the Göttingen Graduate Center for Neurosciences,
Biophysics and Molecular Biosciences (GGNB)

by

Katharina Sievers

from Hamm, Germany

Göttingen, 2023

Members of the thesis advisory committee

Prof. Dr. Ralf Ficner (1st Reviewer)

> Department for Molecular Structural Biology
>
> Institute for Microbiology and Genetics
>
> Georg-August-University Göttingen

Prof. Dr. Markus Bohnsack (2nd Reviewer)

> Department of Molecular Biology
>
> University Medical Center Göttingen

Dr. Sarah Adio

> Department for Molecular Structural Biology
>
> Institute for Microbiology and Genetics
>
> Georg-August-University Göttingen

Members of the extended examination board

Prof. Dr. Kai Tittmann

> Department of Molecular Enzymology
>
> Schwann-Schleiden Research Centre
>
> Georg-August-University Göttingen

Prof. Dr. Hauke Hillen

> Department of Cellular Biochemistry
>
> University Medical Center Göttingen

Prof. Dr. Heike Krebber

> Department of Molecular Genetics
>
> Institute for Microbiology and Genetics
>
> Georg-August-University Göttingen

Prof. Dr Henning Urlaub

> Bioanalytical Mass Spectrometry Group
>
> Max Planck Institute for Multidisciplinary Sciences

Date of oral examination: 09th June 2023

PREFACE

This doctoral thesis summarizes my work on the tRNA modifying enzyme tRNA guanine transglycosylase. The underlying work was carried out from July 2019 to April 2023 under supervision by Prof. Dr. Ralf Ficner at the Georg-August-University Göttingen and resulted in the following publication and submitted manuscript:

Katharina Sievers, Luisa Welp, Henning Urlaub and Ralf Ficner. Structural and functional insights into human tRNA guanine transglycosylase. *RNA Biol.* 18, 382–396 (2021). DOI: 10.1080/15476286.2021.1950980

Katharina Sievers, Lukas Sušac, Stefano Da Vela, Melissa Graewert, Simon Trowitzsch, Dmitri Svergun, Robert Tampé and Ralf Ficner. Structural and functional insights into tRNA recognition by human tRNA guanine transglycosylase. *Submitted manuscript.*

My work further resulted in the following publication, which is not part of this thesis:

Katharina Sievers and Ralf Ficner. Structure of angiogenin dimer bound to double-stranded RNA. Acta Cryst. F78, 330-337 (2022) DOI: 10.1107/S2053230X22008317

Parts of this thesis were presented at the following international conferences:

Katharina Sievers, Luisa Welp, Henning Urlaub and Ralf Ficner. Eukaryotic tRNA guanine transglycosylase – structural analysis of subunit interaction and substrate binding. 73. Mosbacher Kolloqium – The World of RNAs, Mosbach, Germany, March/April 2022.

Katharina Sievers, Luisa Welp, Stefano Da Vela, Dmitri Svergun, Henning Urlaub and Ralf Ficner. Eukaryotic tRNA guanine transglycosylase – structural analysis of subunit interaction and substrate binding. RNA Society 27th Annual Meeting, Boulder, CO, USA, May/June 2022.

CONTENTS

1 INTRODUCTION

Nucleic acids were first discovered in 1869 by Friedrich Miescher as a novel, phosphor-rich substance isolated from leucocyte nuclei[1]. The significance of these new molecules as the physical form of genetic information was only proven 75 years later through a today famous series of experiments using mice and two strains of pneumococci[2], it would be another nine years until the discovery of the DNA double helix[3]. At last, the elucidation of the genetic code, a breakthrough built on decades of earlier research, re-shaped our perception of the living world forever[4].

RNA was originally treated with much less attention, primarily being regarded as intermediaries in Cricks "Dogma of Molecular Biology"[5]. However, scientists quickly realized that RNA could actually be much older than DNA, leading to the popular idea of an "RNA world" that might have existed during the earliest days of life[6].

In modern cells, RNAs fulfill a multitude of roles: They are the mobile, short-term storage of information that was described by Crick, they are adaptor molecules, regulatory elements, perform catalysis, and are a major structural component of large cellular machinery such as the ribosome.

The following work is a case study of an enzyme uniquely involved in RNA metabolism and a captivating example of adaptation and evolution at the molecular scale.

1.1 tRNA modification

Transfer RNAs (tRNAs) are the adaptor molecules at the center of the translation machinery: In the context of a ribosome, tRNAs recognize and bind to a complimentary mRNA codon triplet via their own anticodon. This results in a specific amino acid, bound to the tRNA 3' end, being linked to the growing polypeptide chain. Thus, tRNAs physically bridge the genetic code with the amino acid alphabet of proteins.

Although many structured RNAs have been discovered afterwards, tRNAs, with their characteristic three-dimensional L-shape probably remain the most iconic. Typically encompassing about 75 nucleotides in length, a canonical tRNA contains 3 short stem loops: The T-arm, the D-arm and the anticodon arm as well as a variable loop and a terminal

acceptor arm. These elements form two extended helices, comprised of acceptor arm and T-arm or anticodon arm and D-arm. A cluster of interactions chiefly involving the D- and T-arm forms the tRNA core which fixes the two extended helices at a near 90 °C angle, giving the molecule its distinct L-shaped appearance.
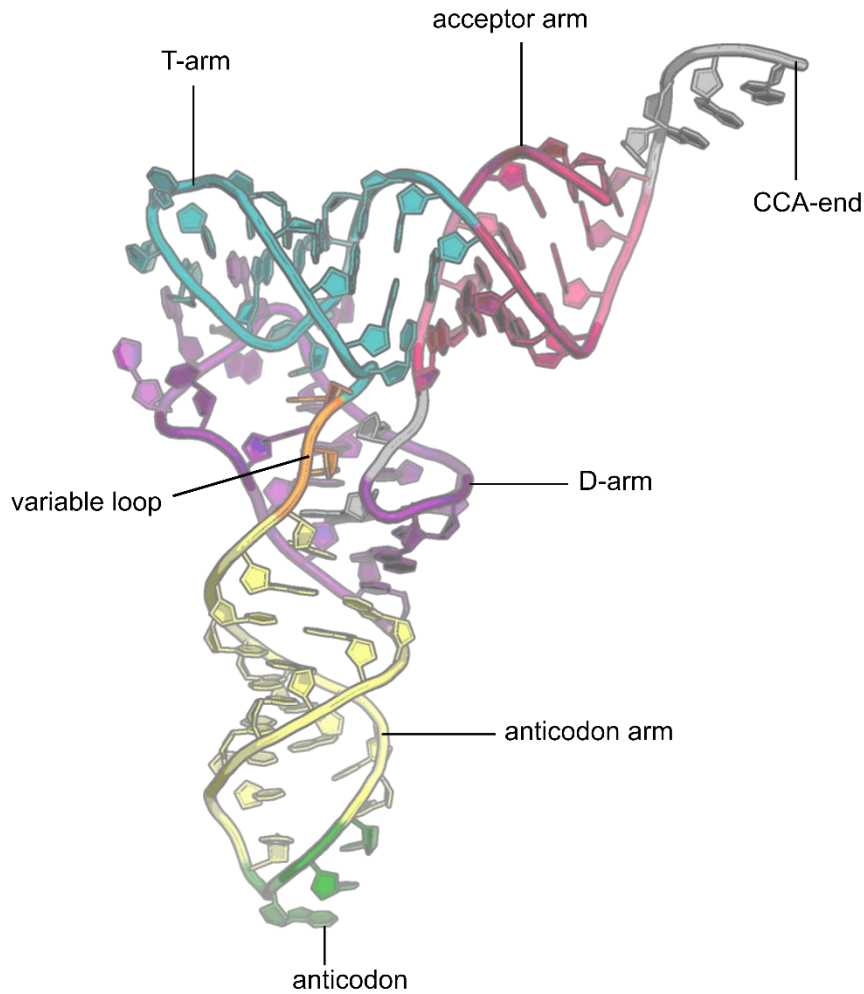
Figure 1: tRNA architecture

Crystal structure of yeast tRNA^{Asp} (PDB-ID: 2TRA), characteristic elements of the canonical L-shape fold are individually colored and labelled.

However, tRNAs are not transcribed from the genomic DNA ready-made: Their primary transcripts include a 5'-leader and a 3'-trailer sequence, which are removed after transcription[7]. The 3' end is then modified by addition of a universal CCA-end[8], which

becomes the anchor for aminoacylation by dedicated aminoacyl-tRNA synthetases[9]. Some pre-tRNAs also contain introns, which require splicing occurring independently from the mRNA-splicing spliceosome[10,11].

In addition, mature tRNAs contain not only the four canonical bases adenine, guanine, cytidine, uridine, but also many different chemical derivatives which are introduced by post-transcriptional RNA modification (Figure 2). RNA modification is a process highly specific to certain RNA molecules and positions. Notably, tRNAs are modified to a much greater extend and with much higher chemical diversity than all other known RNAs[12]. To date, close to 100 different modifications are known to occur in tRNAs[13]. Human cytoplasmatic tRNAs alone contain 40 different known modifications, averaging 13 modifications per tRNA molecule[14,15]. Chemically, tRNA modifications include methylation, acetylation, thiolation, deamination, isomerization, cyclization and conjugation with amino acids, sugars or other organic building blocks[16].

Many of these modifications occur in the tRNA body that is formed by the tRNA D-arm, T-arm and variable loop. Here, pseudouridine (ψ), a uridine isomer, and various methylations are especially numerous. Despite its chemical simplicity, methylation is an effective way to block the formation of hydrogen bonds and thus trigger substantial conformational rearrangements. In human mitochondrial tRNA^{Lys}, methylation of a single adenine at position 9 to m^{1}A is sufficient to shift the dynamic equilibrium from a diverse mixture to the functional fold[17–20]. Mitochondria, like chloroplasts, have their own set of tRNAs, remnants of their prokaryotic origin. However, many mitochondrial tRNAs are characterized by biased nucleotide use or a reduced secondary structure[21], probably rendering posttranscriptional modifications even more important in these tRNAs for stabilizing the correct fold[22].

Because of its 2' hydroxyl group, RNA differs from DNA by typically forming an A-form helix. RNA structured in an A-form helix is characterized by a 3'-endo conformation of the ribose sugar, as opposed to an even mixture of 2'-endo and 3'-endo form that is found in unstructured RNA. For this reason, RNA modifications that favor 3'-endo conformation have a stabilizing effect on RNA helices. Examples of this effect are 2'-O-methylation and modification to pseuouridine[23].

uridine　　　cytosine　　　adenosine　　　guanosine

pseudouridine (Ψ)　　　5-methylcytosine (m^{5}C)　　　N1-methyladenosine (m^{1}A)　　　5-methyluridine (m^{5}U)

2'-O-methylation　　　inosine (I)　　　2-methylthio-N^6-isopentenyladenosine (ms^{2}i^{6}A)

wybutosine (yW)　　　queuosine (Q)
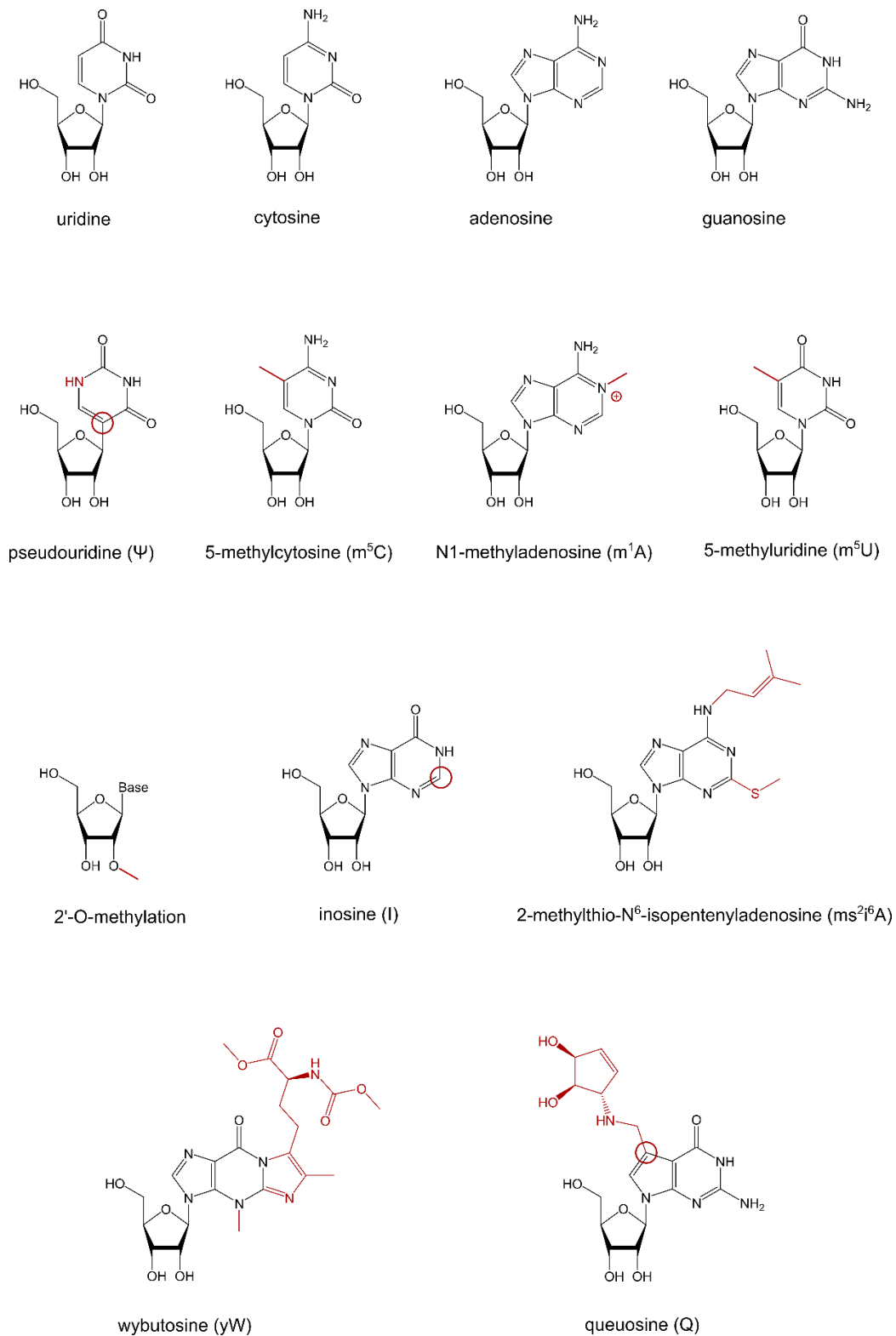
Figure 2: Selected tRNA modifications

Top row: Chemical structures of the four canonical RNA bases. Bottom three rows: Chemical structures of selected tRNA modifications described in the text. Modified bonds and atoms are highlighted in red.

All nucleic acids possess strongly negatively charged phosphate backbones. For that reason, intricately folded RNAs such as tRNAs are intrinsically governed by the opposing forces of hydrogen bonds and nucleobase π-π stacking, and the repulsive forces of backbone phosphates. Some modifications, such as m^5C methylation at position 40 in yeast tRNA[Phe], were shown to improve the binding of positively charged magnesium ions[24,25], and are thus expected to help shield anionic phosphates and cause a more compact overall conformation of the tRNA[26].

In summary, modifications of the tRNA structural core collectively act as modulators of structural flexibility, thereby optimizing the global and local architecture of the molecule for tRNA functionality[26].

In addition to its intramolecular interactions, the interactions formed with other molecules also govern a tRNA's modification pattern. On one hand, all tRNAs must be similar enough to one another to be recruited by the same common elongation factor and fit into the same tRNA binding sites of the ribosome. On the other hand, each tRNA species requires specific aminoacylation by the correct aminoacyl-tRNA synthetase. Several modifications, mainly located in the anticodon region, are known to help overcome this paradox by providing additional specificity elements that act as determinants or antideterminants for specific aminoacyl-tRNA synthetases[27–30].

A third group of modification is formed by the many modifications of the anticodon loop that affect translation. Although conceptually very simple, codon-anticodon base pairing is a structurally complex process innately linked to the ribosome environment. Within the ribosome decoding center, the anticodon (nucleotides 34-36) forms a minihelix structure with the mRNA codon triplet. While tight spatial conditions strongly enforce Watson-Crick base pairs to be formed at the first two codon bases, the third codon base is free to form a wider variety of non-canonical pairings, a process in which the ribosome is an active participant[31,32]. This phenomenon, known as base "wobbling", is the mechanistic explanation why 61 codon triplets can be deciphered by a much smaller set of tRNAs[33]. Consequently, the "wobble" base of the anticodon, position 34, is the most frequently modified nucleotide in tRNAs.

The original wobble hypothesis assumes that uridine pairs with either adenine or guanine at the third codon position[33]. However, in bacteria and eukaryotic organelles, uridine can also pair with cytidine and uridine at this position, a phenomenon known as "super-wobbling" or "four-way wobbling"[34]. In principle, this allows a single tRNA species to decode 4 synonymous codons varying at the last position (a 4-codon box) and is an effective tool to further limit the size of the minimal required tRNA set. Modification of the wobble uridine, in particular m^5U-based derivatization, is thought to suppress super-wobbling and thus allowed 4-codon boxes to split into two non-synonymous 2-codon boxes during the evolution of the genetic code[34]. In contrast, wobble adenine deamination to inosine (I) expands a tRNAs decoding properties, as I34 may pair with A, C and U, while strongly selecting against G-ending codons[33,35,36].

Located directly adjacent to the anticodon triplet, the nucleobase at position 37 is also frequently modified. This position almost exclusively contains a purine (adenine or guanine base) and is strongly co-varied with the identity of the base at the first position of the decoded codon triplett[37]. Modifications to A37 and G37, such as 2-methylthio-N6-isopentenyladenosine (ms^2i^6A) or wybutosine (yW), are frequently bulky and thought to stabilize weak (A-U or U-A) pairs at the neighboring position[37].

Queuosine (Q), a 7-deazaguanosine derivative containing a cyclopentene-*cis*-diol attached via an aminomethyl linker[38,39], is a similarly bulky modification which occurs exclusively at position 34 of certain tRNAs, and it is the main interest of this work.

1.2   The biological significance of queuosine modification

Queuosine is found at the wobble position of four tRNAs that share the G34-U35-N36 anticodon (i.e. tRNA^{Asp}, tRNA^{His}, tRNA^{Tyr}, tRNA^{Asn}, N = any nucleobase)[40]. First identified in *Escherichia coli*[41–44], it was later found in the same tRNAs of many eukaryotic species[45–48]. Interestingly, this includes not only cytosolic tRNAs, as eukaryotic mitochondrial tRNAs were also shown to be Q-modified[49–51]. Today, it is clear that queuosine and its free base queuine (q) occur almost universally in both bacteria and eukaryotes. Known exceptions are *Saccharomyces cerevisiae, Candida albicans* and *Arabidopsis thaliana,* whose tRNAs do not contain queuosine[47,52–54].

1.2.1 Q-modification and translation

The exclusive occurrence of queuosine at anticodon position 34 raises the question whether this modification does affect either aminoacylation or the decoding properties of its tRNAs.

Aminoacyl-tRNA synthetases (Aa-TS) are structurally well-characterized proteins and several complex structures have been published that show the interaction of an Aa-TS and their substrate tRNA. Although Aa-TS belong to two evolutionary and structurally distinct families (referred to as class I and class II), they recognize broadly similar identity elements, mainly involving the tRNA acceptor stem and the anticodon triplet.

The crystal structure of *E. coli* tRNA[Asp] and its Aa-TS reveals that Q34 is bound in a way that orients its C7 atom to the outside of the binding site (Figure 3a)[55]. While its 7-deazaguanine core forms three specific hydrogen bonds via its Watson-Crick Edge (which is identical to guanine), its aminomethyl-cyclopentenediol moiety does not form any close contacts. In a second crystal structure of *E. coli* tRNA[Asp] in complex with *Thermus thermophilus* aspartyl-tRNA synthetase, the cyclopentenediol does form two additional hydrogen bonds, but to do so it adopts a rotated conformation compared to the first structure, illustrating its conformational flexibility[56]. In both structures, the geometry of recognition and the orientation of the 7-dezapurine core is very similar to that of the equivalent guanine in the complex formed by tRNA[Asp] and aspartyl-tRNA synthetase from *S. cerevisae*, an organism naturally devoid of Q[57]. Interestingly, the space that accommodates the bulky queuosine extension in *E. coli* and *T. thermophilus* aspartyl-tRNA synthase is blocked by a lysine side chain in the yeast enzyme (Figure 3b)[57].

Although structural data is available for both a tRNA[Tyr]-tyrosyl-TS complex and a tRNA[His]-histidyl-TS complex, the crystallized tRNAs exclusively contain guanine at position 34[58,59]. Nevertheless, the data shows that guanine 34 is similarly bound in a way that orients its N7 atom away from the binding site[58,59]. Interestingly, the structure of a *T. thermophilus* tRNA[His]·Aa-TS complex features a coordinated water molecule adjacent to the G34 N7 atom[58], possibly filling a space otherwise occupied by a secondary amine in Q34.

a   **b**
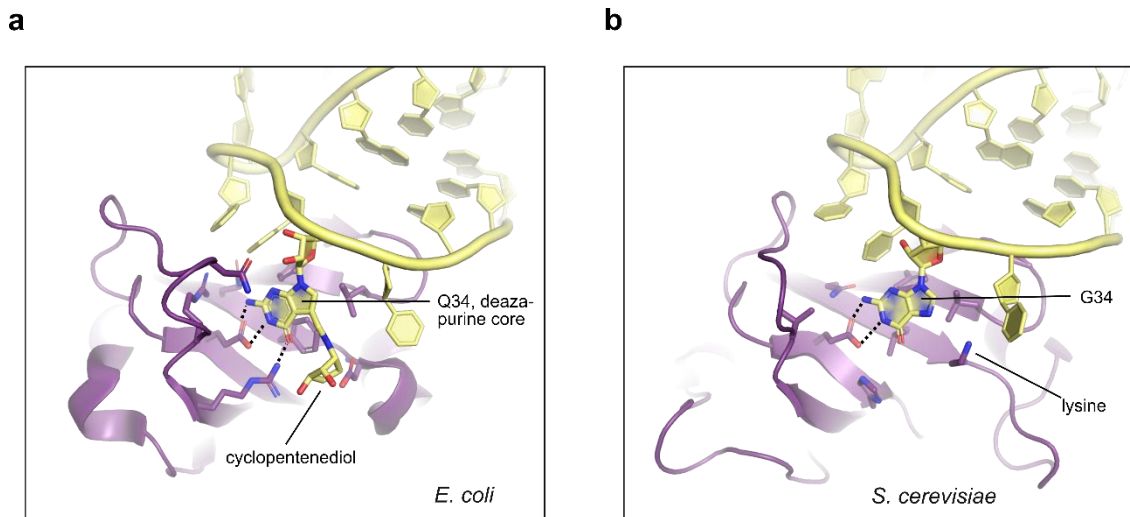
Figure 3: Aspartyl-tRNA-synthetases in complex with tRNA^Asp

*Two crystal structures of aspartyl-tRNA synthetase (purple) in complex with tRNA^Asp (yellow). **a)** Aspartyl-TS·tRNA^Asp complex from E. coli, containing queuosine at tRNA position 34 (PDB-ID: 1C0A). **b)** Aspartyl-TS·tRNA^Asp complex from S. cerevisiae, an organism naturally devoid of queuine (PDB-ID: 1ASY). The bound tRNA contains guanine at position 34.*

Many prokaryotes do not produce a dedicated Aa-TS for tRNA^Asn. Instead, a non-discriminating aspartyl-tRNA synthetase will recognize and load both tRNA^Asp and tRNA^Asn. Thus mischarged Asp-tRNA^Asn is subsequently converted to Asn-tRNA^Asn by an amidotranferase[60,61]. The crystal structure of such a non-discriminating aspartyl-TS from *Pseudomonas aeruginosa* bound to tRNA^Asn shows the familiar orientation of G34 oriented with its N7 atom facing the outside of the binding site[61].

Functional data comparing the aminoacylation of Q34- vs G34-tRNA is scarce, however the existing studies found no or only small differences between the two substrate types[62–64]. Taken together, while some Aa-TS of Q-containing organisms show signs of adaptation to accommodate a queuosine extension, these findings do not suggest that Q-modification is a significant modulator of aminoacylation.

Once reaching the ribosome, an aminoacylated tRNA first enters at the ribosomal A-site. A cognate (matching) tRNA is recognized by a stable minihelix formed between its anticodon and the mRNA codon, which results in conformational changes in the ribosome. These changes stabilize tRNA binding and trigger the release of its aminoacyl end into the P-site, where the growing polypeptide is transferred from the previous tRNA, forging a

new peptide bond. The mRNA is then shifted by one codon, transferring the new peptidyl tRNA to the P-site and the now deacylated tRNA to the E(exit)-site, which restores the ribosome for the next round of elongation[65].

In most organisms, each of the four G/QUN- tRNA isoacceptors is tasked with decoding both codons of their respective 2-codon box, each containing a NAU and a NAC codon. Early studies thus tried to find a direct effect of Q-modification on the innate stabilities of codon-anticodon pairs with U- or C-ending codons. Most of these works suggested that the presence of Q34 exerts a stabilizing effect on wobble pairing with U-ending codons, although the effect was often subtle and contradictory results were reported as well[40,64,66–68]. However, all of these early works suffer not only from technical limitations but also the limited understanding of the structural foundations of codon recognition and translation at the time.

In 2015, the crystal structure of a ribosome caught in the act of decoding a UAC codon with a Q-modified tRNA[Tyr] at its P-site revealed that the third position C-Q pair does not deviate from the expected Watson-Crick geometry[32]. The cyclopentenediol moiety of the modified base occupies the major grove of the codon-anticodon minihelix, sharing this space with the bulky isopentyl-chain of ms^2i^6A found at position 37 in the same tRNA (Figure 4a). It is possible that this helps to rigidify the anticodon loop in the ribosomal context by tightening the space available to alternative conformations or even to pre-organize it, however no functional data is currently available to support these ideas.

Similarly, no structural information is available showing Q34-tRNA during initial codon recognition at the ribosomal A-site, in the decoding of a U-ending codon or even in the interplay with anticodon loop modifications present in other tRNAs species.

Interestingly, the authors do show the Q-mediated destabilization of a first position C·A mismatch within the A-site (Figure 4b). Here, the cyclopentene moiety of the wobble base Q forms hydrogen bonds with the mismatched first position C, causing it to break the geometry of the helix stack[32]. While it is unclear to what extent this interaction might occur *in vivo*, this observation does raise the possibility that Q-modification might play a role as a discriminating element against near-cognate codons.
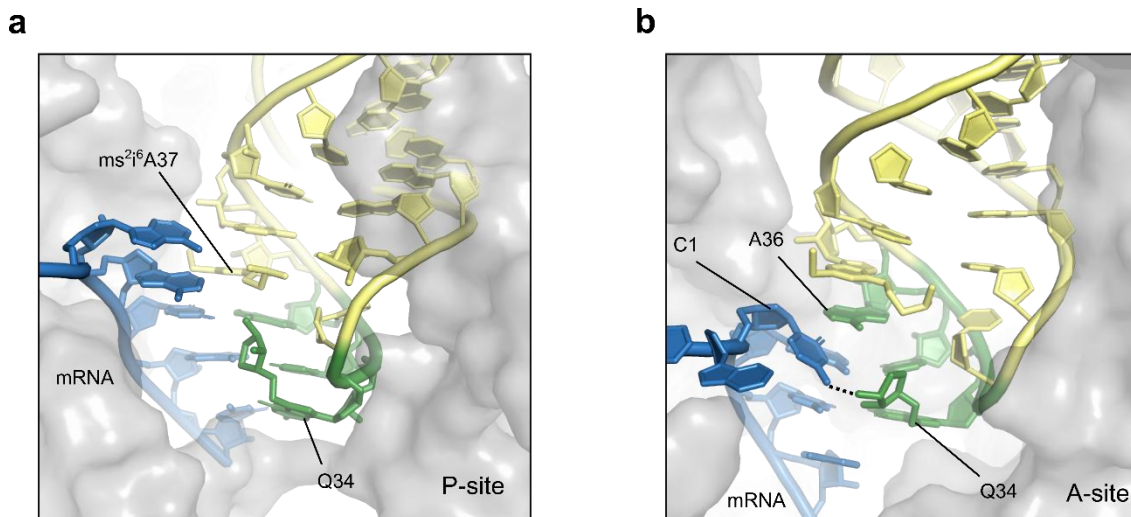
Figure 4: Queuosine in the context of a decoding ribosome

*Crystal structures of bacterial decoding events involving Q-containing tRNA. **a)** E. coli Q34-tRNA^Tyr paired to a cognate UAC codon in the context of the bacterial ribosomal P-site (PDB-ID: 4WZD). **b)** E. coli Q-34-tRNA^Tyr interacts with a near-cognate CAC codon (first position C·A mismatch) at the ribosomal A-site (PDB-ID: 4WQ1). For both structures, mRNA is shown in blue, tRNA is shown in yellow, the tRNA anticodon is highlighted in green. The ribosomal grip at both sub-sites is visualized in surface representation.*

A similar observation was reported on second position misreading errors by tRNA^Asp in *E. coli* that were found to be significantly increased in the absence of queuosine[69]. However, the same study showed that for tRNA^Tyr, Q-modification increased its second-position error rate, showing that this effect cannot be generalized[69].

In *Trypanosoma brucei*, absence of queuosine impaired translation of a reporter luciferase exclusively containing NAU codons, while both the NAC codon equivalent and the mixed codon wildtype were unaffected[70]. Q-hypomodification in *T. brucei* also increased +1 frameshifting events at tRNA^Tyr-decoded UAU codons, while the UAC codon was unaffected[71]. A similar effect was previously observed for tRNA^Tyr and tRNA^His which also caused increased frameshifting at U-ending test codons when Q-hypomodified[72]. The specific type of frameshifting that was tested is caused by P-site slippage and is thought to occur more frequently when the A-site decoding event is slowed down[72]. Thus, increased frameshifting in the absence of Q is an indirect measure of decreased decoding efficiency at the tested U-ending codons.

Recently, extensive investigation of decoding speed in human cells showed that tRNA[Asp], tRNA[Tyr], tRNA[His] and tRNA[Asn] were all translated more slowly in the absence of Q-modification[73]. Importantly, QUN-decoded near-cognate codons were similarly affected and also experienced reduced translational speed in the absence of Q[73]. The authors further showed that for tRNA[Tyr], tRNA[His] and tRNA[Asn], U-ending codons were effected more strongly, suggesting that Q-modification increases the rate of NAU decoding[73]. Finally, reduced translational speed in the absence of Q was shown to be accompanied by the accumulation of misfolded protein[73]. Similar experiments in *Schizosaccharomyces pombe* also revealed an effect on translational speed by Q-modification. However, here, Q-modifications seemed to exclusively speed C-ending His and Asp codons, while U-ending Asn and Tyr codons were slowed down[74]. Q-modification was also found to effect translation accuracy, as it suppressed second-position misreading of the near-cognate glycine codon GGC by tRNA[Asp] [74].

Finally, a genome-wide analysis of codon-choice across the *Drosophila* genus showed that NAU vs NAC codon usage was co-varied with the level of Q-modified tRNA across developmental stages, suggesting that differential codons are advantageous in the presence and absence of Q[75]. In particular, high levels of Q-modification correlated with increased use of C-ending over U-ending codons.

In summary, the available data suggests that Q-modification influences the decoding properties of QUN-tRNAs at its cognate NAU/NAC codons but also at near-cognate codons. Q-modification was found to affect both translation speed and accuracy, but it appears to do so in a strongly context-dependent manner. Although the effect was not consistent, Q-modification often differentially affected the decoding of NAU and NAC codons, revealing a possible link between tRNA modification and codon use. The example of covarying codon choice in *Drosophila* supports this idea, although the underlying mechanism is left unclear. Another example of a potential link between codon use and Q-modification is the much cited example of the *Shigella flexneri* transcription factor VirF, a global regulator of virulence, which is encoded with an unusual 80% NAU-bias[76]. In *Shigella*, a lack of Q-modification was found to impair VirF translation sufficiently to permanently induce a state of non-virulence[77,78].

1.2.2 Q-modification, m⁵C methylation and tRNA fragmentation

The relationship between Q-modification and translation is further complicated by the realization that queuosine, like many tRNA-modifications[79], is involved in a cross-talking mechanism.

For queuosine, this affects the concomitant m⁵C methylation at position 38 of tRNA^{Asp}, which is stimulated by the presence of queuosine. This was first discovered in *S. pombe*, where the presence of queuine in the growth medium strongly affected methylation[80]. Specifically, queuine affected methylation by Pmt1, a homolog of mammalian methyltransferase Dnmt2, which targets position 38 of certain tRNAs, including tRNA^{Asp}. The relationship between Q-modification and Dnmt2-dependent methylation was also confirmed to occur in other organisms, including human cells[73,80].

The stimulatory effect was further reproduced *in vitro*, directly showing that Q34-tRNA^{Asp} is more effectively methylated than G34-tRNA^{Asp} [80,81]. Attempts to elucidate the functional basis of Dnmt2 stimulation by queuosine revealed a very minor increase in affinity between *S. pombe* Dnmt2 and tRNA^{Asp} upon Q-modification of the tRNA[81]. Q34 is likely to come in close contact with the Dnmt2 active site during methylation at position 38, however the details of such an interaction remain unknown.

Of note, Dnmt2-dependent methylation was reported to protect tRNAs against stress-induced cleavage by the small nuclease angiogenin[82]. Thus, Q-dependent stimulation of Dnmt2 might indirectly inhibit fragmentation of tRNA^{Asp}. Importantly, loss of Dnmt2-dependent methylation increased stress sensitivity in *Drosophila melanogaster*, likely because tRNA-derived fragments are involved in the cellular stress response[82]. Interestingly, Q-modification was also reported to confer a protective effect to tRNA^{Asn} and tRNA^{His} that was independent from m⁵C modification[83]. In contrast, while a recent sequencing-based approach did uncover an overall link between tRNA-hypomodification and fragmentation, Dnmt2-dependent methylation in particular was not linked to fragmentation[84]

In summary, these findings suggest that Q-modification further affects other tRNA modification and processing events. However, the very nature of this interdependence makes the contribution of an individual modification difficult to study and the mechanisms of these effects are still largely unclear.

1.2.3 Q-modification and queuine in metabolism, development and cancer

On a systemic level, Q-modification levels appears to vary greatly between different tissues and developmental stages: In mice and rats, young animals show very low levels of Q-modified tRNAs, which increase significantly with age[66,85]. Similarly, induced differentiation of leukemia cells was accompanied by a marked increase of Q-modified tRNA[86–88]. In various insect species, including *Drosophila melanogaster*, the level of Q-modification was found to undergo marked changes correlated with metamorphosis and aging although these changes were not consistent across species[45,89,90].

Early studies on an *E. coli* mutant lacking Q-modified tRNA found no obvious growth defects, declaring it a non-essential modification under normal conditions[64]. Similarly, *Caenorhabditis elegans* and *Chlamydomonas reinhardtii*, a single-celled algae, both grew normally in the absence of Q[91,92].

In contrast, several works have found links between the free base queuine and oxidative metabolism, and in particular the enzyme lactate dehydrogenase (LDH)[93–96]. Recently, queuine depletion of HeLa cells was shown to promote Warburg-type metabolism, which is characterized by aerobic glycolysis and lactic acid fermentation in the cytosol[97]. In eukaryotes, queuine is a micronutrient (discussed in detail in chapter 1.3.3). Experiments with mice artificially reared to be devoid of queuine and Q-modification showed that neither is essential under normal growth conditions[73,98]. Similar results were obtained with knock-out mice enzymatically incapable of Q-modification[99]. However, Q-deficiency severely compromised the animals' tyrosine biosynthesis, causing severe neurological symptoms and death if tyrosine, normally a non-essential amino acid, was not administered externally[100]. Later, this was attributed to an increased oxidation of the cofactor tetrahydrobiopterin (BH4), which is required for hydroxylation of phenylalanine to tyrosine[99].

Consistent with its link to Warburg metabolism[97], Q-hypomodification was also shown to naturally occur in many types of cancer, including leukemia and lymphoma[101,102], two types of brain tumors[103], lung cancer[104] and ovarian cancer[105]. Furthermore, severe Q-hypomodification appears to correlate with tumor aggressiveness and stage as well as poor patient survival[101,104,105].

1.3 Queuosine metabolism

Queuosine is a highly unusual RNA modification, because it is created not by derivatization of the existing nucleobase, but by a complete base exchange involving the breakage of the original N-glycosidic bond. For this reason, queuosine biosynthesis starts independently of tRNA and requires a total of eight enzymes of which most are specific to the queuosine pathway. Notably, *de novo* synthesis of queuosine only occurs in bacteria, while eukaryotes exclusively depend on salvage of the free queuine base, which is then incorporated into tRNA.

1.3.1 *Queuosine biosynthesis in bacteria*

Queuosine biosynthesis starts from guanosine triphosphate (GTP) which is converted to 7,8-dihydroneopterin-3'-triphosphate by GTP cyclohydrolase I, an enzyme shared with tetrahydrofolate (THF) and tetrahydropterin (BH4) biosynthesis[106,107]. The catalyzed reaction starts with the hydrolysis of the purine ring at the C8 atom, followed by deformylation and re-cyclization of the ribosyl moiety, finally generating a pterin ring structure[108,109].

Next, QueD catalyzes the formation of 6-carboxy-5,6,7,8 tetrahydropterin and acetaldehyde[110,111]. The former is further converted by the SAM dependent enzyme QueE, which catalyzes the characteristic carbon replacement of the N7 atom to generate 7-deaza-7-carboxyguanine[112]. An ammonia and ATP-dependent reaction catalyzed by the enzyme QueC converts the carboxy group into a nitrile, yielding 7-cyano-7-deazaguanine[113–115]. This compound is a key intermediate of the pathway and is commonly referred to as preQ$_0$[116]. PreQ$_0$ is then converted to another key compound, preQ$_1$, by the enzyme QueF[117–119]. Chemically, this reaction is an NADPH/H+ dependent reduction of the nitrile to a primary amine, generating 7-aminomethyl-7-deazaguanine.
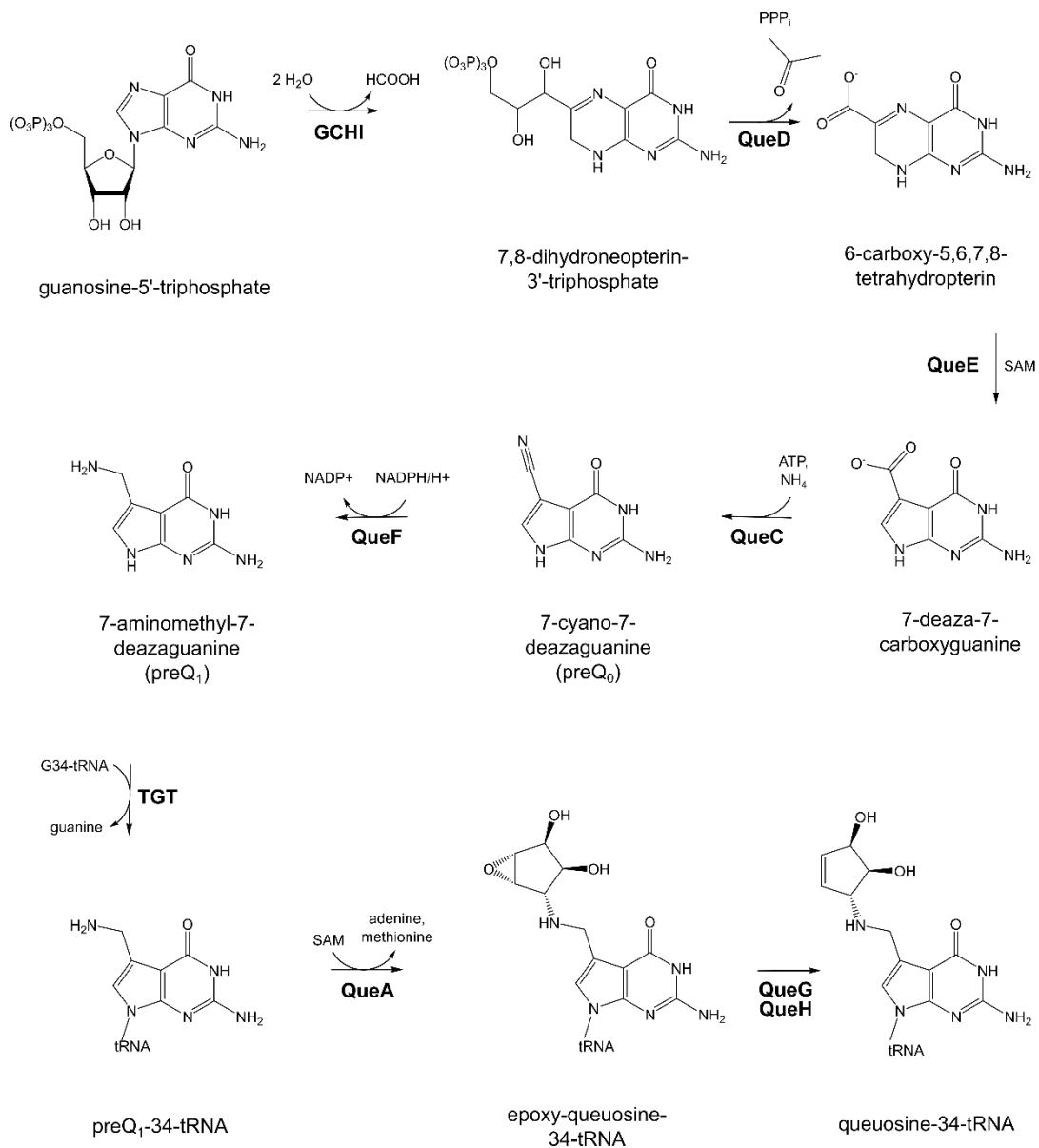
Figure 5: Bacterial queuosine biosynthesis

Pathway of bacterial queuosine de novo biosynthesis starting from guanosine-5'triphosphate (GTP). The pathway requires eight enzymes: GTP cyclohydrolase I (GCHI), QueD, QueE, QueC, QueF, tRNA guanine transglycosylase TGT, QueA and either QueG or QueH, which are inversely distributed among bacteria. The names and structures of each intermediate compound are provided as well as the known co-substrates and co-products of each reaction.

The intermediate preQ1 then serves as the substrate to the pathway's unique base exchange reaction, catalyzed by the enzyme tRNA guanine transglycosylase (TGT) which will be discussed in detail in chapter 1.4. The product of the catalyzed reaction is $preQ_1$34-U35-N36-tRNA and all subsequent steps occur in the context of this tRNA: First, the enzyme

QueA uses the ribose moiety of S-adenosylmethionine to attach a cyclic epoxy group to the primary amine of preQ1, yielding the reaction product epoxy-queuosine-34-tRNA[120,121]. Finally, the epoxide is opened to cyclopentenediol, yielding queuosine-34-tRNA. Interestingly, this reaction is catalyzed by two unrelated and mechanistically different enzymes, QueG[122] and QueH[123], that show complementary distribution among bacteria.

1.3.2   Salvage of preQ$_0$, preQ$_1$ and queuine in bacteria

Queuosine biosynthesis is a costly, energy and resource consuming pathway and bacteria appear to possess multiple salvage mechanisms to re-utilize precursors. Furthermore, not all bacteria are capable of queuosine *de novo* synthesis. Several organisms (e.g. *Clostridium ramosum*, *Haemophilus somnus* and *Acidimicrobium ferrooxidans)* are known to lack the genes responsible to synthesize preQ$_0$ (*queD*, *queE* and *queC)* but do contain the genes required for the subsequent steps of the queuosine pathway (*queF, tgt, queA* and *queG* or *queH*)[123]. Alternatively, *queF*, catalyzing the conversion to preQ$_1$ is also missing (leaving only *tgt*, *queA* and *queG* or *queH*, e.g. in *Rubrobacter xylanophilus* and *Syntrophomonas wolfei*)[123]. These types of gene sets strongly suggest that the respective organisms depend on the uptake and subsequent use of externally sourced preQ$_0$ or preQ$_1$.

Recently, YhhQ was identified as a preQ$_0$/preQ$_1$ importer in *E. coli*, an organism fully capable of queuosine *de novo* synthesis[123]. While the transporter was shown to be able to import both precursor types, import of preQ$_0$ appeared to be preferred in *E. coli*. YhhQ homologs are widespread among bacteria and are also found in many species genetically incapable of preQ$_0$ biosynthesis. However, they are also found in organisms additionally lacking the queF gene and thus the ability of preQ$_0$ conversion to preQ$_1$, suggesting that the transporter might have varied substrate specificity in different organisms[123].

The YhhQ transporter is not the only importer of queuosine precursors: The *E. coli* genes *qrtT* and *queT* encode substrate-specific components of an ECF-type transporter[124,125]. Both genes are frequently genetically associated with genes of the queuosine metabolism or under the control of a preQ$_1$ induced riboswitch[126,127]. Recent work confirmed two QueT homologs in *Clostridium difficile* to function as preQ$_1$ transporters[128].

Importantly, all bacterial species depending on salvage for Q-modification still possess the critical enzyme of the queuosine biosynthesis pathway, tRNA guanine transglycosylase

(TGT), to catalyze the necessary base exchange reaction. In the most extreme cases, *tgt* is the only queuosine-related gene found in some genomes (ie *Corynebacterium diphtheriae* and *Actinomyces coleocanis*)[123], suggesting that these species salvage and directly incorporate the free queuine base. This was recently demonstrated for *Chlamydia trachomatis*, a human pathogenic bacterium, that appears to possess a YhhQ homolog adapted to import queuine. In this species, the TGT enzyme is atypical and is likewise adapted to accept the divergent substrate base[128].
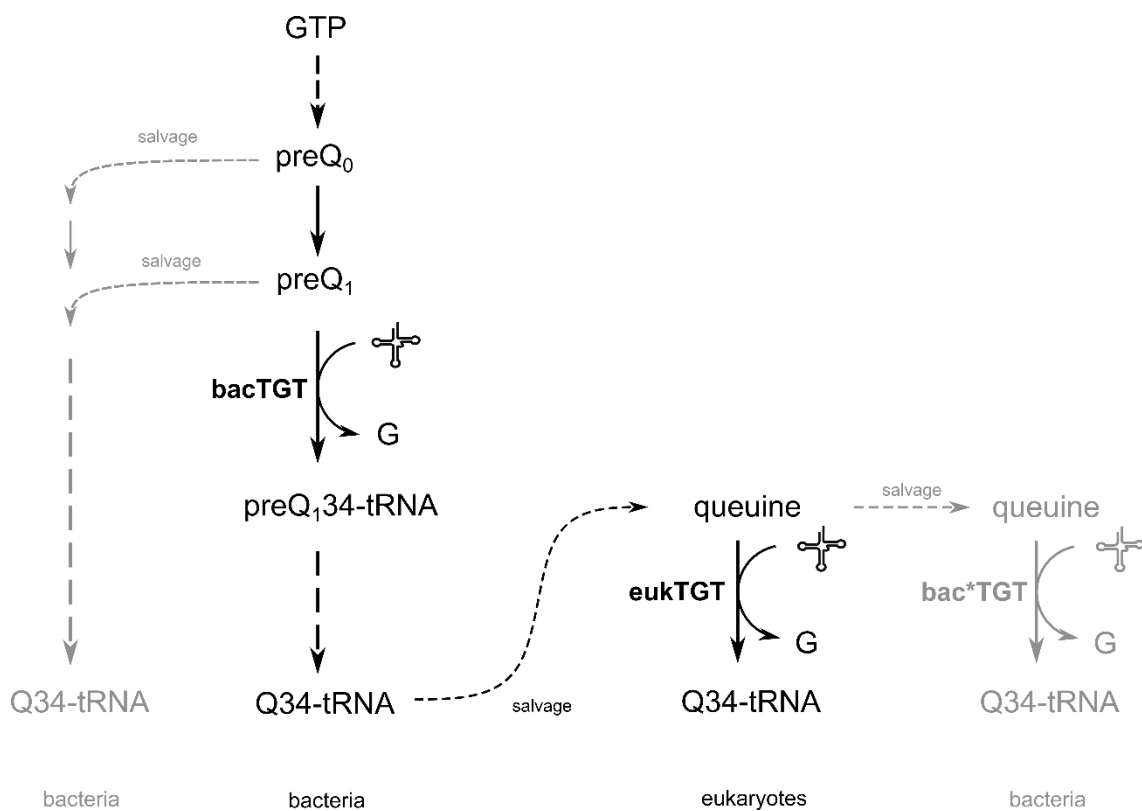
Figure 6: Queuosine metabolism in bacteria and eukaryotes

Overview of queuosine metabolism showing queuosine de novo biosynthesis (2nd column) and different modes of salvage: 1st column: Salvage of queuosine precursors in bacteria, followed by standard processing to yield Q34-tRNA. 3rd column: Salvage of queuine in eukaryotes, followed by direct incorporation by eukTGT. 4th column: Queuine salvage by human pathogenic bacteria (Chlamydia trachomitis-type[128]), followed by direct incorporation by an atypical bacterial TGT (bac*TGT).

1.3.3 Queuine salvage and incorporation in eukaryotes

In eukaryotes, Q-modification is entirely dependent on the uptake of external queuine, because the enzymatic machinery for *de novo* synthesis is universally missing. In essence, this means that each queuine base incorporated into eukaryotic tRNA was originally synthetized by a bacterial cell. Sources of queuine available to eukaryotes are both nutritional and, for the animal kingdom, gut bacterial. This makes queuine a nutrient in eukaryotes and its limited availability is likely the reason why vastly different levels of Q-modifications are observed in different tissues and developmental stages. Specifically, a substrate-limitation to modification could be the explanation why low Q-modification levels are typically observed for fast-growing developmental stages and tissues[75,129].

Eukaryotic cells import both queuosine and the free queuine base via yet unknown transmembrane transporters[130,131]. Queuine can be used directly, because it is the natural substrate of eukaryotic TGTs. Thus, the base exchange reaction catalyzed by eukTGT directly yields queuosine-34-tRNA, without the requirement of further downstream reactions. Coincidently, this makes eukTGT functionally identical to the TGT found in some human pathogenic bacteria[128], although profound structural differences suggest that this is an example of convergent evolution[128].

Recently, Qng1, a homolog of DNA hydrolases, was identified as a conserved salvage enzyme in eukaryotic queuosine metabolism[132]. Subsequent structural and biochemical studies could show that Qng1 is a queuosine-nucleotide N-glycosylase releasing queuine from queuosine-5′-monophosphate [131,133,134]. To date, it is unclear whether queuosine-5′-monophosphate is sourced from processive 5′-to-3′ degradation of Q-containing tRNAs via the rapid decay pathway, or whether yet unknown enzymes provide a link to queuosine import[131].

In addition to Q-modification of cytosolic tRNAs, Q-modification of mitochondrial GUN-tRNAs is also dependent on eukaryotic TGT[50]. Although mitochondrial association or location has been reported for eukTGT[135,136], it is currently unclear how eukTGT comes into contact with its substrate mt-tRNAs, as eukTGT contains none of the known targeting signal for mitochondrial import[137].

1.3.4   *Queuosine glycosylation and glutamylation*

In both eukaryotes and bacteria, some queuosine-containing tRNAs are subject to further derivatization of the cyclopentenediol moiety.

In bacteria, Q34-tRNA[Asp] is the substrate of a glutamyl-queuosine-tRNA[Asp] synthetase[138,139]. Descended from aminoacyl-tRNA-synthetases, the enzyme exploits structural similarity between the tRNA[Glu] amino acid acceptor stem and the tRNA[Asp] anticodon stem to aminoacylate the ribose-like *cis*-diol moiety of the wobble position queuosine[138,140].

Similarly, it has long been known that eukaryotic cells further derivatize queuosine by glycosylation (Figure 7)[46]. Specifically, cytosolic tRNA[Tyr], predominantly contains not queuosine but β-*homoallyl*-galactosyl-queuosine (galQ) at position 34 [46,129] while cytosolic tRNA[Asp] contains α-*allyl*-mannosyl-queuosine (manQ)[141].

queuosine   β-*homoallyl*-galactosyl-queuosine   α-*allyl*-mannosyl-queuosine
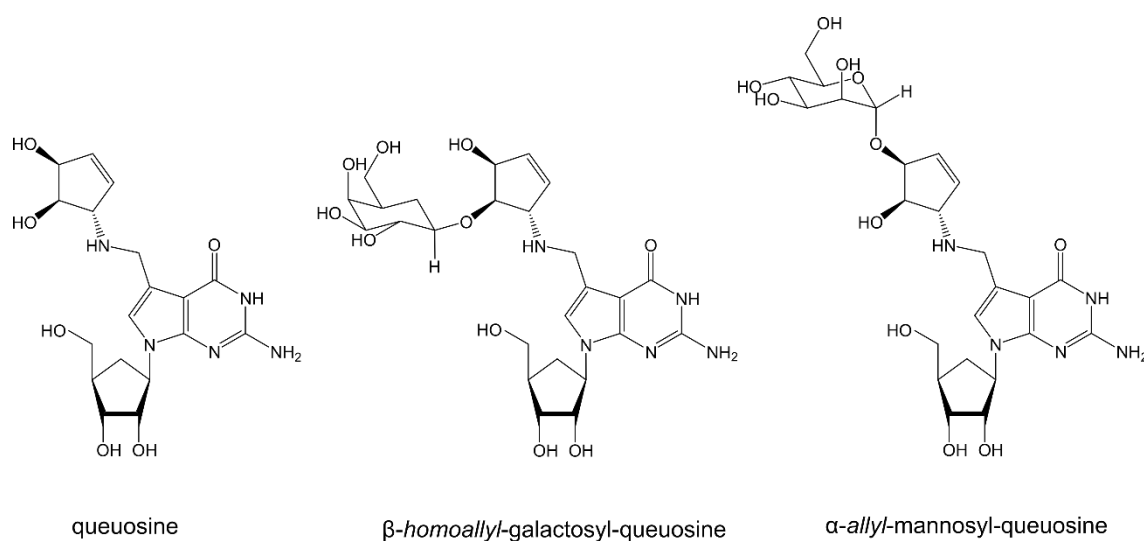
Figure 7: Queuosine and naturally occurring glycosyl-queuosine derivatives

Chemical structures of queuosine, β-homoallyl-galactosyl-queuosine and β-allyl-mannosyl-queuosine, the two naturally occurring glycosyl-queuosine derivatives in eukaryotes. Galactosyl-queuosine is exclusively found in cytosolic tRNA[Tyr], while mannosyl-queuosine is exclusively found in cytosolic tRNA[Asp].

To date, the enzymes involved in queuosine glycosylation are still unknown. Since the type of queuosine glycosylation is specific to certain tRNA types, it is reasonable to assume that glycosylation occurs in the context of these tRNAs, subsequently to queuine

transglycosylation by TGT. GalQ and ManQ are found exclusively in cytoplasmic tRNAs while mitochondrial mt-tRNA^{Asp} and mt-tRNA^{Tyr} both contain regular queuosine at position 34[50,51], suggesting that unlike TGT, the enzymes producing manQ and GalQ do not come in contact with mitochondrial tRNAs.

It is unclear why queuosine derivatization by glycosylation and glutamylation occurs, and why it occurs only in specific tRNAs. However, it is of note that all of these derivatizations make the already bulky queuosine modification even bulkier, certainly influencing its special properties in the ribosomal environment during decoding.

1.3.5   Archaeosine

Queuosine is a modification specific to bacteria and eukaryotes and does not occur in archaea. However, archaea produce the related 7-formamidino-7-deazaguanosine, better known as archaeosine (G$^+$), which is exclusively found at position 15 of several archaeal tRNAs, a site not modified in the other two phyla[142–144].

The key step in archaeosine biosynthesis is the incorporation of preQ$_0$ into tRNA, a base-exchange reaction catalyzed by archaeal TGT (arcTGT)[145]. Several variants exist for further processing: In euryarchaeota, preQ$_0$-tRNA is converted to archaeosine-tRNA by an ATP- and glutamine-dependent amidinotransferase (ArcS)[146]. In some crenarchaeota, ArcS is functionally replaced by an enzyme related to QueF (termed QueF-Like or QueF-L) which utilizes free ammonia instead of glutamine[147,148]. GAC-QueC, a fusion protein containing a glutamine amidotransferase class-II domain and a QueC homolog, replaces QueF in the remaining crenarchaeal genomes[149]. Heterologous expression in *E. coli* caused a non-physiological accumulation of G$^+$34-tRNA, suggesting that GAC-QueC is the last missing archaeosine synthase[149]. However due to the great differences that separate bacterial and archaeal 7-deazapurine metabolism, the enzyme awaits more thorough biochemical testing[150].

Figure 8: Archaeosine biosynthesis

Schematic representation of archaeosine biosynthesis, showing its two characteristic steps: Incorporation of preQ$_0$ by archaeal TGT and further conversion to archaeosine-tRNA. The second step is catalyzed by various enzymes among archaeal species, of which two are known (ArcS and QueF-Like), while a third is strongly suspected (GAC-QueC).

1.4 tRNA guanine transglycosylase

The enzyme tRNA guanine transglycosylase (TGT) catalyzes the key reaction in the deazapurine metabolism: The base exchange of the genetically encoded guanine. Representatives of this family of enzymes occur in bacteria, eukaryotes and archaea and all of them share an evolutionary origin. However, because each domain of life exhibits a different type of deazapurine metabolism, assigning divergent roles to their TGT enzymes, bacterial, eukaryotic and archaeal TGTs are structurally and functionally distinct.

1.4.1 Bacterial and eukaryotic TGT

Bacterial TGT (bacTGT) and eukaryotic TGT (eukTGT) are most similar in their structure and function because both enzymes catalyze the exchange of guanine 34 for queuine or a queuine precursor. The structure of TGT enzymes is based on a triosephosphate isomerase-like $(\beta\alpha)_8$ barrel at its core[151]. By convention, the secondary structure elements that make up this $(\beta\alpha)_8$ core are numbered β1-8 and α1-8[152]. However, the $(\beta\alpha)_8$ barrel fold is augmented by several TGT-specific insertions, including a three-stranded, N-terminal β-sheet forming a lid-like structure (βA-βC), an insertion containing both a 2 or 3-stranded β-sheet and an additional α-helix (αA-βF) located between β3 and α3, and finally, an elaborate zinc-binding domain (αB-αG/H) largely situated in between β8 and α8 (Figure 9). This subdomain contains a single structural zinc ion that is coordinated by the side chains of

three cysteines (C318, C320 and C323, *Zymomonas mobilis* numbering) and a histidine (H349).

Figure 9: Conserved architecture of bacterial and eukaryotic TGT

The conserved fold shared by bacterial TGT and the two subunits of eukaryotic TGT (QTRT1 and QTRT2) is shown. Top row: Schematic representation of secondary structure elements within the central $(\beta\alpha)_8$ barrel core (grey) and insertions (yellow, orange, pink). Bottom row: Crystal structures of bacterial TGT (PDB-ID: 1Q2R), eukaryotic QTRT1 (PDB-ID: 6H45) and QTRT2 (PDB-ID: 6FV5). The color-scheme is consistent between subfigures, characteristic elements are labelled.

Both bacterial and eukaryotic TGT are functionally dimeric proteins. Due to steric reasons, only one tRNA is simultaneously bound by the dimer, which means that for each tRNA molecule, only one of the two dimer subunits is catalytically active, while the other plays a supporting role[153,154]. Bacterial TGT is a homodimer, and its dimerization interface thus

follows 2-fold rotational symmetry. The two subunits interact largely via their zinc binding domains. Specifically, helix αE provides three aromatic residues (W326, Y330, H333, *Z. mobilis* numbering) to form a "hot spot" with residue P92 of the opposing subunit (Figure 10)[155,156]. In both copies of the hot spot motif, the aromatic residues engage in parallel displaced and edge-to-face π-π stacking, thus stabilizing the dimer interface. The aromatic cluster is shielded from water access by the loop connecting β1 and α1. The same loop provides two main chain carbonyls (A48 and A49), which, together with a third carbonyl (M93) lock the αE aromats in place. Finally, the interface contains several salt bridges, chiefly between residues of the β1α1 loop and the apex of αE-αF turn.
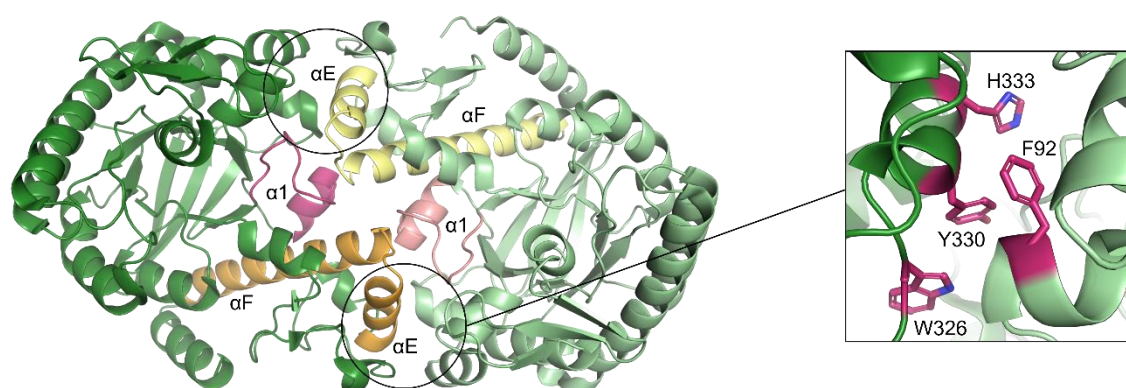
Figure 10: Dimer association in bacterial TGT

Crystal structure of bacterial TGT (PDB-ID: 1Q2R) highlighting the major contributions (helices αE, αF, α1 and adjacent loop) to the symmetric dimer interface. The locations of two identical aromatic "hot spots" are marked by circles, the inset shows a detailed view of this motif.

The TGT active site is located at the center of the $(\beta\alpha)_8$ barrel and involves two catalytic aspartates (D280 and D102, Figure 11)[152]. Additional residues stabilize the (deaza)purine via hydrophobic and π-π stacking interactions (Y106 and M260) and form extensive hydrogen bonds that specifically recognize the guanine-type Watson-Crick face (D102, D156, Q203, mainchain G230)[151,152]. These elements equally accommodate either the genetically encoded guanine or the preQ1 base which bacTGT incorporates. If preQ1 is

bound to the active site, the main chain carbonyl of L231 serves as an anchor point for the additional primary amine[151].
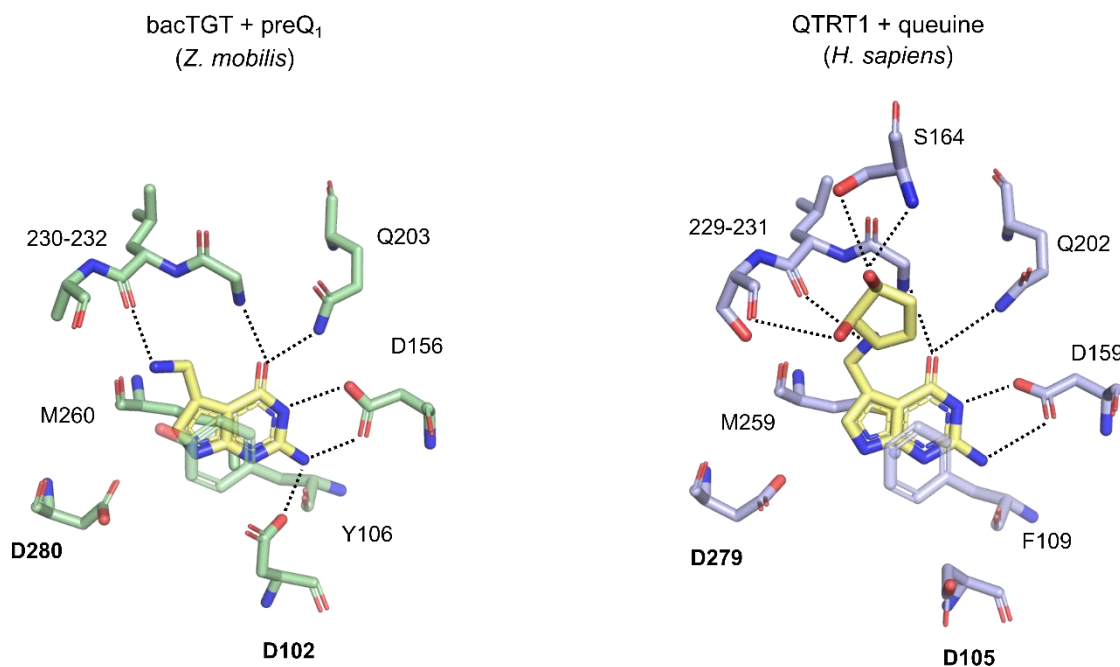
Figure 11: Comparison of TGT active sites

Details of the conserved active sites of bacterial TGT and eukaryotic TGT from two crystal structures. Left: Active site residues of Z. mobilis TGT bound to preQ₁ (PDB-ID: 1P0E). Right: Active site residues of H. sapiens QTRT1 bound to queuine (PDB-ID: 6H45). The equivalent aspartates D102/D105 are flexible and adopt variable orientations in different crystal structures.

Eukaryotic TGT generally differs from bacterial TGT in two major ways: Firstly, by being optimized to accept queuine, not preQ1, in its active site, and secondly, by typically forming a functional heterodimer. The two dimer subunits are homologous, but only one contains a functional active site (QTRT1), while the accessory subunit (QTRT2) is not catalytically active[154,157]. Compared to bacTGT, QTRT1 contains an additional C-terminal helix, αH, otherwise, its overall architecture is largely unchanged (Figure 9)[158]. In contrast, QTRT2 is altered at two of its insertions, as αA and βD are replaced by a flexible loop obstructing the would-be active site, while the βGβH sheet is separated by an unresolved additional loop (Figure 9)[157]. Because both subunits are homologs of each other and of bacterial TGT, it

appeared likely that their dimerization would follow the bacterial enzyme's model. However, this was previously unproven as structural data of the eukaryotic heterodimer was missing prior to this work.

The QTRT1 active site differs from bacTGT in subtle ways to accommodate the differential substrates: While the two catalytic aspartates and the residues binding the (deaza)purine core have direct homologs (D279 and D105 as well as F109, M259, D159, Q202 and mainchain G229), a critical valine-to-glycine mutation (G232) provides the necessary room to accommodate the cyclopentene-*cis*-diol moiety. The mainchain of L230 (the equivalent of L231 in *Z. mobilis*) recognizes the secondary amine of the linker, while the *cis*-diol forms additional hydrogen bonds to S164 and the S231 main chain carbonyl (Figure 11)[158].

1.4.2 *Archaeal TGT*

Archaeal TGT shares its evolutionary origin with both bacTGT and eukTGT. This becomes apparent by the modified $(\beta\alpha)_8$ fold that is shared by all TGT enzymes, as well as a highly similar active site, containing homologs for all catalytic and functional residues found in bacTGT and eukTGT[159]. However, arcTGT also features additional tRNA-binding domains, a likely adaptation to the differential tRNA position targeted by the archaeal enzyme[159,160]: Unlike bacTGT and eukTGT, it catalyzes a base exchange at position 15, not 34, and thus requires a very different orientation of its substrate tRNA. Guanine 15 is also a much more challenging target base than guanine 34, because unlike the latter, which is easily accessible, guanine 15 is located at the center of the tRNA core and thus requires partial unfolding of the tRNA L-form to be accessed.

Archaeal TGT forms a functional homodimer, but its dimer association is fundamentally different from bacTGT[159]. The interface is mainly formed by direct interaction of the two zinc-binding domains on one side, and the two C-terminal regions of the $(\beta\alpha)_8$ domain on the other. Both contact areas are surprisingly hydrophilic, containing many polar and charged amino acid residues. There is no equivalent of the bacterial "hotspot" motif in archaeal TGT.

Three additional, closely associated PUA (pseudouridine synthase and archaeosine transglycosylase) domains with high sequence homology to the RNA-binding domains of pseudouridine synthase are C-terminally fused to the $(\beta\alpha)_8$ domain[159,161]. A crystal structure

of the arcTGT-tRNA complex reveals that these domains collectively bind the tRNA acceptor arm and core in an orientation that allows the tRNA D-arm to unfold and enter the active site of the second subunit (Figure 12)[160]. The tRNA binding site of the PUA domains is strongly positively charged, suggesting that RNA binding is facilitated by an interplay of shape complementarity and attractive electrostatic forces with the negatively charged phosphate backbone of the tRNA[160]. Due to the differential dimer arrangement, the two active sites of the arcTGT dimer face opposite directions and thus allow for two tRNAs to bind at the same time[160].
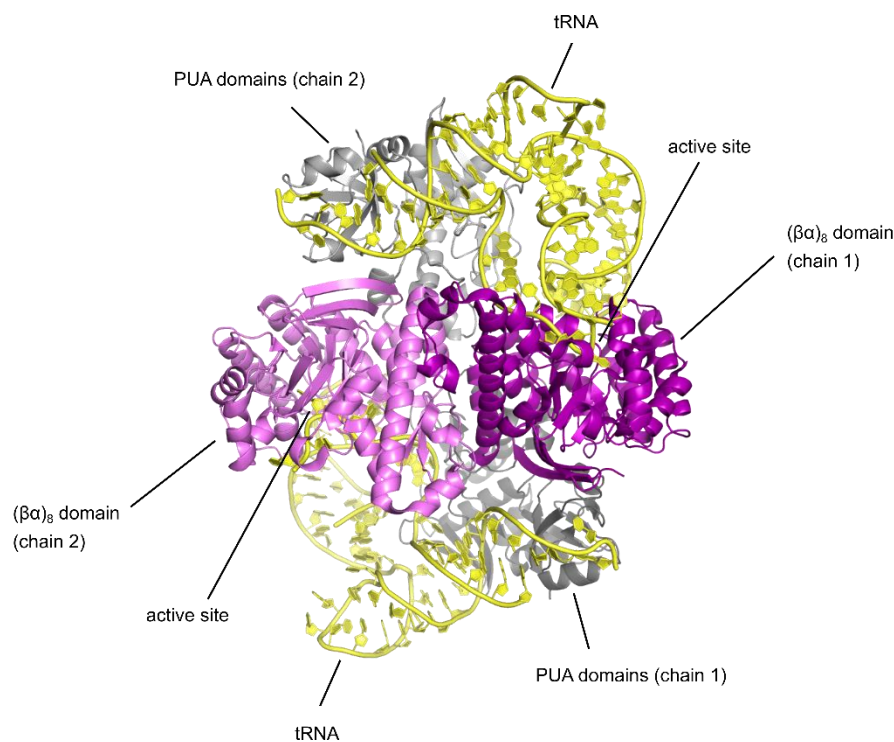
Figure 12: Archaeal TGT domain organization and tRNA binding

A crystal structure showing the divergent domain organization of archaeal TGT bound to two tRNA molecules (PDB-ID: 1J2B). In addition to a catalytic (βα)8 domain shared with bacterial and eukaryotic TGT, arcTGT contains three closely associated tRNA-binding domains per chain. These domains, combined with an alternative dimer interface, allow arcTGT to bind two tRNA molecules at a time.

1.4.3 TGT reaction mechanism

The accumulated crystal structures of TGT enzymes from all domains of life, together with functional data, allow to deduce the TGT reaction mechanism with confidence (Figure 13). Despite overall differences in domain and subunit composition, all TGTs share a highly conserved active site with two catalytic aspartates in identical positions[151,158,159]. This suggests a shared reaction mechanism, which in the following is described using human amino acid numbering:

First, a suitable substrate tRNA binds to the active site, where the genetically encoded guanine (position 34 or 15) is recognized through formation of several hydrogen bonds[152,159,162]. Then, Asp279 performs a nucleophilic S_N2 attack on the C1′ atom of the target nucleoside via its charged carboxylate group. This transfers an electron to the guanine N9 atom, from where it relocates to the N7 atom, which then accepts a proton from a water molecule coordinated by the L230 and S231 main chain amides. A water molecule coordinated in this way is visible in some crystals structures of TGT with bound guanine[159,162]. The result of this electron transfer is the formation of a new ester linkage between the ribose C1′ atom and the Asp279 side chain, replacing the N-glycosidic bond to the guanine base. Such a covalent intermediate was crystallized for *Z. mobilis* TGT[152]. Both guanine and the formed hydroxide are then free to defuse from the active site. This allows the appropriate deazapurine (queuine, preQ$_1$ or preQ$_0$) to bind to the vacated active site. In eukaryotic and bacterial TGT, this is accompanied by a flip of the L230-S231 peptide bond to allow the formation of a stabilizing hydrogen bond between the L231 main chain carbonyl and the primary or secondary amine of preQ$_1$ or queuine respectively[152,158,162,163]. In archaeal TGT, the homologous peptide does not flip upon preQ$_0$ binding: Because the equivalent nitrogen atom is fully substituted (cyano group) it is unable to act as a hydrogen bond donor, instead it accepts a hydrogen bond from the unflipped main chain amide[159].

In the second half-reaction, the charged carboxylate of the second catalytic aspartate, Asp105, likely transfers an electron to the N3 atom of the 7-deazapurine, from where it is passed onto the N9 atom. This causes its deprotonation, enabling it to perform a second nucleophilic S_N2 attack on the C1′atom. As a result, the donated electron is transferred to

the Asp279 carboxyl, which restores the enzyme and forges a new N-glycosidic bond between ribose and deazapurine[164].

The characteristic C7 atom shared by the 7-deazapurines queuine, preQ$_1$ and preQ$_0$ means that a second reaction cycle is not possible, because the carbon atom prevents the necessary charge transfer of the first half reaction. Thus, the only outcome is for the now base-exchanged tRNA to dissociate from the enzyme, taking with it a proton that will quickly be transferred to a solvent water molecule. The divergent ability of a C7 carbon and a N7 nitrogen to transfer a charge is also the reason why the incorporation of a 7-deazapurine is irreversible, while a guanine-to-guanine exchange is not[164–167].

The described reaction mechanism can be expected to follow ping-pong kinetics, which was experimentally shown to be the case for *E. coli* TGT[168]. Recently, kinetic evidence was published which suggests that eukaryotic TGT might instead operate by a bi-bi mechanism[169]. However, such a mechanism, which assumes simultaneous binding of both guanine 34 and queuine, is incompatible with a single shared binding site, a contradiction the authors fail to properly address[169]. For this reason, and because of the extremely high degree of active site conservation, this work assumes that the reaction mechanism above is shared by TGT enzymes from all domains of life, including eukaryotic TGT.

The TGT mechanism also predicts that TGT should be able to incorporate a diversity of 7-deazaguanine derivatives, given that their extended chains fit the TGT binding pocket. The structure of human TGT with bound queuine actually shows that the cyclopentenediol moiety points to the outside of the binding pocket, which could mean that elaborately derivatized queuine analogs might be suitable substrates[158]. This was shown to be the case by several studies[165,170] and prompted the use of eukaryotic TGT but also bacterial TGT as a site-specific labelling tool in biotechnology and medicine[171–173].
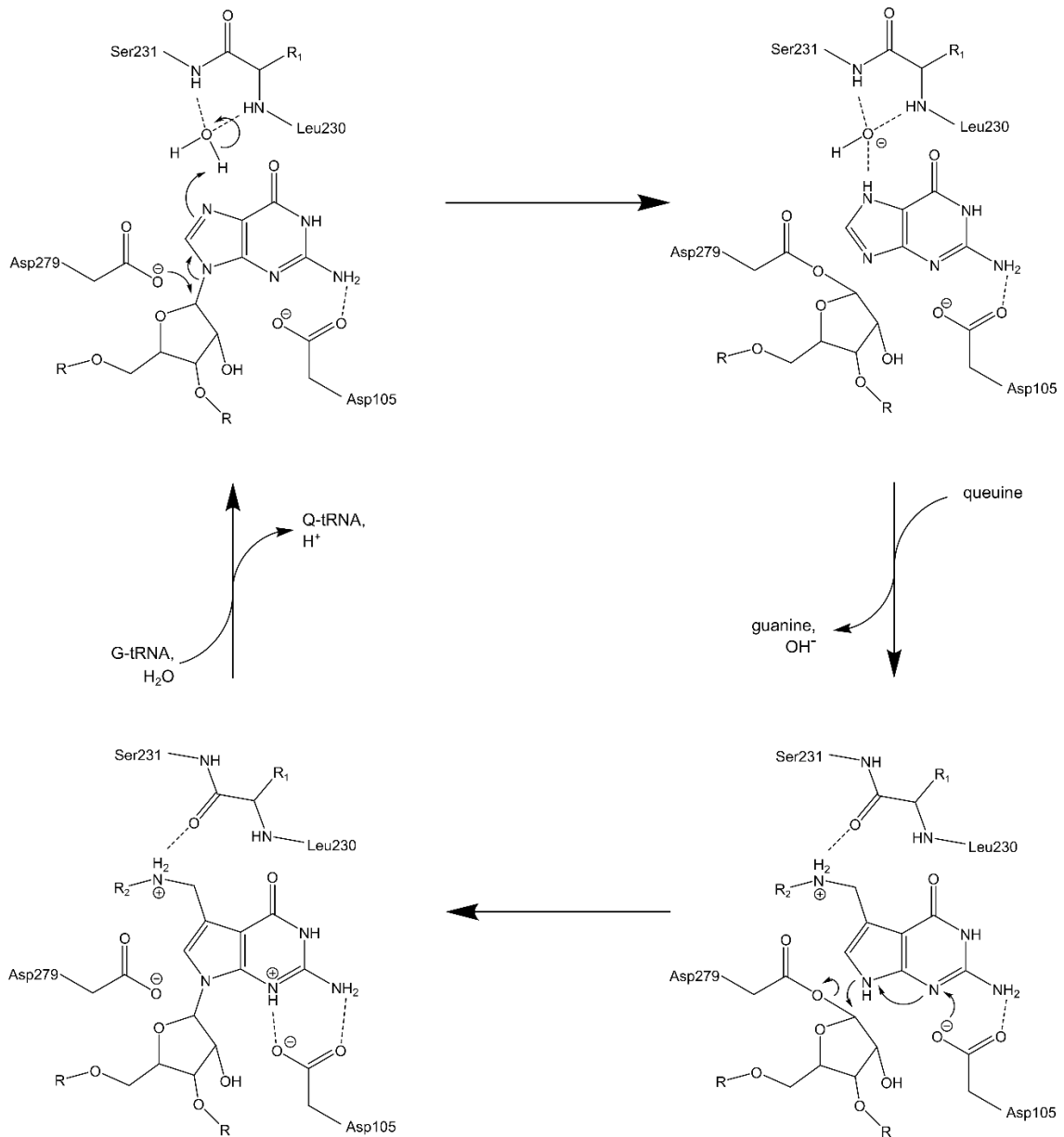
Figure 13: Conserved TGT mechanism

Reaction scheme depicting the two half reactions of the TGT ping-pong mechanism in eukaryotes and bacteria. Catalytic amino acids are shown as present in H. sapiens TGT. However, equivalent amino acids are present in bacterial TGT. R=tRNA, R_1=leucine side chain, R_2=hydrogen (preQ$_1$) or cyclopentenediol (queuine). After excision of guanine 34 completes the first half reaction, an exchange of the free base bound at the active site can occur. During this exchange, the L230-S231 peptide flips to accept a hydrogen bond from the primary/secondary amine of preQ$_1$/queuine. The reaction scheme also holds true for archaeal TGT with minor differences: The natural substrate of arcTGT is preQ$_0$, thus a cyano group is present in the second half reaction instead of a primary/secondary amine. This causes the equivalent of the L230-S231 peptide to stay in a single orientation in both half-reactions because the equivalent hydrogen bond is formed between the main chain amide and the preQ$_0$ cyano group.

1.4.4   tRNA binding and RNA substrate specificity

While tRNA binding by arcTGT is fully understood, this is not the case for bacterial or eukaryotic TGT. The most valuable piece of information comes from a partial crystal structure showing the interaction between a *Z. mobilis* TGT dimer and a short RNA mimicking the anticodon stem loop of tRNA^{Tyr} [152]. This structure reveals that the anticodon loop is bound in an unusual "zig-zag"-like conformation, in which every other base of the loop is flipped outwards[152]. However, while this conformation is very different from the anticodon conformation found in crystallized tRNA, or tRNA bound to an aminoacyl-tRNA-synthetase, the orientation of nucleotides 33-35 closely matches the stretch of RNA within the active site of archaeal TGT[152,160].

The structure further revealed that U35, which is shared by the substrate G34-U35-N36-tRNAs, is sandwiched between the side chains of K42 and V282 where it forms specific hydrogen bonds to R289, R286 and T285 via its C2 and C4 carbonyls[152]. Specific hydrogen bonds are also formed to U33 (which is shared by all tRNAs), and C32, although the latter is only recognized by a single hydrogen bond to its N3 atom, which does not discriminate against cytidine. A36 only forms hydrogen bonds via its ribose and phosphate, consistent with it being the discriminatory base among the four substrate tRNAs. These interactions are in agreement with earlier biochemical data which established Y32-U33-G34-U35 (where Y = U or C) to be the critical recognition motif of bacterial TGT[174–176].

The anticodon loop is largely stabilized and held in position by the inserted active site helix αB, while the anticodon stem rests atop the adjacent zinc binding domain of the catalytic subunit[152]. The non-catalytic subunit is minimally engaged in binding the small substrate RNA, forming a minor stacking interaction with adenine 38 and coming in close contact to the 5' end of the anticodon stem. However, this last contact, mediated by the βDβEβF sheet of the non-catalytic subunit, holds much potential, because it suggests that more extensive contacts might be formed if a complete tRNA is bound. The *Z. mobilis* βEβEβF sheet contains two positively charged residues (K125 and R132) that are regarded as likely candidates to support binding of the phosphate backbone in the D-arm area[177]. However, to date, no structural information is available for the complete bacTGT-tRNA complex.
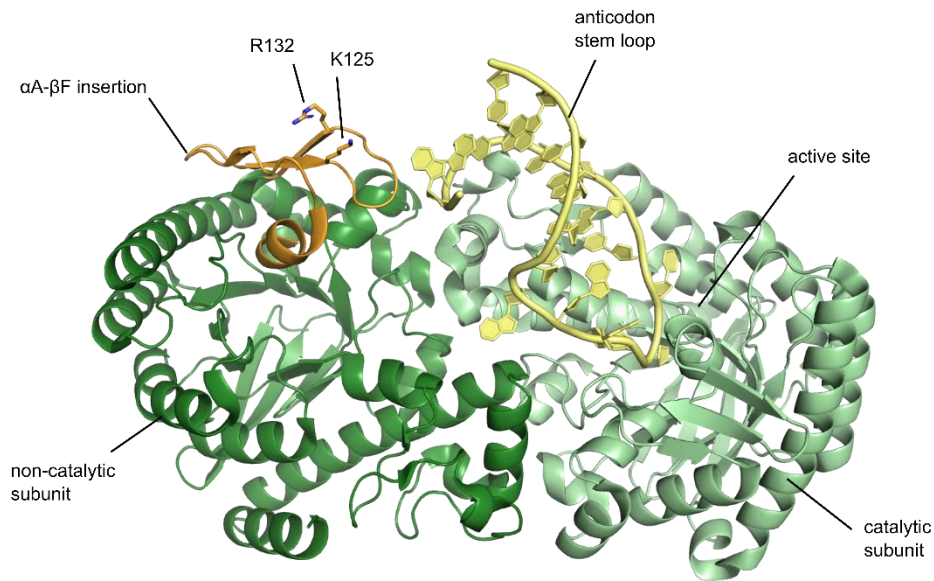
Figure 14: Substrate RNA binding by bacterial TGT

Crystal structure of bacterial TGT bound to a short substrate RNA mimicking the anticodon stem loop (PDB-ID: 1Q2R). The structure shows the atypical conformation of the anticodon loop that is adopted to reach into the active site of the catalytic subunit. The non-catalytic subunit is scarcely involved in binding the short RNA stem loop, however, its αA-βF insertion (orange, including positively charged residues K125 and R132), is in a position where it might contribute to binding a full tRNA.

Prior to this work, information on RNA substrate recognition was even more scarce for eukaryotic TGT. Early experiments on *Xenopus* oocytes suggested that unlike bacterial TGT, which was shown to readily modify stem loop RNA, eukaryotic TGT depended on intact tRNA architecture[174–176,178,179]. However, experiments on bacterial TGT were exclusively conducted *in vitro*, leaving its *in vivo* substrate specificity unclear.

Recently, metabolomic labelling experiments confirmed that tRNA[Asp], tRNA[Tyr], tRNA[His] and tRNA[Asn] are the only targets of Q-modification in *S. pombe*, neonatal mouse liver and human MDA-MB-231 cells[165,170], proving that eukaryotic TGT must be able to discriminate between GUN-tRNAs and suitable YUGU-stem loops of other cellular RNAs.

1.5   Scope of this thesis

This thesis aims to elucidate how tRNA is recognized and bound by eukaryotic TGT and how its binding mode compares to tRNA binding by archaeal and bacterial TGT. The results of this work are summarized in one published manuscript and a second manuscript in preparation.

The first manuscript describes a novel structure of the eukTGT heterodimer in complex with a small RNA mimicking the anticodon stem loop of a substrate tRNA. It describes the dimer interface of eukaryotic TGT and how a substrate RNA is bound by the catalytic subunit. The manuscript further describes putative binding motifs of the non-catalytic subunit and presents biochemical evidence of their involvement in binding of a complete tRNA.

The second manuscript describes the first structure of a TGT·tRNA complex. It provides an analysis of the additional contact sites between tRNA and eukaryotic TGT and biochemical evidence of their significance. Further, it addresses flexibility and disorder in the solution states of the TGT protein and its complex with tRNA and draws conclusions on the specific adaptations of eukaryotic TGT.

Finally, the insights gained by the two novel structures and their accompanying biochemical data are discussed in the broader context of TGT function and evolution, analyzing similarities to bacterial and archaeal TGT as well as the unique characteristics of eukaryotic TGT.

2 STRUCTURE OF HUMAN TGT AND STEM LOOP RNA

This manuscript was originally published in *RNA Biology*:

Structural and functional insights into human tRNA guanine transglycosylase

Katharina Sievers[1], Luisa Welp[2], Henning Urlaub[2,3] & Ralf Ficner[1,4]

Author affiliations:

[1] Department of Molecular Structural Biology, University of Göttingen, Göttingen, Germany

[2] Bioanalytical Mass Spectrometry Group, Max Planck Institute for Multidisciplinary Sciences, Göttingen, Germany

[3] Bioanalytics Group, Institute for Clinical Chemistry, University Medical Center Göttingen, Göttingen, Germany

[4] Cluster of Excellence "Multiscale Bioimaging: From Molecular Machines to Networks of Excitable Cells" (Mbexc), University of Göttingen, Göttingen, Germany

Author contributions:

Experimental design: K.S. and R.F., protein expression and purification: K.S., crystallography, data collection and structure determination: K.S., tRNA purification and complex assembly: K.S., crosslinking, mass spectrometry and crosslinking data analysis: L.W. under supervision by H.U., mutagenesis and biochemical assays: K.S., manuscript writing: K.S., manuscript review and editing: K.S. and R.F.

Taylor & Francis
Taylor & Francis Group

Check for updates

RESEARCH PAPER

Structural and functional insights into human tRNA guanine transglycosylase

Katharina Sievers[a], Luisa Welp[b], Henning Urlaub[b,c], and Ralf Ficner [a,d]

[a]Department of Molecular Structural Biology, University of Göttingen, Göttingen, Germany; [b]Bioanalytical Mass Spectrometry Group, Max Planck Institute for Biophysical Chemistry, Göttingen, Germany; [c]Bioanalytics Group, Institute for Clinical Chemistry, University Medical Center Göttingen, Göttingen, Germany; [d]Cluster of Excellence "Multiscale Bioimaging: From Molecular Machines to Networks of Excitable Cells" (Mbexc), University of Göttingen, Göttingen, Germany

ABSTRACT

The eukaryotic tRNA guanine transglycosylase (TGT) is an RNA modifying enzyme incorporating queuine, a hypermodified guanine derivative, into the tRNAs[Asp,Asn,His,Tyr]. While both subunits of the functional heterodimer have been crystallized individually, much of our understanding of its dimer interface or recognition of a target RNA has been inferred from its more thoroughly studied bacterial homolog. However, since bacterial TGT, by incorporating queuine precursor preQ$_1$, deviates not only in function, but as a homodimer, also in its subunit architecture, any inferences regarding the subunit association of the eukaryotic heterodimer or the significance of its unique catalytically inactive subunit are based on unstable footing. Here, we report the crystal structure of human TGT in its heterodimeric form and in complex with a 25-mer stem loop RNA, enabling detailed analysis of its dimer interface and interaction with a minimal substrate RNA. Based on a model of bound tRNA, we addressed a potential functional role of the catalytically inactive subunit QTRT2 by UV-crosslinking and mutagenesis experiments, identifying the two-stranded βEβF-sheet of the QTRT2 subunit as an additional RNA-binding motif.

Introduction

Queuosine (Q) is an extensively modified nucleoside found at position 34, the wobble position, of tRNA[Asp], tRNAs[Asn], tRNA[His] and tRNA[Tyr], the isoacceptors decoding NAC and NAU codons [1]. In these positions, it is almost universal among both bacteria and eukaryotes.

Queuosine-modification has been shown to regulate translational speed by inverting a tRNA's preference for C- or U-ending synonymous codons, although the direction of this preference seems to depend both on species and codon type [1–5]. In *Shigella flexneri*, a bacterium causing shigellosis, queuosine deficiency leads to a loss of virulence, possibly because its *virF* mRNA is itself Q-modified [6,7]. Among eukaryotes, the presence of queuosine at tRNA position 34 is stimulatory of the methyl transferase Dnmt2 [8,9] and inhibits the 'tRNase' angiogenin [10].

Chemically, queuosine is a guanosine derivative comprised of a 7-deazapurine core and a cyclopentenediol moiety attached via a 7-aminomethyl linker [11,12]. The biosynthesis of queuosine requires eight enzymes in bacteria: Five of them are responsible for converting guanosine 5′-triphosphate (GTP) into the precursor 7-(aminomethyl)-7-deazaguanine (preQ$_1$) [13–19], the enzyme tRNA guanine transglycosylase (TGT) then inserts preQ$_1$ into position 34 of a substrate tRNA, where it replaces the genetically encoded guanine [20,21]. The final two reactions converting preQ$_1$ into queuosine then occur in the context of the tRNA [22–29].

The bacterial TGT enzyme is a homodimer, each subunit is a modified (β/α)$_8$ barrel with multiple insertions, including a zinc-binding domain, which coordinates a single Zn^{2+} ion [30,31]. At the centre of the symmetric dimer interface, two loop-helix motifs form a network of polar interactions with two extensive helix-turn-helix motifs framing the zinc-binding domain of the opposing subunit [32,33]. However, the primary contribution to dimer stability are two aromatic hot spots located in the peripheries of the interface [33,34]. Due to the geometry of the dimer, only one subunit is catalytically active at a time because a tRNA molecule being bound and converted by one subunit blocks the active site of the other by steric hindrance [35,36]. The TGT reaction follows ping-pong kinetics: First, a covalent intermediate is formed between a catalytic aspartate and ribose 34 of the tRNA substrate, leading to the release of free guanine, before preQ$_1$ can take its place in the active site and be incorporated into the tRNA, thus completing the reaction [37].

Although queuosine is found in the tRNAs of most eukaryotes, TGT is the only enzyme of the Q-biosynthesis pathway with a eukaryotic homolog. Instead of producing queuosine and its precursors *de novo*, eukaryotes salvage its free base queuine from gut bacteria or nutritional sources [38–43]. For this reason, the eukaryotic TGT is adapted to insert the fully modified queuine instead of its precursor preQ$_1$ into the tRNA substrate [44–46]. In mammals, queuosine can be further modified by mannosylation or galactosylation [47,48]. Unlike bacterial TGT, eukaryotic TGT is a heterodimer and is comprised of a catalytically active subunit (QTRT1) and a catalytically inactive one (QTRT2) [49,50]. With the exception of a modified binding pocket to

accommodate the bulky cyclopentenediol moiety of queuine, the structure of QTRT1 is very similar to bacterial TGT [51]. The catalytically inactive QTRT2 is homologous and shares the overall $(\beta/\alpha)_8$ fold architecture, but its active site and several other structural elements are degenerate or modified [52].

Since both subunits of the eukaryotic TGT are homologs of the bacterial TGT, it is likely that their dimerization follows its model. However, the lack of a crystal structure has so far impeded thorough understanding of the heterodimer's subunit arrangement.

Detailed knowledge of the dimer is also necessary to understand how TGT enzymes bind their substrate tRNAs. Footprinting data of bacterial TGT suggests interaction mainly with the tRNA's anticodon arm [53]. Experiments with in vitro transcribed minimal RNA constructs confirmed that a stable stem loop with a $Y_{32}U_{33}G_{34}U_{35}$ sequence in a 7-membered loop is sufficient to be recognized and converted by bacterial TGT [54,55]. Such a stem loop RNA was used in the only crystal structure of RNA-bound TGT, which revealed a drastically changed conformation of the anticodon loop and specific recognition of the $U_{33}G_{34}U_{35}$ bases, while the remainder of the RNA was bound independent from sequence via its sugar-phosphate backbone [35]. The only data addressing the substrate specificity of eukaryotic TGT is based on in vivo experiments using a Xenopus oocyte model which suggest that queuine is only incorporated into tRNAs with intact three-dimensional architecture [56,57]. This is in contrast to the minimalist substrate requirements of bacterial TGT and raises the question of whether the eukaryotic TGT·RNA complex differs from the bacterial one.

Here, we present the first crystal structure of human TGT in its heterodimeric and RNA-bound form, serving not only to understand subunit association in eukaryotic TGT but also its interaction with and recognition of a stem loop RNA substrate. In addition, we performed UV-crosslinking and mutagenesis experiments on which we based a model of how a full tRNA is bound by human TGT.

Results

Crystal structure of a human TGT·RNA complex

In preparation for crystallization of a human TGT·RNA complex, we assembled a complex of heterodimeric TGT and a 25-mer stem loop RNA containing a '$Y_{32}U_{33}G_{34}U_{35}$' anticodon loop sequence [35]. Such a stem loop RNA is the known minimal substrate for bacterial TGTs [55] but we verified that in vitro it is also converted by the human TGT (S 1). For crystallization, the complex was assembled in the presence of excess 9-deazaguanine (9dzG) to chemically trap the covalent TGT-RNA intermediate [35].

We obtained rod-shaped crystals from PEG (1500, 3350 or 4000)-based crystallization conditions at pH 5.5–6.5. Crystals appeared after 2–4 days, reached up to 150 μm in size and grew at both 4°C and 20°C. We collected datasets of diffraction images from several crystals using synchrotron radiation and identified the crystals to belong to either space group C2 or P2$_1$.

We obtained initial phases by molecular replacement using the structures of human QTRT1 (PDB-ID: 6H42) and mouse QTRT2 (6FV5) as search models. Although various search combinations were tried, only the heterodimeric form led to drastically improved R-factors during initial refinement. Manual inspection of the resulting electron density revealed a large volume of additional density in which the stem loop RNA was placed (S 2). The best dataset (from crystal grown in 0.1 M MMT pH 6, 25% (w/v) PEG 1500 at 4°C) was refined at a resolution of 2.88 Å and to R-factors of 21.17% (R_{work}) and 24.84% (R_{free}) (Table 1).

The asymmetric unit contains one RNA molecule and two polypeptide chains (QTRT1 and QTRT2), each coordinating a Zn^{2+} ion (Fig. 1A). 9-Deazaguanine (9dzG) is bound to the active site of QTRT1. The first 15 amino acid residues of chain A (QTRT1) are missing, although two of them are remnants of the cleaved N-terminal His-tag and numbering of the model therefore starts with P14. The model is complete at both the QTRT1 C-terminus and the QTRT2 N-terminus, and only the very last residue (S415) is missing from the QTRT2 C-terminus. Other areas of missing density will be discussed below.

Both subunits in this new structure of RNA-bound human TGT (hTGT) have the fold that is characteristic for TGT proteins and which consists of a central $(\beta/\alpha)_8$ barrel with several insertions, including a zinc-binding domain. For this reason, we have adapted the established nomenclature [35,52] to refer to their secondary structure elements (See S 3 for a topology diagram). There is continuous density linking ribose 34 and the catalytic aspartate 279 while the density for 9dzG has no connection to the RNA (Fig. 1B). It is therefore clear that the structure does indeed represent the covalent TGT-RNA intermediate.

Table 1. Data collection and refinement statistics

Data collection	
X-ray source	Synchrotron (BESSY II, MX 14.1)
Wavelength (Å)	0.9184
Resolution (Å)	50.00-2.88
Space group	C121
a, b, c (Å)	161.84, 56.96, 102.96
α, β, γ (°)	90.0, 124.93, 90.0
Wilson B (Å^2)	67.81
R_{meas} (%)[1]	11.6 (112.1)
I/σ (I)[1]	13.83 (1.81)
CC$_{1/2}$[1]	99.9 (87.6)
Completeness (%)[1]	98.9 (99.8)
Redundancy	6.7
Refinement	
Resolution (Å)	42.20-2.88
No. of reflections	16550
R_{work} (%)	21.17
R_{free} (%)	24.84
Mean B value (Å^2)	88.54
Protein	88.78
RNA	86.24
R.m.s. deviations	
Bonds (Å)	0.008
Angles (°)	1.414
Ramachandran favored (%)	96.21
Ramachandran outliers (%)	0.00
Rotamer outliers (%)	4.6
Clash score	7.91

[1]Numbers in parentheses are for the highest resolution shell.
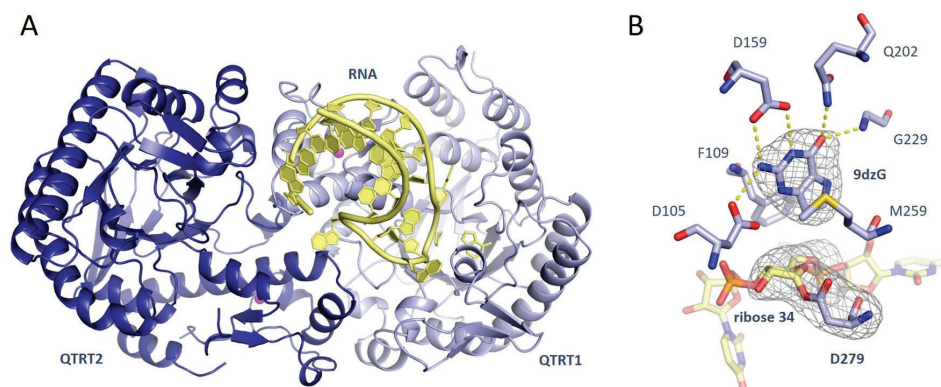
Figure 1. Crystal structure of human TGT with covalently bound RNA.
A: Structural overview of the heterodimeric TGT from *Homo sapiens* as a covalent intermediate with a 25-mer RNA stem loop. The catalytic subunit (QTRT1) is shown in light blue, the non-catalytic subunit (QTRT2) is shown in dark blue, the RNA stem loop is shown in yellow. The 9dzG molecule bound at the active site is shown in yellow stick representation. The two Zn^{2+} ions are depicted as pink spheres. **B**: Active site of human TGT with ribose 34 covalently bound to catalytic aspartate 279 and 9dzG coordinated by D105, F109, D159, Q202, G229 and M259. An mFo-DFc electron density omit map for D279, ribose 34 and 9dzG contoured at σ = 5.0 is shown as a grey mesh.
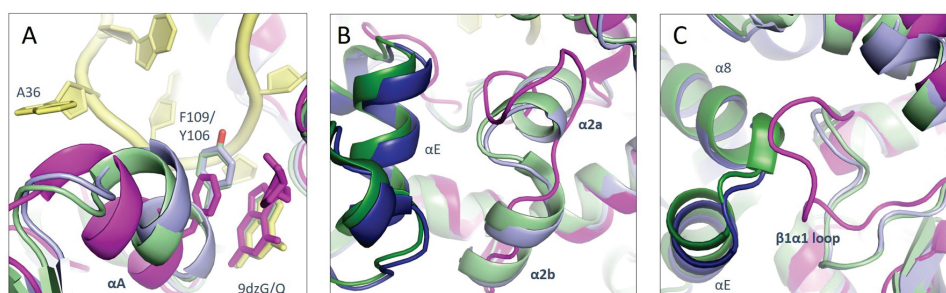
Figure 2. Conformational rearrangements of hTGT.
Comparison of hTGT structure (blue and yellow) with queuine-bound QTRT1 (PDB-ID: 6H45, depicted in pink) and RNA-bound bacterial TGT (PDB-ID: 1Q2R, depicted in green). **A**: Conformational shift of QTRT1 helix αA and equivalent residues F109/Y106 (human/*Zymomonas mobilis*) upon RNA binding. **B**: Formation of QTRT1 helices α2a and α2b upon dimerization. **C**: Re-orientation of QTRT1 β1α1 loop at dimer interface and interaction with helices αE and α8 of the opposing subunit (QTRT2/bacTGT).

The 9dzG base co-locates with that in the bacterial structure of a covalent RNA intermediate (PDB-ID: 1Q2R) and the 7-deazaguanine moiety in the structure of human QTRT1 soaked with queuine (6H45) [35,51]. The surrounding active site is largely identical to the available QTRT1 structures 6H42 and 6H45 which represent its apo and queuine-bound form. One of the few differences between these two structures is the conformation of S231 and G232 which are flipped to accommodate queuine's cyclopentenediol moiety in 6H45. In the RNA-bound hTGT structure, the G/Q binding pocket is occupied by 9dzG, which lacks the cyclopentenediol extension, and, while showing some flexibility, S231 and G232 occupy positions most similar to the apo structure.

Other parts of the QTRT1 subunit have more severely altered conformations compared to the apo structure: Helix αA (108–113), which is located near the active site, is shifted closer to the 9dzG base bound at the catalytic centre (Fig. 2A). This new position is identical to that occupied by the equivalent helix in the structure of RNA-bound TGT from *Zymomonas mobilis* (1Q2R), while in RNA-free structures of the bacterial homodimer (e.g. 1PUD), helix αA co-locates with those of the human QTRT1 subunit (6H42, 6H45) [30,35,51], illustrating that this change is caused by binding of the RNA rather than dimerization. The position of adenine 36 right at the end of helix αA deems it responsible for its displacement. Within the helix, residues Q110 and S113 form hydrogen bonds with the phosphate backbone of nucleotides 35 to 36. Helix αA also contains F109 which is partly responsible for stabilizing the base in the active site via pi-stacking interaction.

Amino acid residues 74–89, unstructured in the non-dimeric QTRT1 structures, form two helices α2a and α2b in the structure of hTGT (Fig. 2B). Despite being in close vicinity to U35, this change seems to be a result of heterodimerization as equivalent helices are present not only in the bacterial RNA-bound structures but also in structures of the RNA-free bacterial homodimer [30,35].
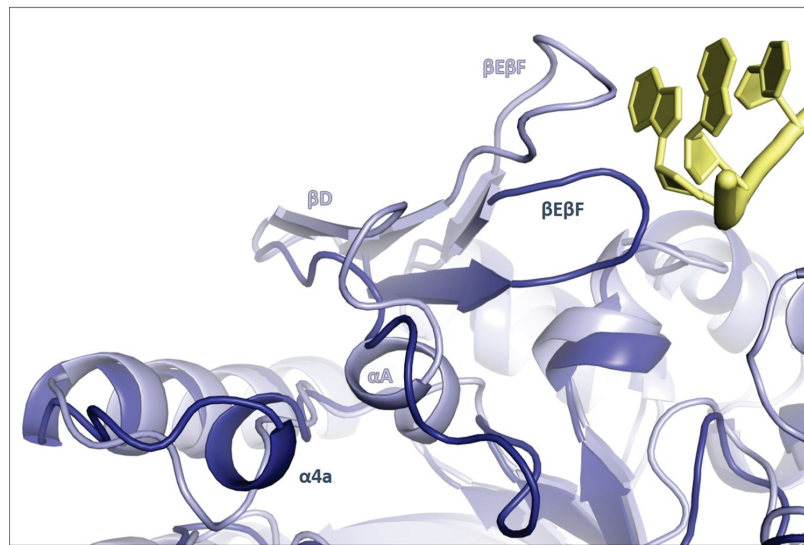
Figure 3. Structural differences between QTRT1 and QTRT2.
The comparison of QTRT2 (dark blue) with superimposed QTRT1 (light blue) reveals altered secondary structure elements in the region near the 5′ end of the stem loop RNA (yellow). QTRT2 secondary structure elements are labelled in dark blue, QTRT1 elements are labelled in light blue.

Similarly, the QTRT1 loop-helix motif composed of β1α1-loop [47–58] and preceding helix α1 [59–65] take a different course in the hTGT structure (Fig. 2C) while the sharply angled turn between helices αE and α8 (327–335 and 339–366) of the same subunit is slightly twisted. Both of these motifs are part of the dimer interface and occupy identical positions in structures of the bacterial dimer [30]. The altered position of helix αE also causes a small change in the neighbouring loop containing residues 301–311 which is also identical to that in bacterial dimers [30,35]. This loop contains several positively charged amino acid residues and acts as a platform for the backbone of nucleotides 29–32.

The new hTGT structure is the first crystallographic representation of the human non-catalytic subunit QTRT2. However, upon inspection it immediately becomes clear that it is extremely similar the published structure of murine QTRT2 (6FV5) [52]. Like the mouse protein, human QTRT2 overall resembles bacterial TGT or the catalytically active QTRT1, but the would-be active site region appears degenerate, as key residues and secondary structure elements are changed or missing.

Helix αA and β-sheet βD are absent in QTRT2 and the corresponding stretch encompassing residues 108 to 121 is without a secondary structure (Fig. 3). The course of this unfolded stretch partly diverges from that in the mouse QTRT2 structure (residues 101 to 107) and appears highly flexible as indicated by high atomic displacement parameters (ADPs). The reason for this is an unfavourable interaction with the equally flexible unpaired adenine 25 of a symmetry mate which is stacking with Y107 but directly interferes with the course of the preceding main chain as it is seen in the mouse structure (S 4). The

subsequent βEβF sheet (residues 113–124), two-stranded due to the missing βD, is angled much closer to the centre of the subunit in QTRT2 (Fig. 3). Although it too exhibits locally increased ADPs, the position of the motif is identical to that of the mouse structure.

The structure of hTGT also confirms the presence of an additional small helix spanning residues 148–151 that we named α4a (Fig. 3). The area is rich in positively charged amino acid residues and makes crystal contact with the phosphate backbone of a symmetry related RNA (S 5) which forces it into a more indented conformation compared to the murine structure.

Finally, QTRT2 has an insertion of about 30 amino acid residues, however, as in the mouse structure, electron density for this insertion spanning residues 291 to 326 is completely missing, and we thus did not include it in model building.

Changes relating to heterodimerization are more subtle in QTRT2 compared to QTRT1 because the previously published mouse structure is that of a similarly configured homodimer [52]. Part of the β1α1-loop (residues 37 to 42) is shifted towards the interface to engage with QTRT1 residues 337–339. This also entails a minor change of the preceding α1 helix [42–53]. Similarly, the interface region 86–92 adopts a slightly altered conformation and the helix-turn-helix motif formed by helices αE and α8 of this subunit (residues 361–400) also shows a minor twist.

The dimer interface of QTRT1 and QTRT2

The structure of hTGT is the first crystallographic account of the dimer interface formed between eukaryotic QTRT1 and QTRT2. Dimerization mainly occurs via the two zinc-binding domains of the subunits and follows the overall architecture
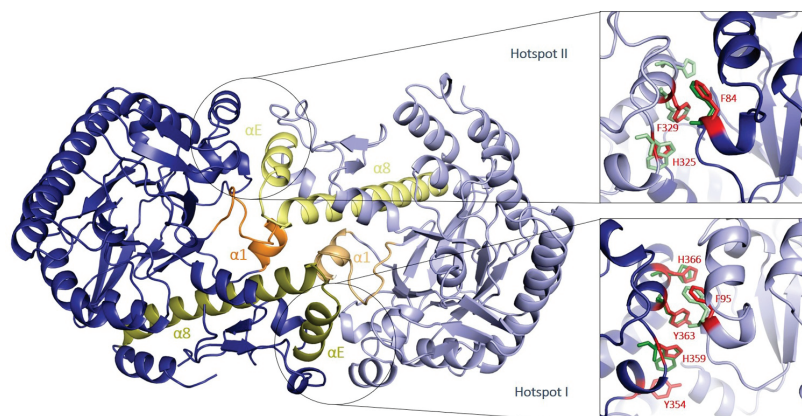
Figure 4. Dimer interface of QTRT1 and QTRT2.
The dimer interface of QTRT1 (light blue) and QTRT2 (dark blue) is primarily formed by two helix-turn-helix motifs (pale and dark yellow) interacting with two loop-helix motifs (light and dark orange) of the opposing subunit. The peripheries of the interface contain two aromatic hotspots. Hot spot residues are shown in red, corresponding residues from *Zymomonas mobilis* are shown in green for comparison.

of the bacterial homodimer: The interface is formed by two extensive helix-turn-helix motifs that consist of helices αE and α8 of both subunits interacting with the two loop-helix motifs comprised of the α1 helices and preceding β1α1 loops (Fig. 4).

The interface of hTGT also includes equivalents for the two characteristic aromatic hot spots of the bacterial homodimer [33,34]. Being a heterodimer, these two hot spots are not identical in eukaryotic TGT and will henceforth be referred to as hot spot (HS) I and II (Fig. 4).

HSI is comprised of QTRT1 F95 and QTRT2 residues H366, Y363 and H359. It thus has direct equivalents for the *Z. mobilis* residues F92, H333 and Y330. H359 occupies the position of the five-ring of *Z. mobilis* W326. The loss in hydrophobic area due to this change is compensated by the extension of the hot spot by an additional tyrosine (Y354).

HSII appears degenerate: Only QTRT1 F84 is conserved, F329 and H325 take the place of *Z. mobilis* Y330 and W326. There is no additional aromatic residue to compensate for the loss of the bulky tryptophan and *Z. mobilis* H333 is replaced by an alanine.

The two aromatic hot spots are located at the outer edges of the dimer interface, with most residues of the feature being provided by the two αE helices. The interior of the interface is characterized by a network of hydrogen bonds and polar interactions. Some of these interactions are formed by the hot spot residues themselves: In HSI, H366 and Y363 bond to the main chain carbonyls of Q51 and A52, consistent with their bacterial homologs. Because the equivalent residues (A332 and F329) have non-polar side chains, these interactions are lost in HSII.

In bacterial TGT, a key feature of the interface is the salt bridge between a glutamate sitting at the very apex of the helix-turn-helix motif and a lysine of the facing β1α1 loop (E339 and K52 in *Z. mobilis*). In human TGT, this interaction is conserved in the interface half containing HSI and formed between QTRT2 E372 and QTRT1 K55, although the terminal amide of QTRT1 Q51 is located at almost equal distance and

might provide an additional hydrogen bond with E372. In the interface half of HSII, the apex region of the helix-turn-helix motif has a more extended conformation. As a result, an aspartate (D337) instead of a glutamate is sufficient to bond with K38 located in the N-terminal region of the QTRT2 β1α1 loop. This lysine is not the equivalent of *Z. mobilis* residue K52, instead it replaces the Q51 found in the first half of the interface. In addition, the interaction with the QTRT2 β1α1 loop in this second half of the interface is strengthened by QTRT1 N338 binding to several of its backbone functionalities as well as QTRT1 T339 bonding with QTRT2 H44.

Other interactions contributing to the polar interactions of the interface are QTRT2 Y354 (the additional tyrosine of HSI) bonding to the main-chain amide of QTRT1 E60, QTRT2 N358 binding QTRT1 N97 in the first half and QTRT1 H325 (part of HSII) bonding to QTRT2 H47 in the second half of the interface.

In the centre of the dimer interface, the two α1 helices of the subunits interact directly as QTRT1 E60 forms hydrogen bonds with the QTRT2 sidechains of H48 and N52.

Active site and binding of the RNA stem loop

The binding of the stem loop RNA substrate by human TGT appears to follow the model of the previously published bacterial complex [35]. The RNA is folded into a stem loop that is comprised of a stem of six helically stacked base pairs, a 5′ overhang of one base and a loop of seven unpaired nucleotides. The helical stem rests on the zinc-binding domain of the QTRT1 subunit, while the loop points into the C-terminal face of its (β/α)$_8$ barrel core where the active site is located. As such, the RNA is bound almost exclusively by the QTRT1 subunit.

As reported for the bacterial RNA-complex, the loop region of the RNA adopts an unusual conformation which is quite different from that of the anticodon loop of a free tRNA: While the first unpaired base, C32, is roughly in plane with
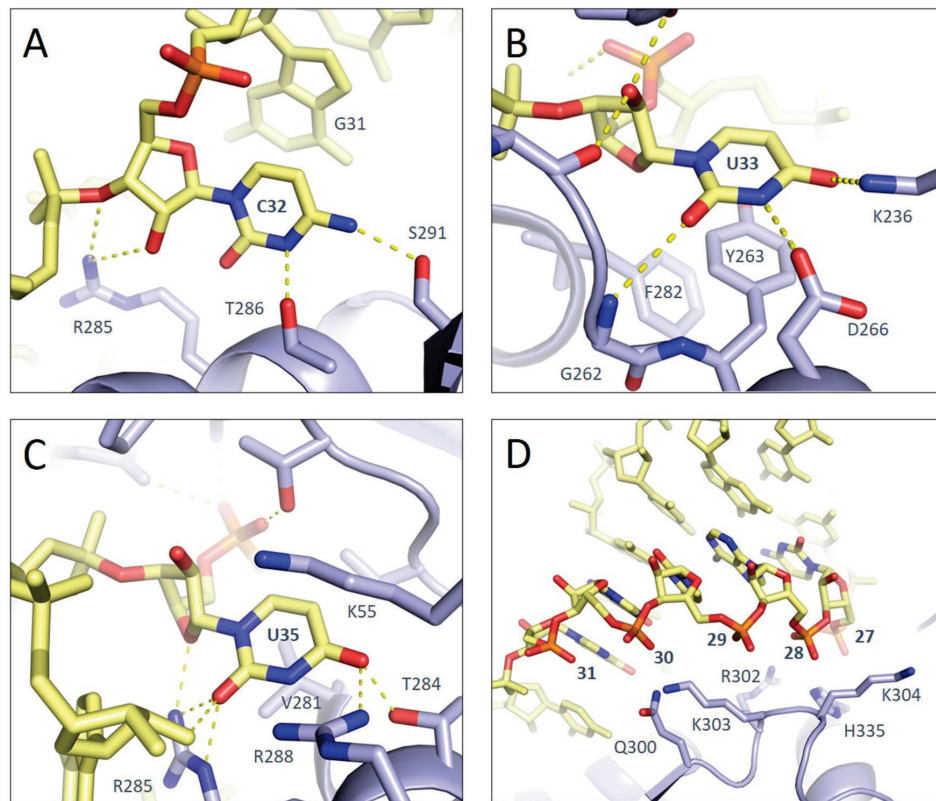
Figure 5. Sequence-specific and sequence-independent binding of RNA substrate.

RNA nucleotides are depicted in yellow stick representation, QTRT1 is depicted as cartoon and sticks in light blue. **A**: C32 forms weakly sequence-specific polar contacts with T286 and S291. **B**: U33 is stacked by Y263 and F282 and recognized specifically by K236, D266 and G262. **C**: C35 is stabilized between K55 and V281 and forms sequence-specific contacts with T284, R288 and R285. **D**: The helical stem of the RNA is bound sequence-independently via its negatively charged phosphate backbone. Nucleotides 27–31 (numbered) interact with positively charged QTRT1 residues Q300, K303, R302, H335 and K304.

the helical stacking of the stem, U33 is flipped out [35]. Nucleotides 35 to 38 are in a zig-zag conformation in which A36 and A38 are likewise flipped to the outside of the loop.

Knowing that bacterial TGTs recognize their RNA substrate by only the bases of the $Y_{32}U_{33}G_{34}U_{35}$ motif, it is of particular interest to see which bases of the loop are recognized in a sequence-specific manner by the human TGT. The first loop nucleotide, C32, is positioned only roughly in plane with the preceding helically stacked bases. It is stabilized in this position by forming a hydrogen bond with T286 and a polar interaction with S291 via its N3 and N4 nitrogens (Fig. 5A). This differs from the bacterial structure, where C32 is in plane with the helix stack and S291 is replaced by a glutamine.

U33 is stabilized in its flipped conformation via pi-stacking interaction with Y263, which is in turn stacked to F282. It accepts hydrogen bonds from K236 and the main-chain amide of G262 via its O2 and O4 carbonyl functions and forms an additional hydrogen bond with D266 via its N3 nitrogen (Fig. 5B). With the exception of K236, which does not exist in the bacterial protein, this way of binding is

conserved, although the base is stabilized by hydrophobic packing with a lysine, not a tyrosine, in *Z. mobilis*.

The remnant ribose of G34 is covalently bound to D279 via its C1 atom, thus representing the covalent RNA-protein intermediate that is the result of the first half of the TGT reaction mechanism (Fig. 1B). D297 is held in place by its second terminal oxygen accepting a hydrogen bond from Y257. The C1 of ribose 34 is located at a distance of 4.2 Å from the C9 atom of the 9dzG base bound in the G/Q binding pocket, illustrating that a conformational change would be necessary for the formation of the new covalent bond and completion of the base exchange. The 9dzG base is stacked between M259 and F109, which is rotated slightly out of plane by the RNA-induced conformational change of αA. Specific recognition of the deazapurine occurs through several hydrogen bonds with its Watson–Crick Edge: The second catalytic aspartate D105 accepts a hydrogen bond from the N2, D159 accepts two more hydrogen bonds from the N1 and N2 and the O6 forms two hydrogen bonds with Q202 and the main-chain amine of G229.

U35 is stacked between K55 and V281. It forms specific contacts by its O4 accepting two hydrogen bonds from T284 and R288 and O2 accepting hydrogen bonds from R285, which also forms a second bond with the ribose O4′ of the same nucleotide (Fig. 5C). All of these interactions are conserved and have direct equivalents in the *Z. mobilis* structure.

While the flipped base A36 does not form any close contacts, A37 is stacked by R285 and R288 forms a hydrogen bond with O2′. A38 is the only base that is bound by two residues of the QTRT2 subunit: It is stabilized via hydrophobic interaction with L373 and polar interaction with N371. In the *Z. mobilis* structure, the stabilization of the base is achieved by an isoleucine at the same position. The polar interaction is formed with a main-chain carbonyl, but from both structures it seems unlikely that this single interaction is sufficient for sequence-specific recognition, especially in hTGT where the sidechain carbonyl is not at all held in position by any neighbouring residues.

Finally, QTRT1 F289 forms a stacking interaction with C39 thus holding it in position. As C39 and G31 form the first base pair of the stem, this interaction also serves to stabilize the helical stack. Unlike the loop, the helical stem is bound in a manner that is completely independent from sequence, mostly via its negatively charged phosphate backbone.

Due to the orientation of the stem loop, only the strand that includes nucleotides 26–30 makes contact with the protein, while the opposite strand (nucleotides 39–44) is positioned 'in mid-air'. The phosphate 30 forms two hydrogen bonds with K303 and Q300. The remaining phosphates of nucleotides 29–26 do not form dedicated hydrogen bonds. However, several positively charged or polar residues are located in the near vicinity (R302, K304 and H335), the closest at a distance of less than 5 Å (Fig. 5D).

Potential sites for tRNA binding

Inspection of the surface electrostatics of the heterodimer reveals that the RNA binding face exhibits two well-defined positively charged patches (Fig. 6). The first one extends from the active site to the zinc-binding domain of the QTRT1 subunit and represents the primary-binding site of the stem loop RNA. A second positively charged patch is located on the QTRT2 subunit, which is mostly formed by helices α4a and α4b. We prepared a model of the human tRNA^{Asp} based on the published structure of its yeast equivalent (PDB-ID: 2TRA) and superimposed it to the helical stem of the RNA in the complex structure (S 6). In the resulting model, the acceptor stem of the aligned tRNA comes in close vicinity to the positively charged patch on the surface of QTRT2, suggesting that this patch binds the acceptor stem of a substrate tRNA via its negatively charged phosphate backbone.

According to the superimposed model, the two-stranded βEβF-sheet of the QTRT2 subunit also contributes to binding of the tRNA: Due to its complementary shape it is able to protrude into the groove that is formed by the tRNA's D-arm, where it is well positioned to form hydrogen bonds and Van der Waals interactions (Fig. 8A).

Analysis of UV-crosslinks of a TGT·tRNA complex

Aiming to gain experimental evidence for the involvement of the QTRT2 subunit in binding of a complete tRNA, we performed UV-induced crosslinking of a TGT·tRNA complex and analysed the crosslinked peptides using mass spectrometry. We identified 14 crosslinked peptides representing 12 unique crosslinks. However, many of the rarer crosslinks (<5 crosslink spectrum matches (CSMs)/replicate) are in locations that are biologically not plausible, such as the rear face of the dimer with respect to its active site. For that reason, we considered only those crosslinks with more than 5 CSMs in each replicate. We also excluded the two crosslinks at the QTRT1 and QTRT2 N-termini because we consider them to be artefacts caused by increased terminal flexibility. The remaining crosslinks involve QTRT1 residues G232, F289, Y131, K303 or 304 and QTRT2 residue W116 (Table 2). While the crosslinked QTRT1 residues are located around the crystallographically identified binding site of the stem loop RNA, QTRT2 W116 confirms the involvement of the βEβF-sheet of the non-catalytic subunit (Fig. 7). It was
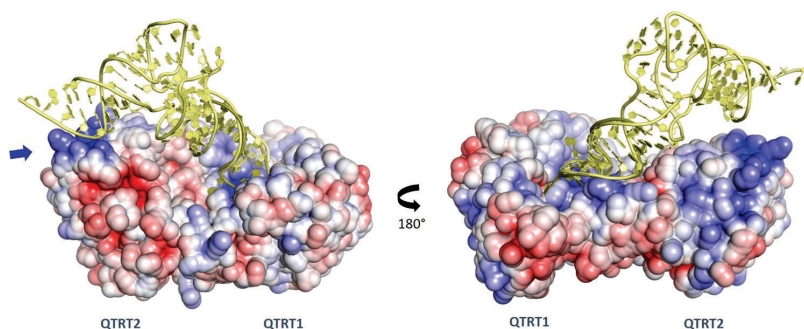
Figure 6. Surface electrostatics of the hTGT heterodimer and superimposed model of tRNA^{Asp}.
Two different views on the TGT heterodimer surface electrostatics (blue = positive charge, red = negative charge) are depicted. Two positively charged areas are visible: The first corresponds to the primary-binding site of the crystallized stem loop RNA (dark yellow), the second is located on the surface of the QTRT2 subunit (indicated by a blue arrow). A model of human tRNA^{Asp} (light yellow) superimposed to the stem loop RNA comes in close contact to the positively charged area of QTRT2 via its acceptor stem.
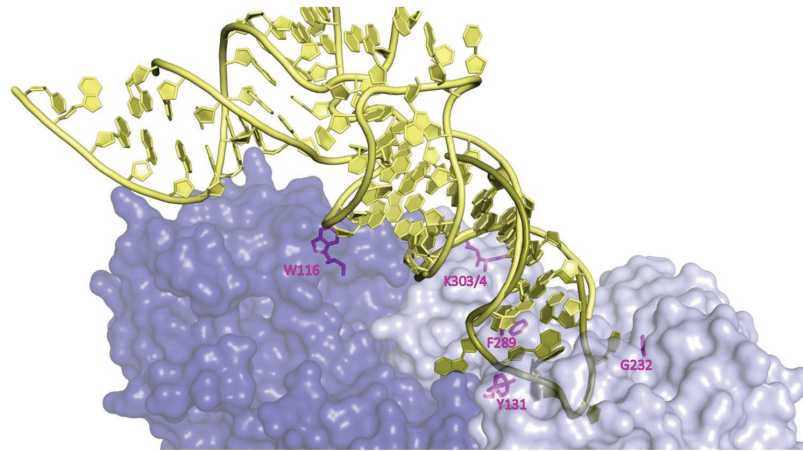
Figure 7. UV-Crosslinking of a TGT·tRNA complex.
Surface representation of QTRT1 (light blue) and QTRT2 (dark blue) with amino acid residues involved in crosslinks with tRNA^{Asp} shown in magenta. The crystallized stem loop RNA is shown in dark yellow, a superimposed tRNA^{Asp} model is shown in pale yellow.
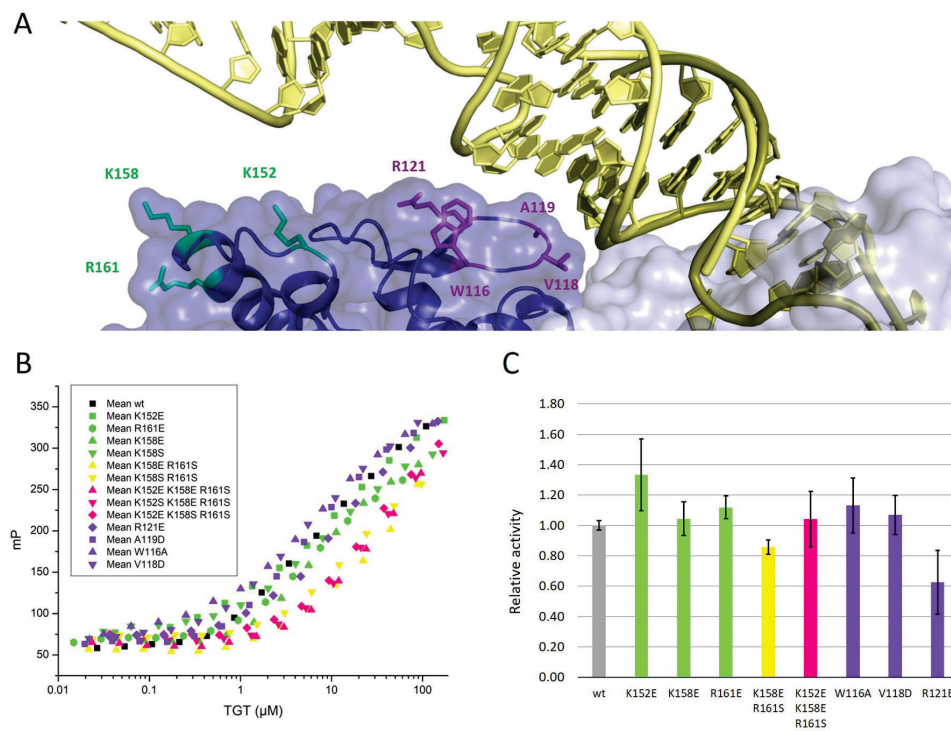
Figure 8. Mutagenesis of potential tRNA binding regions.
A: Surface representation of QTRT1 (light blue) and QTRT2 (dark blue) with stem-loop RNA (dark yellow) and a superimposed tRNA^{Asp} model (pale yellow). Amino acid residues that underwent mutagenesis are shown as coloured stick representations (purple: βEβF-sheet, green: positively charged patch). **B**: Fluorescence polarization-based affinity assay with TGT mutants and labelled tRNA^{Asp}. Individual points represent the average of three triplicates, error bars were omitted for clarity. K_D values and their errors derived from each curve are listed in Table 3. **C**: Relative Q-incorporation activity of TGT mutants from three replicates with standard deviations shown as error bars.

Table 2. UV-crosslinking results

Peptide sequence[1]	CSMs in each replicate			>5	Position	Crosslinked base
	1	2	3			
MkLSLTK	11	19	16	Yes	QTRT2 K2	C
SVSVwSVAGR	11	18	13	Yes	QTRT2 W116	U
DVPGFAIGGLSgGESK	12	9	17	Yes	QTRT1 G232	U (C)[2]
gPMAGAATQASLESAPR	14	15	8	Yes	QTRT1 G-2	C
SPyDGNETLLSPEK	12	12	11	Yes	QTRT1 Y131	U
fGSALVPTGNLQLR	6	11	6	Yes	QTRT1 F289	C (U)[2]
FRSPyDGNETLLSPEK	4	7	6	No	QTRT1 Y131	U
kkVFEK	6	5	5	No	QTRT1 K303/4	C
kYQEDFNPLVR	5	6	5	No	QTRT2 K339	C
kVFEK	5	4	5	No	QTRT1 K304	C
IkNLGK	5	4	4	No	QTRT2 K18	C
LLSSVTAELPEDkPR	2	4	4	No	QTRT2 K247	C
LAQLkELIHR	1	4	5	No	QTRT2 K407	C
SDkLAQLK	2	3	4	No	QTRT2 K402	C

[1]Lower case letter represents crosslinked amino acid residue.
[2]Bases in parentheses represent a less abundant sub-population.

crosslinked exclusively to a uracil, corroborating the nearby placement of U11 in the superimposed tRNA model.

Mutagenesis of putative QTRT2 binding regions

To further investigate the involvement of the two suspected tRNA binding regions of the QTRT2 subunit, the βEβF-sheet and the positively charged patch involving helices α4a and α4b, we created a series of QTRT2 mutants. For the positively charged patch, we chose K152, K158 and R161 because they are solvent-exposed and do not interact with neighbouring residues in the hTGT structure and created single, double and triple mutants. The charge of each residue was either neutralized (mutation to serine) or inversed (mutation to glutamate), however, the combination of K158E and R161E resulted in presumably misfolded protein that could not be purified.

We tested the affinity with fluorescently labelled tRNA^{Asp} and performed activity tests with each of the remaining mutants (Fig. 8). The affinity of the K158E and R161E single mutants was identical to that of the wildtype, for which we determined a K_D of 7.91 ± 0.86 μM (Table 3). The K152E and K158S mutants exhibited marginally reduced affinity with a less than 2-fold increased experimental K_D (12.51 ± 1.88 μM, 13.28 ± 3.54 μM). The binding curves of the K158S R161S and K158E R161S double mutants and K152E K158E R161S, K152S K158E R161S and K152E K158S R161S triple mutants were all noticeably shifted (Fig. 8B). Since these curves do not reach saturation, they could not be fitted, but upon visual inspection it is clear that the K_D of these mutants is well above 20 μM.

For the βEβF-sheet, we created the following single-point mutations: R121E, A119D, V118D and W116A. Mutants V118D and W116A were indistinguishable from the wildtype in affinity tests, the experimental K_D of the A119D mutant was marginally reduced (5.48 ± 0.42 μM). In contrast, the R121E mutation caused a 4-fold increased K_D (16.00 ± 1.09 μM).

We also determined the relative activity of some of the mutants (Fig. 8C). Despite the observed reduction of affinity of the double and triple mutants, the relative activity of all mutants of the positively charged patch deviated by less than 30% from that of the wildtype: The K158E R161S double mutant had activity reduced to 80% of that of the wildtype and the activity of the K152E single mutant was 1.3-fold increased, while all other mutants of the positively charged patch fell somewhere in between. The βEβF mutants W116A and V118D too had wildtype-like activity. With the relative activity reduced to 60% of the wildtype activity, the R121E mutation had the most drastic effect.

Discussion

Despite half a century of research on tRNA guanine transglycosylase (TGT), our understanding of eukaryotic TGT especially is still fragmentary. In this publication, we presented the first crystal structure of a eukaryotic TGT in its heterodimeric and RNA-bound form. With its aid, we were able to gain a thorough grasp of the functional elements that make up the interface of its two subunits. We were also able to analyse how a stem loop RNA is bound by eukaryotic TGT, make a conjecture on the binding of a full tRNA and evaluate whether and how it differs from bacterial TGT.

Comparing the subunits of the heterodimeric structure to the previously published apo-structures of the individual subunits, we saw several changes in conformation. The catalytic subunit QTRT1 was previously crystallized as an unusual homodimer in which both chains are aligned along their $(\beta/\alpha)_8$ barrels, an arrangement considered a crystallographic artefact by the authors [51]. QTRT2 was also crystallized as a homodimer, but it was configured similarly to the hTGT heterodimer. Unsurprisingly, the differences we observe in heterodimeric hTGT therefore mostly involve the regions of the dimer interface. However, most of these changes, such as the formation of QTRT1 helices α2a and α2b, are in line with structures of the bacterial TGT dimer. Like in bacterial TGT, the dimer association in eukaryotic TGT seems to be largely based on the interaction of its α1 helix and preceding β1α1 loop with a helix-turn-helix motif formed by helices αE and α8. Since the eukaryotic dimer interface exhibits a pseudo 2-fold symmetry, both of these elements occur twice. Looking at the two halves of the interface, it becomes clear

that they are unevenly conserved: The first half (involving the helix-turn-helix motif of QTRT2 and the loop-helix motif of QTRT1) is very similar to its bacterial homolog, including a salt bridge at the apex of the helix-turn-helix motif and the configuration of the aromatic hot spot which is thought to be the major contributor to dimer stability in bacterial TGT. In the second half, the interaction is stabilized by alternative bonds and the extent of the aromatic hot spot is significantly reduced. Interestingly, this reduction mostly effects the QTRT1 subunit, which contributes only three aromatic residues to the two hotspots, whereas QTRT2 contributes five. This might be the explanation why QTRT2 has previously been observed to form homodimers in solution, while QTRT1 has not [52].

The altered conformation of QTRT1 helix αA near the active site is the only major change that seems to be caused by the binding of the RNA substrate. It is shared only by the structures of the RNA-bound bacterial TGT [35]. The conformational change of αA causes a rotation of F109, which stacks the (deaza)purine in the active site and, in its rotated conformation, allows it to act like a lid to its binding pocket. This might be a mechanism of induced fit serving to shield the active site from water access and facilitating the nucleophilic attacks on ribose 34. While it is unclear whether the αA shift is induced by initial binding of the tRNA or whether it is the result of the conformational changes that occur during the formation of the covalent RNA-TGT intermediate, the former appears more likely: An equivalent αA conformation is also observed in the post-catalytic state of bacterial TGT bound to preQ$_1$ $_{34}$-RNA, which is likely similar to the initial G$_{34}$-tRNA substrate complex [35]. In addition, conformational changes of the RNA occurring between the covalent intermediate and the formation of the post-catalytic state are limited to nucleotide 34 while the adenine at position 36, which is likely responsible for the shift of αA, occupies identical positions [35].

Recently, a sequential bi–bi mechanism in which queuine is bound before formation of an RNA-complex has been suggested for eukaryotic TGT instead of a ping-pong mechanism [58]. However, from the structure of hTGT it is clear that one base only, guanine 34 or queuine, can simultaneously reside at the active site. Even if, as the authors of the cited work suggest, queuine initially binds to a secondary binding site outside of the catalytic centre, a second queuine molecule

would still need to bind to the active site after the freed guanine is released, which is why we continue to argue for a conserved ping-pong mechanism.

The RNA loop entering the active site groove in the hTGT complex structure has the same unusual conformation as described for the bacterial structure [35]. Nucleotides 33 and 35 are recognized by specific interactions that are largely the same as in the bacterial complex. C32 forms contacts with two sidechain hydroxyls, which likely could also bind a uracil in this position. So while we could show that eukaryotic TGT does not necessarily require an intact tRNA for its substrate, the hTGT structure confirms the previously shown importance of the Y$_{32}$U$_{33}$G$_{34}$U$_{35}$ sequence for recognition [56,57].

All nucleotides of the helical stem are bound via their phosphate backbone only, confirming that its sequence is unimportant for recognition. The helix is angled slightly differently to the bacterial structure. This might be caused by crystal contacts in either structure (in 1Q2R the helix stacks with its symmetry mate to form an positively charged region of QTRT2) or be related to the different angle of the βEβF motif of the QTRT2 subunit. This motif is part of the second large insertion in the (β/α)$_8$ barrel fold and has already been identified as a potential contributor to tRNA binding in 2007 [59]. Back then, it was not yet known that eukaryotic TGT is a heterodimer of homologs, yet, the model based on the bacterial homodimer still holds up: The insertion comprised of residues 96–139 is heavily modified in QTRT2 compared to both QTRT1 and bacterial TGT, but while helix αA and subsequent βD strand are replaced by an unstructured stretch of amino acid residues, the two-stranded βEβF-sheet is conserved. By superimposing a model of human tRNA^{Asp} to the stem loop RNA, we discovered that the motif is shaped perfectly for protruding into the groove formed by the tRNA's D-arm. UV-induced crosslinking of a TGT·tRNA complex confirmed the involvement of the βEβF motif. We created several mutants and showed that its R121E mutant has both decreased affinity with labelled tRNA^{Asp} and reduced relative activity. Other mutants based on the motif were identical to the wildtype in these respects, however, this might either be due to the high flexibility in this area, allowing for the mutated residues to bend away from the RNA or because the previously hydrophobic interactions are replaced by polar contacts with its backbone.

The αA helix that is missing in QTRT2 is part of the active site in QTRT1 and bacterial TGT. Being a homodimer, it is also present in the noncatalytic subunit of the bacterial dimer, as the evolutionary pressure to keep the active site conserved likely much outweighs any potential benefits that might arise from optimizing the αA-βF insertion for tRNA binding. Through evolution of a noncatalytic homolog and the eukaryotic heterodimer, the insertion's function at the active site is decoupled from its role in tRNA binding, thus elevating this evolutionary pressure. Through the replacement of αA and βD with an unstructured loop, the now two-stranded βEβF-sheet is angled much less steeply than it is in bacteria, a conformation that is possibly more favourable for reaching into the tRNA's D-arm groove.

Table 3. Binding affinites of TGT mutants

TGT construct	Experimental K$_D$ (μM)
wildtype	7.91 ± 0.86
QTRT2 K152E	12.51 ± 1.88
QTRT2 K158S	13.28 ± 3.54
QTRT2 K158E	7.83 ± 0.70
QTRT2 R161E	7.81 ± 1.68
QTRT2 K158S R161S	NA (>20)
QTRT2 K158E R161S	NA (>20)
QTRT2 K152E K158E R161S	NA (>20)
QTRT2 K152S K158E R161S	NA (>20)
QTRT2 K152E K158S R161S	NA (>20)
QTRT2 W116A	7.68 ± 0.73
QTRT2 V118D	7.68 ± 0.76
QTRT2 A119D	5.48 ± 0.42
QTRT2 R121E	16.00 ± 1.09

Through inspection of the surface electrostatics, we identified a striking concentration of positively charged residues in the α4a and α4b helices of the QTRT2 subunit. Its interaction with the stem loop of a symmetry mate RNA demonstrates the area's capability of binding the phosphate backbone of an RNA (S 5). In the superimposed model of a TGT-tRNA complex, the positively charged patch is in the vicinity of the tRNA's acceptor stem, but with a distance of approximately 10 Å, it is too far away to form polar contacts with its phosphate backbone. Our crosslinking experiments did not yield any evidence for the involvement of this area for tRNA binding. However, UV-induced crosslinking almost exclusively occurs with pyrimidine bases, so if the patch does bind the 3′ strand of the acceptor stem it would be unlikely to form crosslinks as human tRNA^{Asp} exclusively contains purine bases in this area of the strand. The importance of this positively charged patch was corroborated by the observation that charge-inversed double and triple mutants of some of its positively charged residues had significantly reduced affinity with labelled tRNA^{Asp}. However, we also observed that the dual mutation of residues K158 and R161 to a glutamate resulted in presumably misfolded protein, likely because the two residues are located too closely together. Although we avoided mutating both residues to glutamate, all our double and triple mutants contain a combination of the two residues exchanged either for a serine or a glutamate. For this reason, it is possible that a local conformational change, while not rendering the protein insoluble, is the underlying reason for the observed loss in affinity.

The conformation of a tRNA is not static as is demonstrated by the inversed anticodon loop in RNA-bound TGT or the molten D-Arm in the structure of tRNA bound to another member of the TGT family, the archaeal protein inserting achaeosine into position 15 of the D-arm [60]. It is thus possible that a tRNA binding to the TGT heterodimer does adopt a bent conformation that allows its acceptor stem to make contact with the positively charged patch on the QTRT2 surface. However, while we are convinced of the involvement of the βEβF motif in tRNA binding, the experimental evidence is not sufficient to confidently say the same of the positively charged patch.

Finally, QTRT2 has a unique third insertion which appears disordered in both of its crystal structures. This putative loop of roughly 30 amino acid residues (292–326) has previously been proposed to play a role in orienting a substrate RNA and become ordered upon tRNA binding [52]. While we do not know if this is the case upon binding of a full tRNA, we consider it unlikely due to its remote location far away from both the stem loop RNA in the hTGT complex structure and the position of the superimposed tRNA. Instead, we speculate whether it could serve to anchor the TGT enzyme in the compartmentalized eukaryotic cell. Mitochondrial tRNAs^{Asp,Asn,His,Tyr} are Q-modified in a QTRT1 and QTRT2-dependent manner and QTRT2 in particular has been associated with mitochondrial membranes [49,61], so the function of this QTRT2-specific insertion possibly could be to interact with a cellular structure or membrane-bound protein.

Materials and methods

Expression and purification of heterodimeric *H. sapiens* TGT

Human TGT was co-expressed and purified as a heterodimer (QTRT1 and QTRT2) essentially as described previously [51]. In brief, the proteins were co-expressed with a cleavable 6xHis-tag fused N-terminally to QTRT1 in *Escherichia coli* BL21 (DE3) cells using autoinduction medium (ZYM-5052 medium, 2 mM MgSO$_4$ replaced by 1 mM MgCl$_2$, supplemented with 100 mM ZnCl$_2$) [62]. Cells were initially grown for 3 h at 37°C followed by 50–60 h at 16°C before harvesting. Flash frozen cells were stored at −20°C. For purification, cells were thawed and disrupted using an ice-cold microfluidizer (M-110S Microfluidizer (Microfluidics, Westwood, MA, USA)) in 50 mM HEPES pH 7.5, 100 mM NaCl, 10 mM imidazole. The crude lysate was cleared by ultracentrifugation (1 h, 48,380 g, 4°C) and filtering through a 0.45 µM syringe filter (Filtropur (Sarstedt, Nümbrecht, Germany)). The cleared supernatant was loaded onto a Talon column (HiTrap TALON crude (GE Healthcare) or Clontech HisTALON Superflow (Takara Bio, Kusatsu, Japan)), washed with 1 M LiCl and target protein was eluted with 125 mM imidazole. All chromatographic steps were performed at 4°C. Pooled target protein was incubated with PreScission Protease (1:100 w/w) under mild agitation for 16–18 h at 4°C. Protein was concentrated using an Amicon ultrafiltration device (30 kDa MWCO, Merck) and further purified by Superdex S200 (GE Healthcare) size-exclusion chromatography (20 mM HEPES pH 7.5, 100 mM NaCl). TGT was concentrated to 7–10 mg/mL and, if not used directly, flash frozen in liquid nitrogen and stored at −80°C.

Crystallization, data collection and structure determination

Freshly purified TGT was mixed with 2-fold molar excess of synthetic stem loop RNA (sequence: AGCACGGCUGUAAACCGUGC, (Axolabs, Kulmbach, Germany)) and 5-fold excess 9-deazaguanine (AmBeed, Arlington Hts, IL, USA), diluted to a final protein concentration of 2 mg/mL and incubated on ice for 30 min. For crystallization, the complex solution was mixed 1:1 or 2:1 with screening conditions as sitting drops in a 3 Lens 96-well crystallization plate (SWISSCI, High Wycombe, UK) using a mosquito pipetting robot (SPT Labtech, Melbourn, UK). The crystallization plate was tightly sealed and incubated at either 4°C or 20°C. Crystals were harvested from 0.1 M MMT (DL malic acid, MES, Tris in 1:2:2 molar ratio) pH 6, 25% (w/v) PEG 1500 and 0.1 M Bis-Tris pH 5.5, 25% (w/v) PEG 3350 and 0.1 M sodium cacodylate pH 6.5, 25% (w/v) PEG 4000 after 3 months, where necessary cryoprotected with PEG 1500 (30% (w/v) final concentration, MMT grown crystals only) and stored in liquid nitrogen until further use.

X-ray diffraction data were collected at beamline MX 14.1 operated by the Helmholtz–Zentrum Berlin (HZB) at the BESSY II electron-storage ring, Berlin-Adlershof, Germany equipped with a PILATUS3 S 6 M detector. Diffraction images were indexed, integrated and scaled using the XDS-

package [63]. The structure the heterodimer was solved by molecular replacement with models 6H45 and 6FV5 (PDB-IDs) using PHASER [64]. Model adjustment, including placement of the RNA stem loop (PDB-ID: 1Q2R) and 9-deazaguanine, and building of QTRT2 residues divergent from the mouse protein was done in Coot [65]. Refmac05 was used for structure refinement in iterative cycles with manual model adjustment [66]. Atomic displacement parameters of the final model were refined using TLS parameterization in PHENIX [67].

Structural data representation and analysis

Structural figures were prepared using PyMol.

Surface electrostatics of the sidechain-completed hTGT heterodimer were calculated using the Adaptive Poisson-Boltzman method (APBS) as implemented within PyMOL [68].

Model of *H. sapiens* tRNA^{Asp} and structure superposition

A model of human tRNA^{Asp} was prepared based on the coordinates of *Saccharomyces cerevisiae* tRNA^{Asp} (PDB-ID: 2TRA) by mutating the base sequence in Coot to fit the human tRNA. The tRNA model was superimposed to the TGT·RNA complex by aligning bases 25–31 and 39–42 in PyMOL.

In vitro transcription and purification of tRNA^{Asp}

Human tRNA^{Asp} was transcribed *in vitro* from annealed DNA oligonucleotides (Merck) using T7 RNA polymerase (4 mM rNTPs, 25 mM MgCl$_2$, 1× HT buffer (30 mM HEPES pH 8.0, 10 mM DTT, 6 mM MgCl$_2$, 2 mM Spermidine, 0.01% Triton X-100)). The transcript was loaded onto a ResourceQ column (GE Healthcare) in 20 mM Hepes pH 7.5, 50 mM KCl and eluted in a shallow KCl gradient (245 to 732.5 mM in 150 mL). Fractions containing tRNA were pooled, precipitated with ethanol and the dried pellet dissolved in water.

Preparation of TGT·tRNA complex

TGT protein was mixed with 1.5-fold molar excess of tRNA^{Asp} and incubated on ice for 30 min. The TGT·tRNA complex was purified by size-exclusion chromatography using a Sephadex 200 Increase 10/300 GL column (GE Healthcare) in 20 mM Hepes pH 7.5, 100 mM NaCl and concentrated to 1 mg/mL protein using an Amicon ultrafiltration device (30 kDa MWCO, Merck).

UV-crosslinking experiments were done in triplicates from three independently assembled and purified complex samples.

Protein-RNA crosslinking

For each replicate, 40 to 60 μg of purified TGT·tRNA complex were crosslinked by UV irradiation at 254 nm for 10 min on ice using an in-house built crosslinking apparatus as described in [69]. After ethanol-precipitation, the crosslinked complex

was processed as described in [69] with minor modifications. Briefly, the protein-RNA pellet was dissolved in 4 M urea, 50 mM Tris/HCl, pH 7.5, following dilution to 1 M urea with 50 mM Tris/HCl, pH 7.5. Ten μg RNase A (EN0531, Thermo Fisher Scientific), 1kU RNase T1 (EN0531, Thermo Fisher Scientific) and 250 U PierceTM universal nuclease (88,700, Thermo Fisher Scientific) were added and MgCl$_2$ concentration was adjusted to 1 mM. RNA digestion was performed for 4 h at 37°C followed by protein digestion with trypsin (sequencing grade, Promega) at a 1:20 enzyme to protein mass ratio. Sample clean-up was performed using C18 columns (74–4601, Harvard Apparatus) and crosslinked peptides were enriched with in-house packed TiO2 columns (Titansphere 5 μm; GL Sciences, Japan) as described in [69]. Peptides were dried and subjected to MS measurement.

LC-MS/MS analysis and data analysis

Peptide pellets from TiO$_2$ enrichment were dissolved in 2% (v/v) acetonitrile, 0.05% (v/v) TFA. LC-MS/MS analyses were performed on a Q Exactive HF-X (Thermo Fisher Scientific) instrument coupled to a nanoflow liquid chromatography system (1100 series, Agilent Technologies). Sample separation was performed at a flow rate of 300 nl/min using a buffer system consisting of 0.1% (v/v) formic acid (buffer A) and 80% (v/v) acetonitrile, 0.08% (v/v) formic acid (buffer B) and linear gradient from 10% to 45% buffer B in 44 min. Peptides were separated over 58 min. Eluting heteroconjugates were analysed in positive mode using a data-dependent top 20 acquisition method. MS1 and MS2 resolution were set to 120,000 and 30,000 FWHM, respectively. AGC targets were set to 106 and 5×105, normalized collision energy (NCE) to 28%, dynamic exclusion to 21 s, and maximum injection time to 60 and 120 ms (MS1 and MS2). MS data were analysed and manually validated using the OpenMS pipeline RNPxl and OpenMS TOPPASViewer 1.

Mutagenesis

Site-directed mutagenesis was adapted from the supplier's protocol for the QuikChange Site-Directed Mutagenesis kit (Agilent) for using 35–45-mer DNA primers with a back-to-back overlap of 6–8 bases (Merck). Mutagenesis PCR (18 cycles, 54°C annealing temperature) was carried out with Phusion polymerase (Thermo Fisher Scientific).

Queuine incorporation activity tests

Queuine incorporation activity tests were based on the previously described boronate affinity electrophoresis, in which Q-containing RNA migrates more slowly due to interaction with its additional cis-diol [70]. The incorporation reaction was carried out in 10 μL volume: TGT (0.5 μM final concentration) was added to 4 μM of tRNA^{Asp} in the presence of 1 mM queuine [9] in 100 mM HEPES pH 7.5, 20 mM MgCl2, 5 mM DTT. The reaction was incubated for 3 minutes at 37°C (after which approximately 50% substrate conversion is observed for the wildtype enzyme) and stopped by addition of an equal volume of RNA loading dye (New England

Biolabs). RNA samples were separated by affinity electrophoresis (120 V, 30 mA, 80 min, 4°C) in TAE buffer using gels prepared by supplementing the gel mixture (10% (w/v) acrylamide, 42% (w/v) urea) with 5 mg/mL 3-(acrylamido)phenylboronic acid (Merck) before polymerization. Gels were stained with GelRed (Biotium, Fremont, CA, USA), imaged and bands quantified using GelAnalyzer 19.1 (www.gelanalyzer.com). For each lane, the ratio of Q34 tRNA to total tRNA was determined (relative activity) and normalized by the wild-type value. The assay was performed in triplicates stemming from three independent incorporation reactions and affinity gels, with the exception of the R161E mutant for which only two replicates could be obtained.

tRNA labelling and fluorescence polarization affinity measurements

In vitro transcribed tRNA^{Asp} was fluorescein-labelled as described previously [9]. For fluorescence polarization experiments, a two-fold dilution series of TGT (50 µL individual sample volumes) was mixed with 20 nM labelled tRNA in a black 96 well plate (Corning, Corning, NY, USA). Fluorescence polarization was measured after 5 minutes of shaking in a VICTOR Nivo plate reader (PerkinElmer). Triplicates were measured from three independent dilution series. Data evaluation and sigmoidal curve fitting were done with OriginPro 8.5.

Acknowledgments

Funding

Data availability

Coordinates and diffraction data of the hTGT-RNA structure have been deposited within the Protein Data Bank (PDB ID 7NQ4).

Disclosure statement

No potential conflict of interest was reported by the author(s).

Author contributions

Experimental design (K.S., R.F.), protein expression and purification (K. S.), crystallography, data collection and structure determination (K.S.), crystal structure analysis (K.S.), tRNA purification and complex assembly (K.S.), crosslinking, mass spectrometry and crosslinking data analysis (L. W., under supervision by H.U.), mutagenesis and biochemical assays (K. S.), manuscript writing (K.S.), manuscript review and editing (K.S., R.F.).

ORCID

Ralf Ficner 🆔 http://orcid.org/0000-0002-1739-6086

References

[1] Harada F, Nishimura S. Possible anticodon sequences of tRNAHis, tRNAAsn, and tRNAAsp from Escherichia coli. Universal presence of nucleoside Q in the first position of the anticodons of these transfer ribonucleic acids. Biochemistry. 1972;11:301–308.

[2] Meier F, Suter B, Grosjean H, et al. Queuosine modification of the wobble base in tRNAHis influences 'in vivo' decoding properties. Embo J. 1985;4:823–827.

[3] Zaborske JM, Bauer DuMont VL, Wallace EWJ, et al. A nutrient-driven tRNA modification alters translational fidelity and genome-wide protein coding across an animal genus. PLoS Biol. 2014;12:e1002015.

[4] Tuorto F, Legrand C, Cirzi C, et al. Queuosine-modified tRNAs confer nutritional control of protein translation. Embo J. 2018;37:e99777.

[5] Müller M, Legrand C, Tuorto F, et al. Queuine links translational control in eukaryotes to a micronutrient from bacteria. Nucleic Acids Res. 2019;47:3711–3727.

[6] Durand JMB, Dagberg B, Uhlin BE, et al. Transfer RNA modification, temperature and DNA superhelicity have a common target in the regulatory network of the virulence of Shigella flexneri: the expression of the virF gene. Mol Microbiol. 2000;35:924–935.

[7] Hurt JK, Olgen S, Garcia GA. Site-specific modification of Shigella flexneri virF mRNA by tRNA-guanine transglycosylase in vitro. Nucleic Acids Res. 2007;35:4905–4913.

[8] Müller M, Hartmann M, Schuster I, et al. Dynamic modulation of Dnmt2-dependent tRNA methylation by the micronutrient queuine. Nucleic Acids Res. 2015;43:10952–10962.

[9] Johannsson S, Neumann P, Wulf A, et al. Structural insights into the stimulation of S. pombe Dnmt2 catalytic efficiency by the tRNA nucleoside queuosine. Sci Rep. 2018;8:8880.

[10] Wang X, Matuszek Z, Huang Y, et al. Queuosine modification protects cognate tRNAs against ribonuclease cleavage. RNA. 2018;24:1305–1313.

[11] Kasai H, Ohashi Z, Harada F, et al. Structure of the modified nucleoside Q isolated from Escherichia coli transfer ribonucleic acid. 7-(4,5-cis-dihydroxy-1-cyclopenten-3-ylaminomethyl)-7-deazaguanosine. Biochemistry. 1975;14:4198–4208.

[12] Yokoyama S, Miyazawa T, Iitaka Y, et al. Three-dimensional structure of hyper-modified nucleoside Q located in the wobbling position of tRNA. Nature. 1979;282:107–109.

[13] Phillips G, Yacoubi BE, Lyons B, et al. Biosynthesis of 7-deazaguanosine-modified tRNA nucleosides: a new role for GTP cyclohydrolase I. J Bacteriol. 2008;190:7876–7884.

[14] McCarty RM, Somogyi Á, Bandarian V. Escherichia coli QueD Is a 6-carboxy-5,6,7,8-tetrahydropterin Synthase. Biochemistry. 2009;48:2301–2303.

[15] McCarty RM, Somogyi Á, Lin G, et al. The deazapurine biosynthetic pathway revealed: in vitro enzymatic synthesis of PreQ0 from guanosine 5′-triphosphate in four steps. Biochemistry. 2009;48:3847–3852.

[16] Dowling DP, Bruender NA, Young AP, et al. Radical SAM enzyme QueE defines a new minimal core fold and metal-dependent mechanism. Nat Chem Biol. 2014;10:106–112.

[17] Van Lanen SG, Reader JS, Swairjo MA, et al. From cyclohydrolase to oxidoreductase: discovery of nitrile reductase activity in a common fold. Proc Natl Acad Sci. 2005;102:4264–4269.

[18] Lee BWK, Van Lanen SG, Iwata-Reuyl D. Mechanistic studies of bacillus subtilis QueF, the nitrile oxidoreductase involved in queuosine biosynthesis. Biochemistry. 2007;46:12844–12854.

[19] Chikwana VM, Stec B, Lee BWK, et al. Structural basis of biological nitrile reduction. J Biol Chem. 2012;287:30560–30570.

[20] Okada N, Noguchi S, Kasai H, et al. Novel mechanism of post-transcriptional modification of tRNA. Insertion of bases of Q precursors into tRNA by a specific tRNA transglycosylase reaction. J Biol Chem. 1979;254:3067–3073.

[21] Okada N, Nishimura S. Isolation and characterization of a guanine insertion enzyme, a specific tRNA transglycosylase, from Escherichia coli. J Biol Chem. 1979;254:3061–3066.

[22] Slany RK, Bösl M, Kersten H. Transfer and isomerization of the ribose moiety of AdoMet during the biosynthesis of queuosine tRNAs, a new unique reaction catalyzed by the QueA protein from Escherichia coli. Biochimie. 1994;76:389–393.

[23] Mathews I, Schwarzenbacher R, McMullan D, et al. Crystal structure of S-adenosylmethionine: tRNAribosyltransferase-isomerase (QueA) from thermotoga maritima at 2.0 Å resolution reveals a new fold. Proteins Struct Funct Bioinforma. 2005;59:869–874.

[24] Grimm C, Ficner R, Sgraja T, et al. Crystal structure of bacillus subtilis S-adenosylmethionine: tRNAribosyltransferase-isomerase. Biochem Biophys Res Commun. 2006;351:695–701.

[25] Van Lanen SG, Iwata-Reuyl D. Kinetic mechanism of the tRNA-modifying enzyme S-adenosylmethionine: tRNARibosyltransferase-isomerase (QueA). Biochemistry. 2003;42:5312–5320.

[26] Frey B, McCloskey J, Kersten W, et al. New function of vitamin B12: cobamide-dependent reduction of epoxyqueuosine to queuosine in tRNAs of Escherichia coli and salmonella typhimurium. J Bacteriol. 1988;170:2078–2082.

[27] Miles ZD, McCarty RM, Molnar G, et al. Discovery of epoxyqueuosine (oQ) reductase reveals parallels between halorespiration and tRNA modification. Proc Natl Acad Sci. 2011;108:7368–7372.

[28] Payne KAP, Fisher K, Sjuts H, et al. Epoxyqueuosine reductase structure suggests a mechanism for cobalamin-dependent tRNA modification. J Biol Chem. 2015;290:27572–27581.

[29] Dowling DP, Miles ZD, Köhrer C, et al. Molecular basis of cobalamin-dependent RNA modification. Nucleic Acids Res. 2016;44:9965–9976.

[30] Romier C, Reuter K, Suck D, et al. Crystal structure of tRNA-guanine transglycosylase: RNA modification by base exchange. Embo J. 1996;15:2850–2857.

[31] Chong S, Curnow AW, Huston TJ, et al. tRNA-guanine transglycosylase from Escherichia coli is a zinc metalloprotein. Site-directed mutagenesis studies to identify the zinc ligands. Biochemistry. 1995;34:3694–3701.

[32] Immekus F, Barandun LJ, Betz M, et al. Launching spiking ligands into a protein–protein interface: a promising strategy to destabilize and break interface formation in a tRNA modifying enzyme. ACS Chem Biol. 2013;8:1163–1178.

[33] Jakobi S, Nguyen TXP, Debaene F, et al. Hot-spot analysis to dissect the functional protein–protein interface of a tRNA-modifying enzyme. Proteins Struct Funct Bioinforma. 2014;82:2713–2732.

[34] Jakobi S, Nguyen PTX, Debaene F, et al. What glues a homodimer together: systematic analysis of the stabilizing effect of an aromatic hot spot in the protein–protein interface of the tRNA-modifying enzyme Tgt. ACS Chem Biol. 2015;10:1897–1907.

[35] Xie W, Liu X, Huang RH. Chemical trapping and crystal structure of a catalytic tRNA guanine transglycosylase covalent intermediate. Nat Struct Mol Biol. 2003;10:781–788.

[36] Ritschel T, Atmanene C, Reuter K, et al. An integrative approach combining noncovalent mass spectrometry, enzyme kinetics and X-ray crystallography to decipher Tgt protein-protein and protein-RNA interaction. J Mol Biol. 2009;393:833–847.

[37] Goodenough-Lashua DM, Garcia GA. tRNA–guanine transglycosylase from E. coli: a ping-pong kinetic mechanism is consistent with nucleophilic catalysis. Bioorganic Chem. 2003;31:331–344.

[38] Reyniers JP, Pleasants JR, Wostmann BS, et al. Administration of exogenous queuine is essential for the biosynthesis of the queuosine-containing transfer RNAs in the mouse. J Biol Chem. 1981;256:11591–11594.

[39] Ott G, Kersten H, Nishimura S. Dictyostelium discoideum: a useful model system to evaluate the function of queuine and of the Q-family of tRNAs. FEBS Lett. 1982;146:311–314.

[40] Katze JR, Gunduz U, Smith DL, et al. Evidence that the nucleic acid base queuine is incorporated intact into tRNA by animal cells. Biochemistry. 1984;23:1171–1176.

[41] Kirtland GM, Morris TD, Moore PH, et al. Novel salvage of queuine from queuosine and absence of queuine synthesis in chlorella pyrenoidosa and chlamydomonas reinhardtii. J Bacteriol. 1988;170:5633–5641.

[42] Siard TJ, Jacobson KB, Farkas WR. Queuine metabolism and cadmium toxicity in drosophila melanogaster. BioFactors Oxf Engl. 1991;3:41–47.

[43] Gaur R, Björk GR, Tuck S, et al. Diet-dependent depletion of queuosine in tRNAs in caenorhabditis elegans does not lead to a developmental block. J Biosci. 2007;32:747–754.

[44] Shindo-Okada N, Okada N, Ohgi T, et al. Transfer ribonucleic acid guanine transglycosylase isolated from rat liver. Biochemistry. 1980;19:395–400.

[45] Katze BB, McCloskey JA. Queuine, a modified base incorporated posttranscriptionally into eukaryotic transfer RNA: wide distribution in nature. Science. 1982;216:55–56.

[46] Chen Y-C, Brooks AF, Goodenough-Lashua DM, et al. Evolution of eukaryal tRNA-guanine transglycosylase: insight gained from the heterocyclic substrate recognition by the wild-type and mutant human and Escherichia coli tRNA-guanine transglycosylases. Nucleic Acids Res. 2011;39:2834–2844.

[47] Kasai H, Nakanishi K, Macfarlane RD, et al. The structure of Q* nucleoside isolated from rabbit liver transfer ribonucleic acid. J Am Chem Soc. 1976;98:5044–5046.

[48] Okada N, Shindo-Okada N, Nishimura S. Isolation of mammalian tRNAAsp and tRNATyr by lectin-sepharose affinity column chromatography. Nucleic Acids Res. 1977;4:415–423.

[49] Boland C, Hayes P, Santa-Maria I, et al. Queuosine formation in eukaryotic tRNA occurs via a mitochondria-localized heteromeric transglycosylase. J Biol Chem. 2009;284:18218–18227.

[50] Chen YC, Kelly VP, Stachura SV, et al. Characterization of the human tRNA-guanine transglycosylase: confirmation of the heterodimeric subunit structure. RNA. 2010;16:958–968.

[51] Johannsson S, Neumann P, Ficner R. Crystal structure of the human tRNA guanine transglycosylase catalytic subunit QTRT1. Biomolecules. 2018;8:81.

[52] Behrens C, Biela I, Petiot-Bécard S, et al. Homodimer architecture of QTRT2, the noncatalytic subunit of the eukaryotic tRNA-guanine transglycosylase. Biochemistry. 2018;57:3953–3965.

[53] Müller SO, Slany RK. Structural analysis of the interaction of the tRNA modifying enzymes Tgt and QueA with a substrate tRNA. FEBS Lett. 1995;361:259–264.

[54] Curnow AW, Kung FL, Koch KA, et al. tRNA-guanine transglycosylase from Escherichia coli: gross tRNA structural requirements for recognition. Biochemistry. 1993;32:5239–5246.

[55] Nakanishi S, Ueda T, Hori H, et al. A UGU sequence in the anticodon loop is a minimum requirement for recognition by escherichia coli tRNA-guanine transglycosylase. J Biol Chem. 1994;269:32221–32225.

[56] Carbon P, Haumont E, Fournier M, et al. Site-directed in vitro replacement of nucleosides in the anticodon loop of tRNA: application to the study of structural requirements for queuine insertase activity. Embo J. 1983;2:1093–1097.

[57] Grosjean H, Edqvist J, Stråby KB, et al. Enzymatic formation of modified nucleosides in tRNA: dependence on tRNA architecture. J Mol Biol. 1996;255:67–85.

[58] Alqasem MA, Fergus C, Southern JM, et al. The eukaryotic tRNA-guanine transglycosylase enzyme inserts queuine into tRNA via a sequential bi–bi mechanism. Chem Commun. 2020;56:3915–3918.

[59] Stengl B, Meyer EA, Heine A, et al. Crystal structures of tRNA-guanine transglycosylase (TGT) in complex with novel and potent inhibitors unravel pronounced induced-fit adaptations and suggest dimer formation upon substrate binding. J Mol Biol. 2007;370:492–511.

[60] Ishitani R, Nureki O, Nameki N, et al. Alternative tertiary structure of tRNA for recognition by a posttranscriptional modification enzyme. Cell. 2003;113:383–394.

[61] Suzuki T, Yashiro Y, Kikuchi I, *et al*. Complete chemical structures of human mitochondrial tRNAs. Nat Commun. 2020;11:4269.

[62] Studier FW. Protein production by auto-induction in high-density shaking cultures. Protein Expr Purif. 2005;41:207–234.

[63] Kabsch W. XDS. Acta Crystallogr D Biol Crystallogr. 2010;66:125–132.

[64] McCoy AJ, Grosse-Kunstleve RW, Adams PD, et al. Phaser crystallographic software. J Appl Crystallogr. 2007;40:658–674.

[65] Emsley P, Lohkamp B, Scott WG, et al. Features and development of coot. Acta Crystallogr D Biol Crystallogr. 2010;66:486–501.

[66] Murshudov GN, Skubák P, Lebedev AA, et al. REFMAC5 for the refinement of macromolecular crystal structures. Acta Crystallogr D Biol Crystallogr. 2011;67:355–367.

[67] Adams PD, Afonine PV, Bunkóczi G, *et al*. PHENIX: a comprehensive Python-based system for macromolecular structure solution. Acta Crystallogr D Biol Crystallogr. 2010;66:213–221.

[68] Jurrus E, Engel D, Star K, *et al*. Improvements to the APBS biomolecular solvation software suite. Protein Sci Publ Protein Soc. 2018;27:112–128.

[69] Kramer K, Sachsenberg T, Beckmann BM, et al. Photo-cross-linking and high-resolution mass spectrometry for assignment of RNA-binding sites in RNA-binding proteins. Nat Methods. 2014;11:1064–1070.

[70] Igloi GL, Kössel H. Affinity electrophoresis for monitoring terminal phosphorylation and the presence of queuosine in RNA. Application of polyacrylamide containing a covalently bound boronic acid. Nucleic Acids Res. 1985;13:6881–6898.

2.12 Supplementary figures
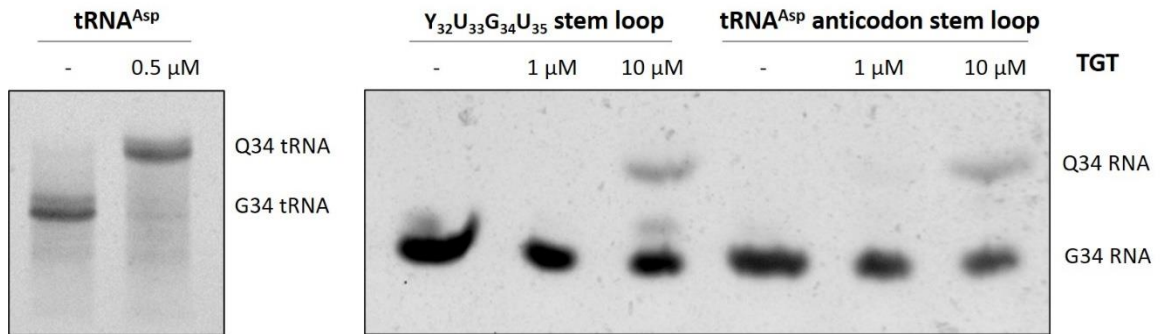
S 1 Q-incorporation into stem loop RNA

Q-incorporation by human TGT into tRNA^{Asp}, a tRNA^{Asp} anticodon stem loop or the $Y_{32}U_{33}G_{34}U_{35}$ stem loop construct used for crystallization. The incorporation reactions contained either 4 µM tRNA or 5 µM stem loop RNA, 1 mM queuine and 0.5 to 10 µM TGT and were incubated for 1 h (tRNA^{Asp}) to 2.5 h (stem loops) at 37 °C. Reaction samples were separated on a boronate affinity electrophoresis gel, which causes retardation of queuine-containing RNA through interaction via its cis-diol.
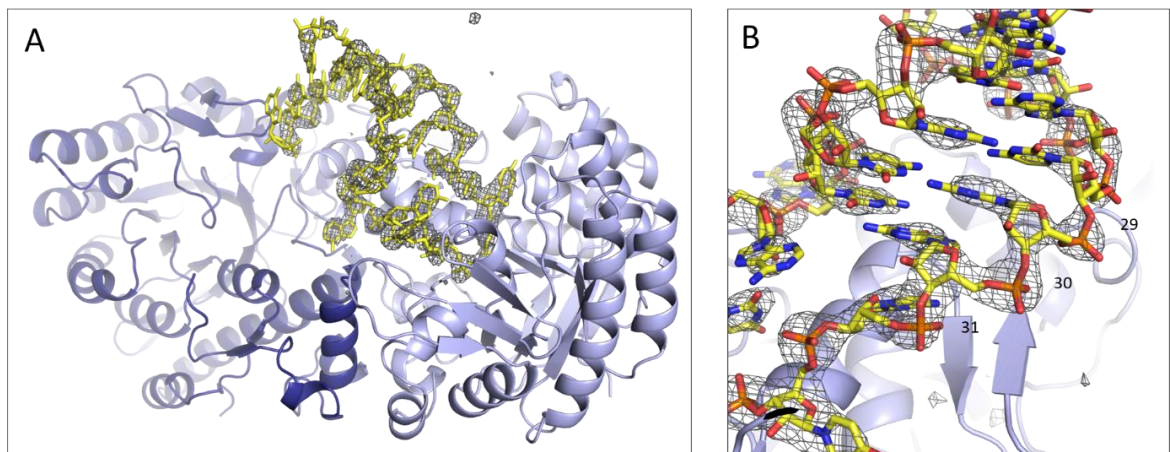
S 2 Electron density of the RNA stem loop

*An mFo-DFc omit map of the RNA stem loop (chain C) contoured at σ = 3.0 is shown as grey mesh. (**A**): Overview of the hTGT-RNA structural model. (**B**): Close-up of the helical stem focusing on nucleotides 29-31.*
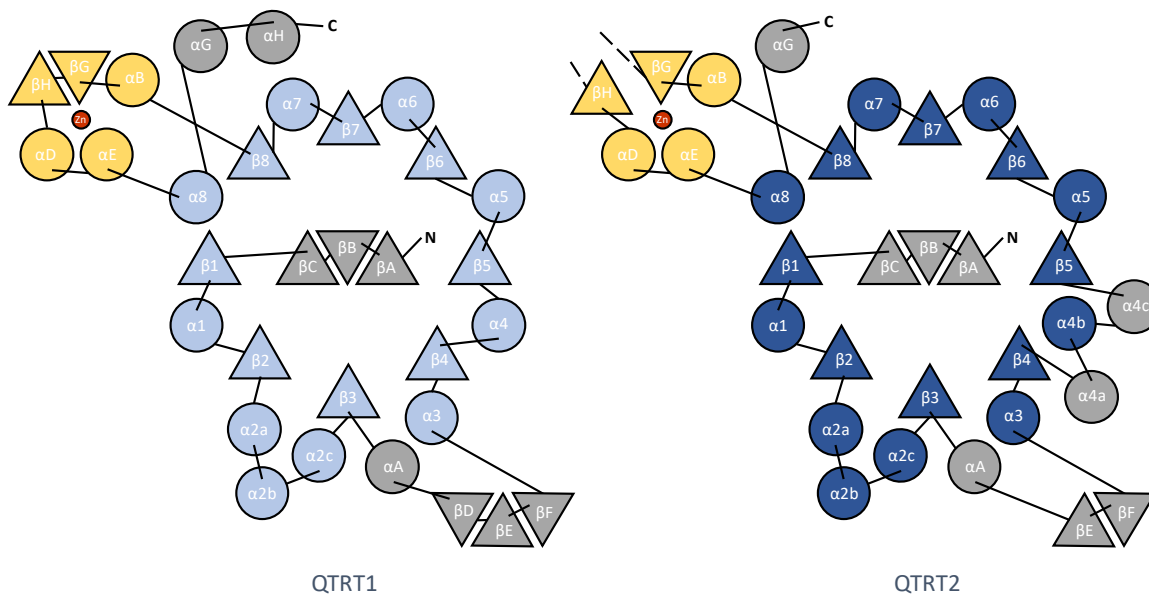
S 3 Topology of human TGT

*The topologies of QTRT1 (**A**) and QTRT2 (**B**) with adapted numbering of secondary structure elements. The $(\beta/\alpha)_8$ core is shown in blue, the zinc binding domain coordinating a single zinc ion (red) is shown in yellow and additional insertions are shown in grey. Triangles represent β-sheets, circles represent α-helices.*
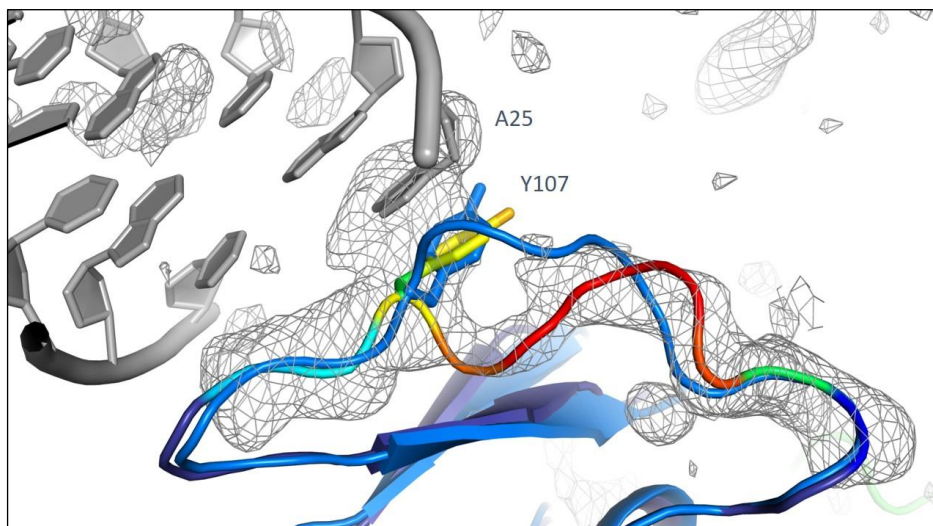
S 4 Unpaired adenine 25 of a symmetry-related RNA forces QTRT2 main chain to adopt an alternative conformation

The course of the main chain of QTRT2 residues 100 - 109 deviates from that in the mouse structure (PDB-ID 6FV5, shown in marine blue). Y107 stacking to A25 of a symmetry-related RNA (grey) in the hTGT structure is shown in stick representation. QTRT2 as seen in the hTGT structure is shown in dark blue with residues 100 - 109 being colored according to B-factor (low: blue, high red). An mFo-DFc electron density omit map for QTRT2 residues 100 – 109 and adenine 25 contoured at σ=2.5 is shown as a grey mesh.
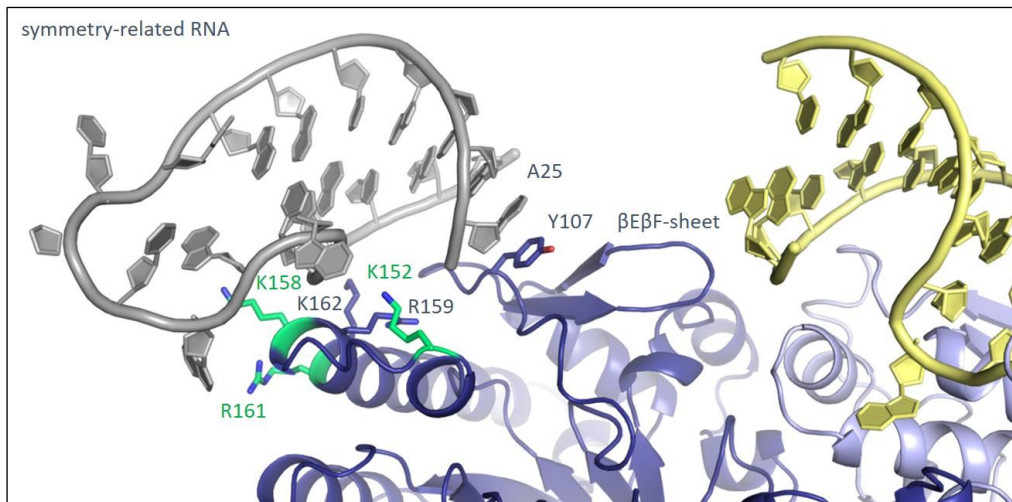
S 5 Interaction between positively charged QTRT2 patch and a symmetry-related RNA

QTRT2 (dark blue) interacts with a symmetry related RNA (grey). Positively charged QTRT2 residues in the area are shown in stick representation, residues that were a target for mutagenesis are colored in green. Additionally, QTRT2 residue Y107 stacking to A25 is also shown in stick representation.
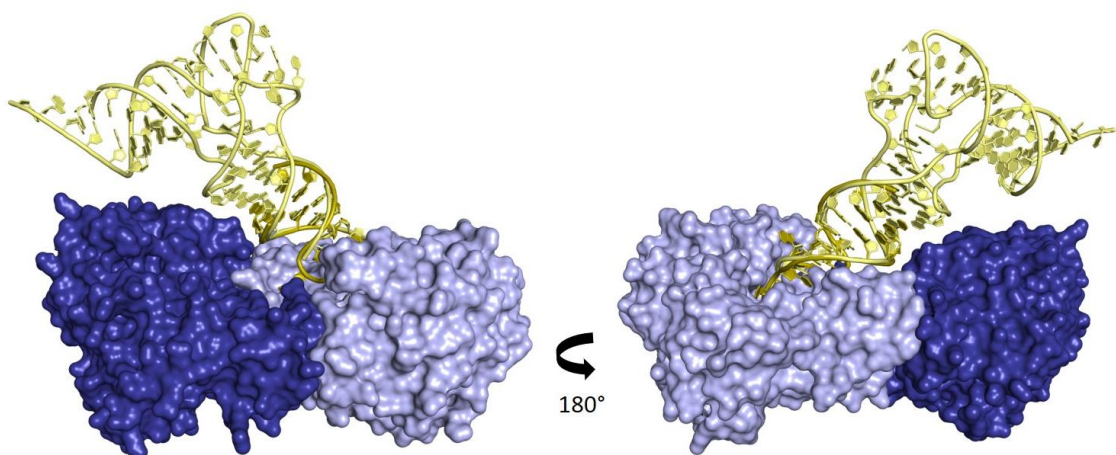
S 6 Model of tRNA-bound complex

A model of human tRNA^{Asp} based on the crystal structure of Saccharomyces cerevisiae tRNA^{Asp} (light yellow) was superimposed to the RNA stem loop (dark yellow) in the hTGT structure. Human TGT is shown in surface representation (QTRT1: light blue, QTRT2: dark blue)

3 STRUCTURE OF HUMAN TGT AND tRNA

This manuscript has been submitted:

Structural and functional insights into tRNA recognition by human tRNA guanine transglycosylase

Katharina Sievers[1], Lukas Sušac[2], Stefano Da Vela[3], Melissa Graewert[3], Simon Trowitzsch[2], Dmitri Svergun[3,4], Robert Tampé[2] and Ralf Ficner[1]

Author affiliations:

[1] Department of Molecular Structural Biology, University of Göttingen, Göttingen, Germany

[2] Institute of Biochemistry, Biocenter, Goethe University Frankfurt, Frankfurt/Main, Germany

[3] European Molecular Biology Laboratory, Hamburg Outstation, EMBL c/o DESY, Hamburg, Germany

[4] Present address: BIOSAXS GmbH, Hamburg, Germany

Author contributions:

Experimental design: K.S., S.T. and R.F., protein, tRNA and complex preparation: K.S., complex vitrification and electron microscopy: L.S., cryo-EM resources: R.T., cryo-EM data processing and model building: K.S., fluorescence polarization, thermal shift and activity assays: K.S., small angle X-ray scattering data collection and analysis: K.S., S.DV. and M.G., small angle X-ray scattering resources: D.S., manuscript writing: K.S., manuscript review and editing: K.S., S.DV., M.G., R.T., L.S., S.T. and R.F.

3.1 Summary

Eukaryotic tRNA guanine transglycosylase (TGT) is an RNA modifying enzyme which catalyzes a base exchange of the genetically encoded guanine 34 of tRNAs[Asp,Asn,His,Tyr] for queuine, a hypermodified 7-deazaguanine derivative. Eukaryotic TGT is a heterodimer comprised of a catalytic and a non-catalytic subunit. While binding of the tRNA anticodon loop to the active site is structurally well-understood, the contribution of the non-catalytic subunit to tRNA binding remained enigmatic, as no complex structure with a complete tRNA was available. Here, we report a cryo-EM structure of eukaryotic TGT in complex with a complete tRNA, revealing the crucial role of the non-catalytic subunit in tRNA binding. We decipher the functional significance of these additional tRNA binding sites, analyze solution state conformation, flexibility and disorder of apo TGT and examine conformational transitions upon tRNA binding.

3.2 Introduction

Queuine (Q) is a hypermodified nucleobase that is found at the wobble position 34 of tRNA[Asp], tRNA[Asn], tRNA[His] and tRNA[Tyr] of bacteria and eukaryotes[1]. These tRNAs share a $G_{34}U_{35}N_{36}$ anticodon (where N = any nucleobase) and each of them decodes both NAC and NAU codons of their respective codon box.

Q-modification regulates decoding efficiency and translation[2–8]. The extent of Q-modification is tissue- and development-specific and atypical levels of Q-modifications are linked to cancer and metabolic disorder[9–11]. Furthermore, Q-modification stimulates m^5C methylation by the enzyme Dnmt2[12–14], is linked to tRNA hypo-fragmentation[15] and was shown to be a requirement of virulence in *S. flexneri*[16,17].

Chemically, queuine is a 7-deazaguanine derivative featuring a cyclopentenediol attached via a 7-aminomethyl linker[18,19]. Although occurring in both bacteria and eukaryotes, queuine is only synthesized by bacteria and all queuine found in eukaryotic RNA has originally been produced by bacteria[20].

Notably, Q- biosynthesis starts outside the context of tRNA: Bacteria first convert GTP to 7-(aminomethyl)-7-deazaguanine (preQ$_1$), which requires five consecutive enzymatic reactions[21–27]. Then, the enzyme tRNA guanine transglycosylase (TGT) substitutes the

genetically encoded guanine 34 of its substrate tRNA for preQ$_1$[28]. Two additional enzymes are required to further convert preQ$_1$ to queuine, now within the tRNA context[29–36]. Because eukaryotes do not produce queuine *de novo*, they possess elaborate uptake and salvage mechanisms to utilize queuine from nutritional and gut bacterial sources,[37–39] which is then directly incorporated into tRNA in a single reaction. This is achieved by the eukaryotic version of TGT (eukTGT) which is adapted to accept the bulkier substrate base but is otherwise similar to bacterial TGT (bacTGT)[40–42]. Interestingly, archaea also produce a 7-deazaguanosine derivative, termed archaeosine, which replaces a guanine in some tRNAs' D-arm via insertion by yet another member of the TGT family[43,44].

Bacterial and eukaryotic TGTs are dimeric proteins, that bind and convert a single tRNA at a time[45,46]. Crystal structures of bacterial and eukaryotic TGT bound to RNA revealed that once bound to TGT, the anticodon loop adopts an inverted "zigzag"-like conformation within the active site[42,47]. Binding of the substate RNA triggers a mobile helix to close off the active site, presumably protecting it from water[42]. The TGT reaction follows ping-pong kinetics[48]: A nucleophilic attack by a conserved aspartate creates a temporary covalent bond to ribose 34, thereby excising the original guanine, which then leaves the active site[47]. The thus vacated binding pocket allows for preQ1 or queuine to bind and, through activation by a second aspartate, form a new N-glycosidic bond with ribose 34. Because the C7 atom of the 7-deazaguanine prevents a necessary charge transfer, this new bond cannot be re-hydrolyzed by TGT, making the Q-incorporation reaction irreversible[49,50].

Both eukTGT and bacTGT form functional dimers. However, bacTGT is a homodimer, while eukTGT is a heterodimer[45,46,51]. This means that in bacTGT, both subunits can act as the catalytically active subunit and tRNA can be bound in two different orientations. The two subunits of eukTGT are paralogs and their dimer interface is very similar to bacterial TGT, but only one subunit (QTRT1) has a functional active site while the other permanently acts as the non-catalytic subunit (QTRT2)[41,42].

To date, the only complex structures of either eukaryotic or bacterial TGT feature a minimal, anticodon stem loop-like RNA bound to the catalytic subunit[42,47]. Functional data shows that such a stem loop is a viable substrate *in vitro* as long as it contains a $Y_{32}U_{33}G_{34}U_{35}$ recognition motif (Y = C or U) at the correct position[52–54]. In fact, Q-incorporation was shown for an mRNA that featured a loop of the correct size[55]. In contrast, *in vivo* data of

experiments on *Xenopus* oocytes highlights the importance of correct three-dimensional tRNA architecture for Q-incorporation[56].

This leaves the pressing question how a complete tRNA is recognized and bound by TGT and whether additional protein-RNA interactions are involved. A potential candidate for an additional interaction site was revealed by analysis of the human TGT crystal structure, which features a striking patch of positively charged amino acids on the surface of the non-catalytic subunit. Affinity experiments with charge-altered mutants suggested that the area does contribute to tRNA binding[42]. In addition, the non-catalytic subunit's βEβF sheet, located in a suitable position to support further tRNA binding, was shown to form a single crosslink with tRNA[Asp][42,57]. Thus, a complete picture of the tRNA-recognition principles of eukTGT is missing to date due to the lack of structural data.

Here, we present a complete structure of the fully assembled TGT·tRNA complex obtained by single particle cryo-EM, proving that the substrate tRNA does indeed make extensive contact to the non-catalytic subunit via both its βEβF sheet and the positively charged N-terminal half of helix α4. The functional significance of these contacts was characterized by determining the affinity and reaction kinetics with different RNA substrates. Finally, we characterized the solution state conformation of apo TGT and the TGT·RNA complex based on solution small-angle X-ray scattering data.

3.3 Results

3.3.1 *Cryo-EM map of human TGT bound to tRNA*

Human TGT was complexed with a silhouette-preserving tRNA construct based on human tRNA[Asp] that had been produced by *in vitro* transcription. The complex was stabilized with excess 9-deazaguanine (9dzG)[47] and purified by size-exclusion chromatography immediately prior to vitrification on cryo-EM grids. Two datasets were processed, and a final map was reconstructed from 463,140 particles (Figure S2 and Figure S3).
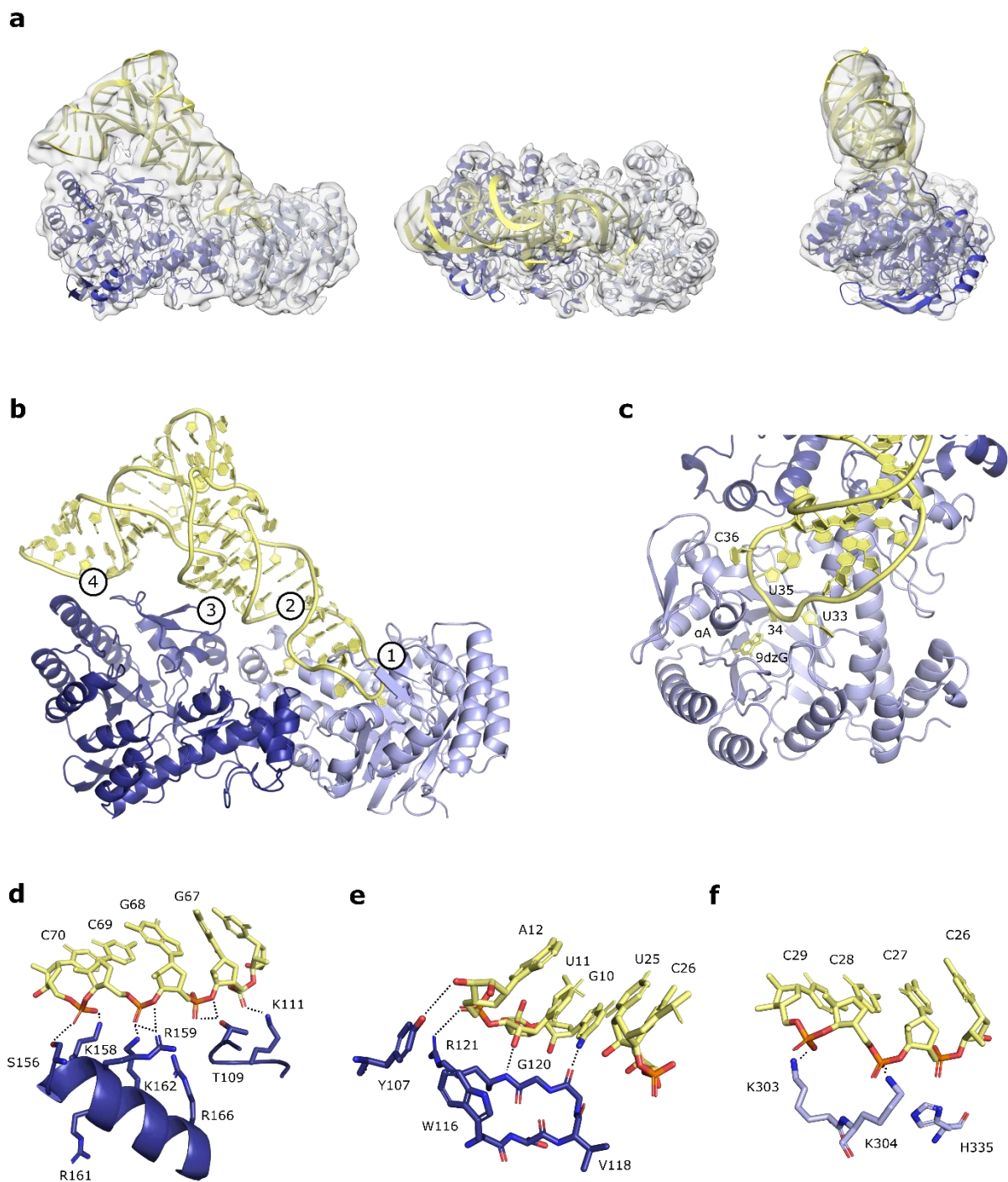
Figure 1: TGT·tRNA cryo-EM structure

a) Cryo-EM map and TGT·tRNA model in three distinct orientations. Catalytic and non-catalytic subunits are shown in light and dark blue respectively, tRNA is shown in yellow. *b)* Complete model of TGT and bound tRNA. Four distinct tRNA-binding regions are indicated. *c)* Details of binding region 1, involving the QTRT1 active site and surrounding elements binding the tRNA anticodon loop. *d)* Details of binding region 4, involving residues of QTRT2 helix α4 and β3βA turn binding the tRNA acceptor stem. *e)* Details of binding region 3, involving QTRT2 βEβF sheet and Y107 binding the tRNA core. *f)* Details of binding region 2, involving multiple QTRT1 residues binding to tRNA anticodon stem.

The map reveals the overall structure of the TGT heterodimer and bound tRNA, which intimately interacts with both TGT subunits (Figure 1a). The Fourier shell correlation resolution of this map is 3.3 Å after application of a refined mask, but local resolution varies from below 3 Å in the center of the protein to above 5 Å in the periphery of the complex (Figure S2a+c).

As low map quality can be caused by different types of heterogeneity, we used 3D Variability Analysis to examine the heterogeneity present in our dataset. This revealed that the dataset is subject to continuous heterogeneity without distinct clusters or states (Figure 2b) and is caused primarily by a "sweeping" movement of the tRNA acceptor stem across the QTRT2 surface (Figure 2a, supplementary movie 2), but also twisting of the TGT subunits and heterogeneity of the CCA-end (supplementary movies 1-3). The observed movement of the tRNA relative to the QTRT2 subunit especially suggests that despite their intricacy, the contacts between tRNA and TGT are not static.
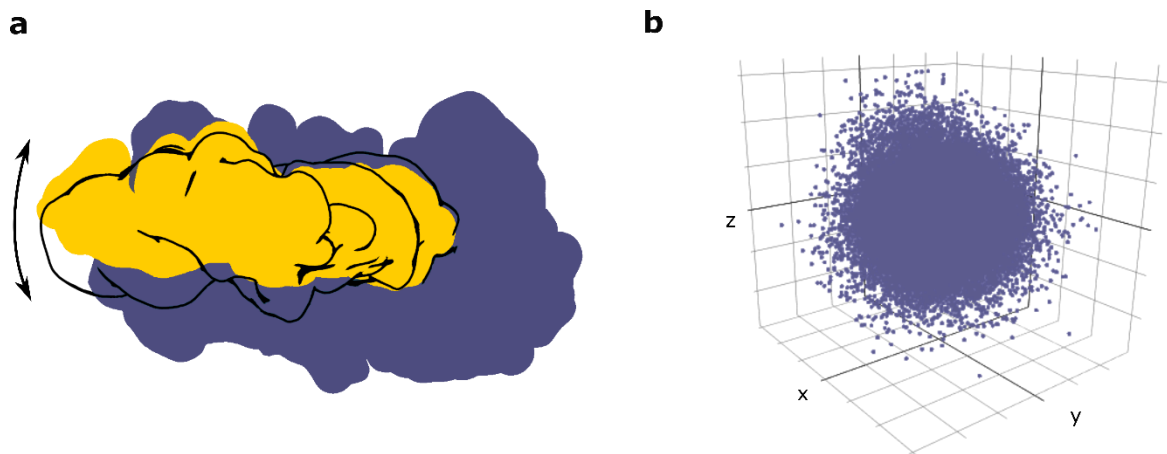
Figure 2: 3D Variability Analysis of cryo-EM data

a) Schematic depiction of "sweeping" tRNA motion against the TGT protein. TGT is depicted as a solid blue outline, tRNA is shown both in solid yellow and as a black outline, representing two different conformations. The figure is based on 3D variability analysis conducted at 8 Å resolution and represents variability mode 2. b) Particle distribution in latent space. Axes x, y and represent the first three variability modes as determined by 3D variability analysis of the clean particle stack.

3.3.2   Model building and description of the tRNA interface

The sharpened cryo-EM map allowed to fit, rebuild, and refine the available atomic model of the TGT heterodimer and a model of the tRNA (Figure 1b). In the refined model, the TGT dimer is slightly wider than in previous crystal structures, with a maximum dimension of 97 Å instead of 92 Å (Cα QTRT1 D208 – QTRT2 E200). Despite varying local resolution, the map quality allowed to trace the main chains along their entire length except for a flexible loop spanning QTRT2 residues 293-329, of which most appear disordered. Local resolution is especially poor near the tRNA's unpaired 5' end (including the CCA-end), and the tRNA was only modelled to encompass nucleotides 1-72. Surprisingly, the map is also weak at the active site of QTRT1: The residual ribose 34, the 9dzG base and F109 of QTRT1 known to engage with the base bound in the active site via stacking interaction are all relatively poorly resolved. This is likely because not all molecules may have contained the stabilizing 9dzG base after size-exclusion chromatography. Regardless, the tRNA appears to bind to the active site in a manner virtually identical to known TGT crystal structures featuring a stem loop RNA[42,47] (Figure 1c). Outside of the active site region, the tRNA is bound to the QTRT1 subunit by hydrogen bond networks between K303 and K304 and RNA backbone phosphates 28 and 29 as well as between H335 and phosphate 27 (Figure 1f and Figure S2g).

The tRNA core heavily interacts with QTRT2's βEβF sheet. Nucleotides 10 and 11 form hydrogen bonds with main chain carbonyl and amines of QTRT2 residues 119-121. In addition, the guanidino group of R121 forms a hydrogen bond with phosphate 12 (Figure 1e and Figure S2f). The same guanidino group also stabilizes the neighboring tyrosine 107 via stacking interaction, which in turn forms a hydrogen bond to the ribose moiety of adenosine 12 (Figure 1e).

The tRNA acceptor stem is exclusively bound via its 3' strand: Phosphates 67 and 68 come in close contact with the short β3βE turn formed by QTRT2 residues 109-111 and form hydrogen bonds with K111 and T109 (Figure 1d and Figure S2e). Phosphate 69 forms extensive hydrogen-bonds with both R159 and K162. Finally, phosphate 70 forms hydrogen bonds to S156 and K158. R166 is in close proximity to the tRNA backbone but does not seem to form any direct interactions with the RNA's phosphate backbone. Nucleotides 71-72 are poorly resolved, appearing to be flexible and not form dedicated contacts to the TGT protein.

In total, the TGT·tRNA buried interface is 1873.7 Å^2 in size, of which 515.3 Å^2 are buried between tRNA and QTRT2 (Table 1). This results in a theoretical solvation free energy of -29.9 kcal/mol (-7.6 kcal/mol between QTRT2 and tRNA). The approximately 32 hydrogens bonds that are formed in total across the interface (15 between QTRT2 and tRNA) further decrease the binding free energy between TGT and its tRNA substrate.

Table 1: PISA[58] analysis of protein-tRNA interfaces

Interface	Interface area (Å^2)	$\Delta^i G^1$ (kcal/mol)[a]	Hydrogen bonds
QTRT1	1358.4	-22.3	17
QTRT2	515.3	-7.6	15
total	1873.7	-29.9	32

[a] $\Delta^i G^1$ indicates the solvation free energy gain upon formation of the interface without the contribution of satisfied hydrogen bonds.

3.3.3 Contribution of the tRNA body increases affinity with TGT

Having uncovered the intricate interactions between the tRNA body and the QTRT2 subunit, the obvious question was of the extent and manner they contribute to enzyme functionality. Analysis of the TGT·tRNA interface suggests a significant contribution of the QTRT2 contacts to binding free energy. Similarly, previous fluorescence polarization affinity experiments using charge-manipulated QTRT2 mutants showed a measurable contribution of residues K158, R161 or K152 to tRNA binding[42]. For a more general assessment of the contribution of the tRNA body to binding, we compared the binding affinities of 3' fluorescently labelled complete full-length tRNA with multiple shortened RNA constructs using fluorescence polarization (Figure 3a, summary of RNA constructs in Table 4). The K_D of fluorescein-tRNA$^{\text{Asp}}$ and TGT was determined as 6.5 ± 0.0 μM and is thus very similar to previously reported data[42]. A fluorescein-labeled RNA construct consisting of only the anticodon stem loop (ASL) of human tRNA$^{\text{Asp}}$, plus an additional terminal G-C pair for improved stability, showed markedly reduced affinity to TGT. Its K_D was determined to be 16.8 ± 3.3 μM. The binding curve of TGT and a synthetic stem loop based loosely on tRNA$^{\text{Tyr}}$ was similar. However, with a calculated K_D of 27.9 ± 6.3 μM, its affinity proved to be even lower than that of the human tRNA$^{\text{Asp}}$-based stem loop. Both

stem loops thus proved to possess binding affinities in the same order of magnitude as the non-substrate control, as the K_D of TGT and a poly-adenine 20-mer (A20 RNA) was determined to be 17.5 ± 0.5 μM.
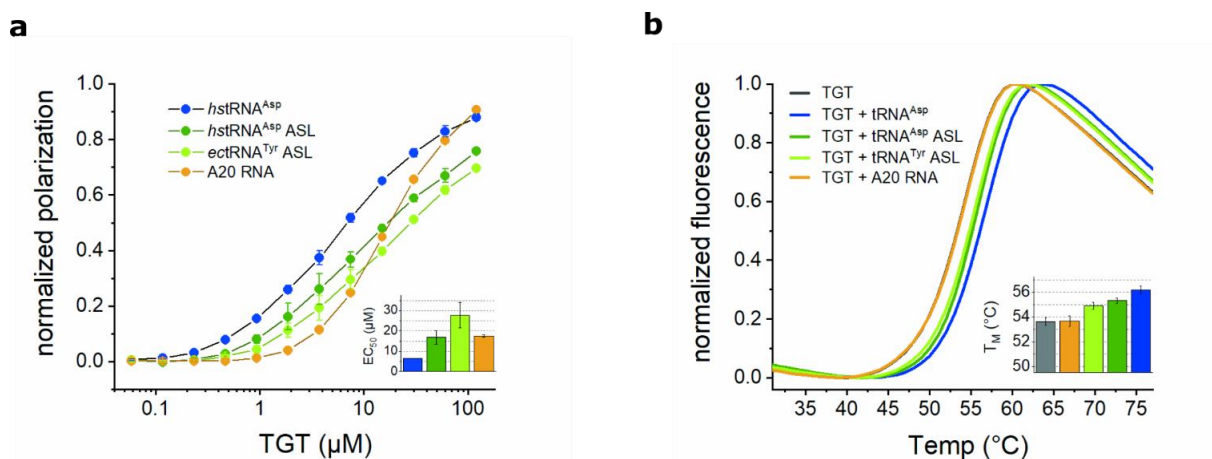
Figure 3: Binding properties of different RNA constructs

a) Fluorescence polarization data of TGT and fluorescently labelled RNA. Normalized binding curves with hstRNA^{Asp}, hstRNA^{Asp} anticodon stem loop (ASL), tRNA^{Tyr} ASL and poly-A 20mer are shown. The inset shows the EC_{50} calculated for each curve. For fitted raw (not normalized) curves see Figure S4. b) Thermal denaturation curves of TGT and TGT in complex with any of the (unlabeled) RNA constructs detailed in a). The inset shows the T_M calculated from each curve.

Table 2: Observed K_D values of different RNA constructs

RNA construct	K_D (μM)
hstRNA^{Asp}	6.5 ± 0.0
hstRNA^{Asp} ASL	16.8 ± 3.3
tRNA^{Tyr} ASL	27.8 ± 6.3
A20 RNA	17.5 ± 0.5

In a different approach to characterize the complex formation of TGT with tRNA and alternative RNAs, we measured thermal stability of TGT in the presence of different RNA constructs. All complexes were mixed, and thermal denaturation was monitored using the protein-specific fluorescent probe SYPRO orange (Figure 3b). TGT alone exhibited a melting temperature of 53.6 ± 0.3 °C. A near identical value was measured for TGT mixed

with 2-fold molar excess of A20 RNA (T_M = 53.6 ± 0.4 °C). Addition of 2-fold molar excess of either *hs*tRNA^{Asp} ASL or tRNA^{Tyr} ASL increased thermal stability to a T_M of 54.8 ± 0.3 °C and 55.3 ± 0.2 °C, respectively. The effect of full *hs*tRNA^{Asp} on thermostability was clearly the strongest, as 2-fold excess increased the measured T_M to 56.2 ± 0.3 °C.

Table 3: Observed Tm of TGT in presence of different RNA constructs

RNA construct	T_M (°C)
TGT	53.6 ± 0.3
TGT + *hs*tRNA^{Asp}	56.2 ± 0.3
TGT + *hs*tRNA^{Asp} ASL	55.3 ± 0.2
TGT + tRNA^{Tyr} ASL	54.9 ± 0.3
TGT + A20 RNA	53.7 ± 0.4

Finally, we looked at the contribution of the tRNA body to enzymatic activity. We used a gel-based activity test and quantified the incorporation of queuine into either *hs*tRNA^{Asp} or *hs*tRNA^{Asp} ASL at various RNA concentrations. As expected, Q-incorporation into the stem loop RNA was much slower than into tRNA at identical concentrations (Figure 4a+b). We determined initial velocities and used Michaelis-Menten kinetics to fit the data and calculate V_{max} and K_M (Figure 4c). For tRNA^{Asp}, the calculated value of K_M = 3.0 ± 0.2 μM is similar to the K_D determined using fluorescence polarization (6.5 ± 0.0 μM). Assuming a single active site per heterodimer, the turnover number k_{cat} was calculated to be 2.8×10^{-2} s^{-1}.

The applied substrate concentrations of tRNA^{Asp} ASL were not sufficient to create substrate-saturated reaction conditions, making it impossible to accurately determine kinetic parameters by non-linear regression. However, a double-reciprocal plot of the same data reveals an obvious tendency: The tRNA^{Asp} ASL datapoints scatter around a slope much steeper than that of the tRNA^{Asp} data (Figure 4d), which is indicative of a significantly higher K_M, while the similar Y-axis interceptions suggest that the values for V_{max} and thus k_{cat} are not much different.
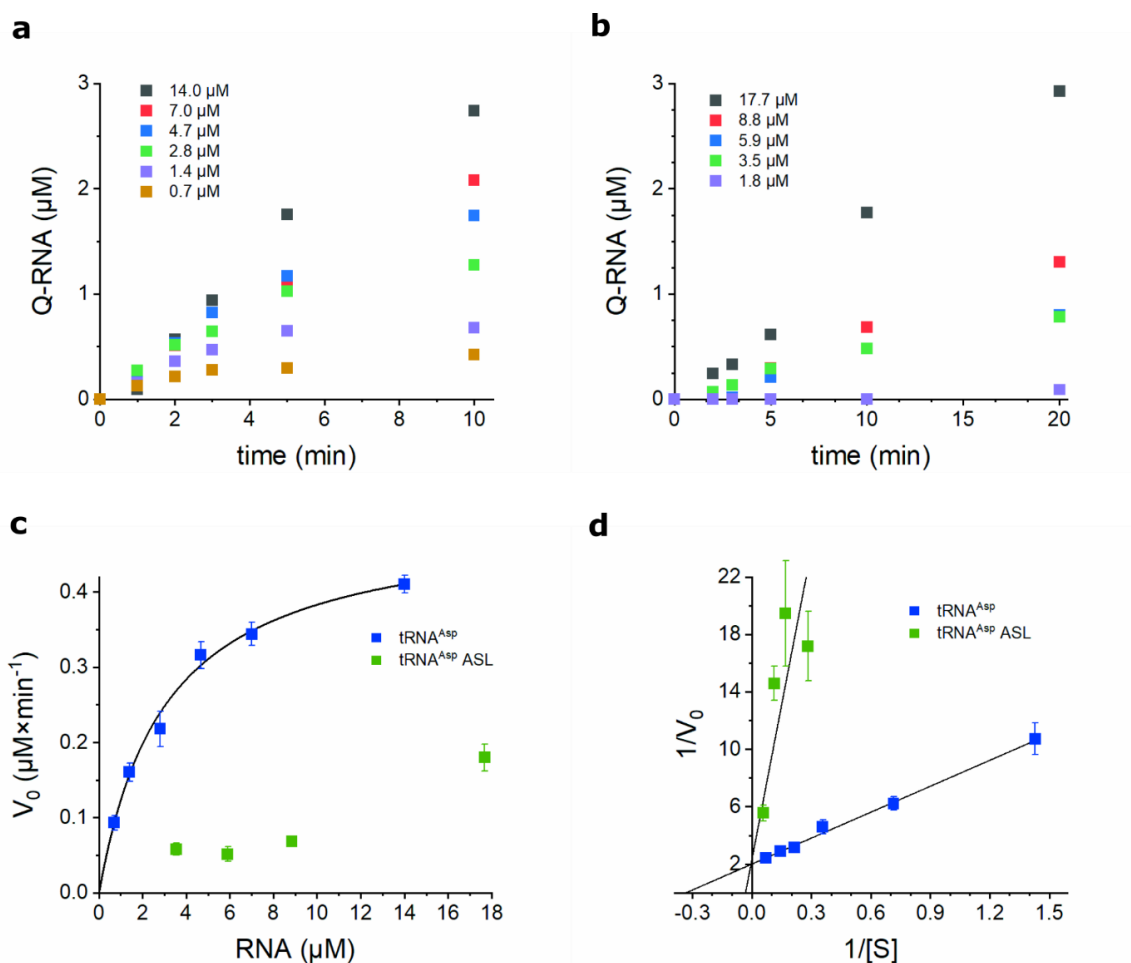
Figure 4: Kinetics of Q-incorporation into tRNAAsp and tRNAAsp ASL

a) Time-course data of Q-incorporation reactions into tRNA^{Asp} (various concentrations). b) Time-course data of Q-incorporation reactions into tRNA^{Asp} ASL (various concentrations). c) Michaelis-Menten plot with initial velocities derived from data shown in a-b) and the result of non-linear regression against tRNA^{Asp} data. d) Double-reciprocal plot of initial velocities derived from data shown in a-b). Error-weighted linear fits of both datasets are shown.

3.3.4 TGT conformation is extended in solution

In the TGT·tRNA cryo-EM structure presented in this work, the TGT is significantly more extended than in previously published crystal structures. This raises the question whether this extension is caused by tRNA binding or is reflective of the protein's solution state. For this reason, we used small angle X-ray scattering (SAXS) to investigate the conformational spread of apo TGT in solution. A SAXS curve of the heterodimeric TGT species was extracted from a SEC-SAXS chromatogram (Figure 5a-b) and subjected to primary data analysis (summarized in Supplementary table 2), revealing a radius of gyration (R_g) of 33 Å.
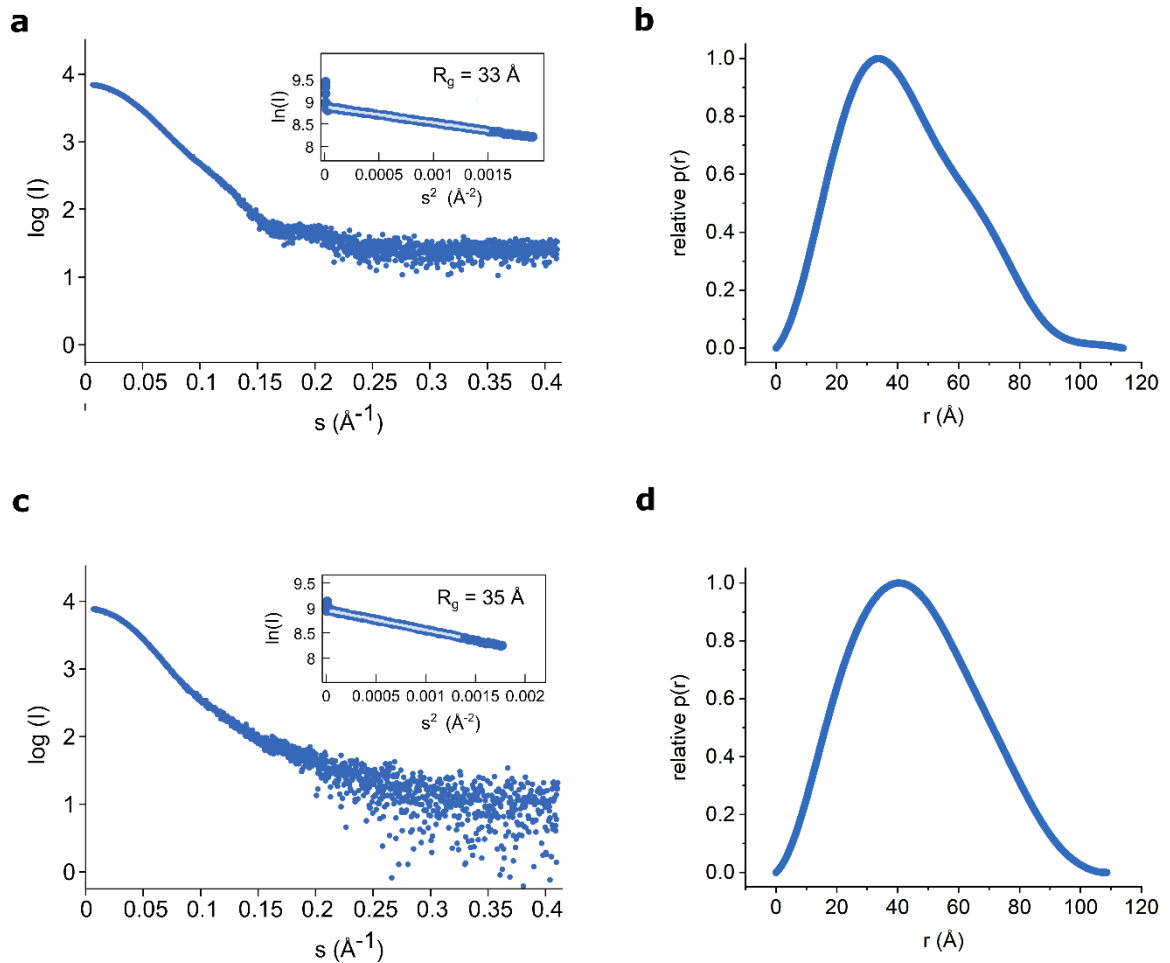
Figure 5: *Small-angle X-ray scattering data of TGT and TGT·tRNA complex*

a) SAXS curve of apo TGT in solution, extracted from SEC-SAXS data, buffer subtracted and averaged (Error bars not shown). Inset shows Guinier-linearized data and fits at low-angles. Deviating datapoints at the lowest angles are caused by un-scattered X-rays passing the purposely small beam stop and thus mark the minimum angle of the collected dataset. Affected datapoints were removed from main figures. c) Same as a) but for TGT·tRNA complex (prepared with GGG-tRNA). b) Pair-distance distribution function of data shown in a). d) Pair-distance distribution function of data shown in c.

TGT contains two main elements that are known to be likely disordered in solution and which need to be considered in the interpretation of the SAXS data: The $\beta G\beta H$ loop spanning QTRT2 residues 292-330 and the QTRT1 N-terminal residues 1-13. Making use of the available crystal structure and cryo-EM data, we used an ensemble optimization method (EOM) to find a representative structure ensemble for the data (Supplementary table 2). In doing so, structure pools, based either on the TGT cryo-EM structure, a previously reported TGT crystal structure (PDB-ID: 7NQ4) or a mixture of both, were

generated by modelling highly flexible/disordered regions as random chains. By comparing the fit of the three optimized ensembles it becomes evident that the ensemble selected from a mixed pool best fits the experimental data (χ^2 = 1.329, Figure 6a). Its fit is marginally better than that of an ensemble selected from an exclusively cryo-EM structure-based pool (χ^2 = 1.371, Figure S6a) and significantly better than that of an ensemble selected from an exclusively crystal-structure based pool (χ^2 = 2.910, Figure S6b). The final mixed ensemble contains structures based on the larger cryo-EM structure and structures based on the smaller crystal structures in an approximate 3:1 ratio, suggesting that TGT predominantly exists in an extended overall conformation in solution. For both subsets of the final ensemble, their respective average radii of gyration were below the pool averages, suggesting that disordered regions consistently adopt moderately compact conformations (Figure 6b). The representative ensemble structures illustrate the space that is occupied by flexible regions (Figure 6c).

SAXS data was also collected for the TGT·tRNA complex (Figure 5c+d, Supplementary table 2). The ensemble optimization analysis was repeated using a structure pool based on the reported TGT·tRNA cryo-EM structure, again modelling disordered regions as random chains. The final ensemble is similar to that of free protein in terms of its relative compactness, suggesting that disordered regions are unaffected by tRNA binding (Figure 6d-f).
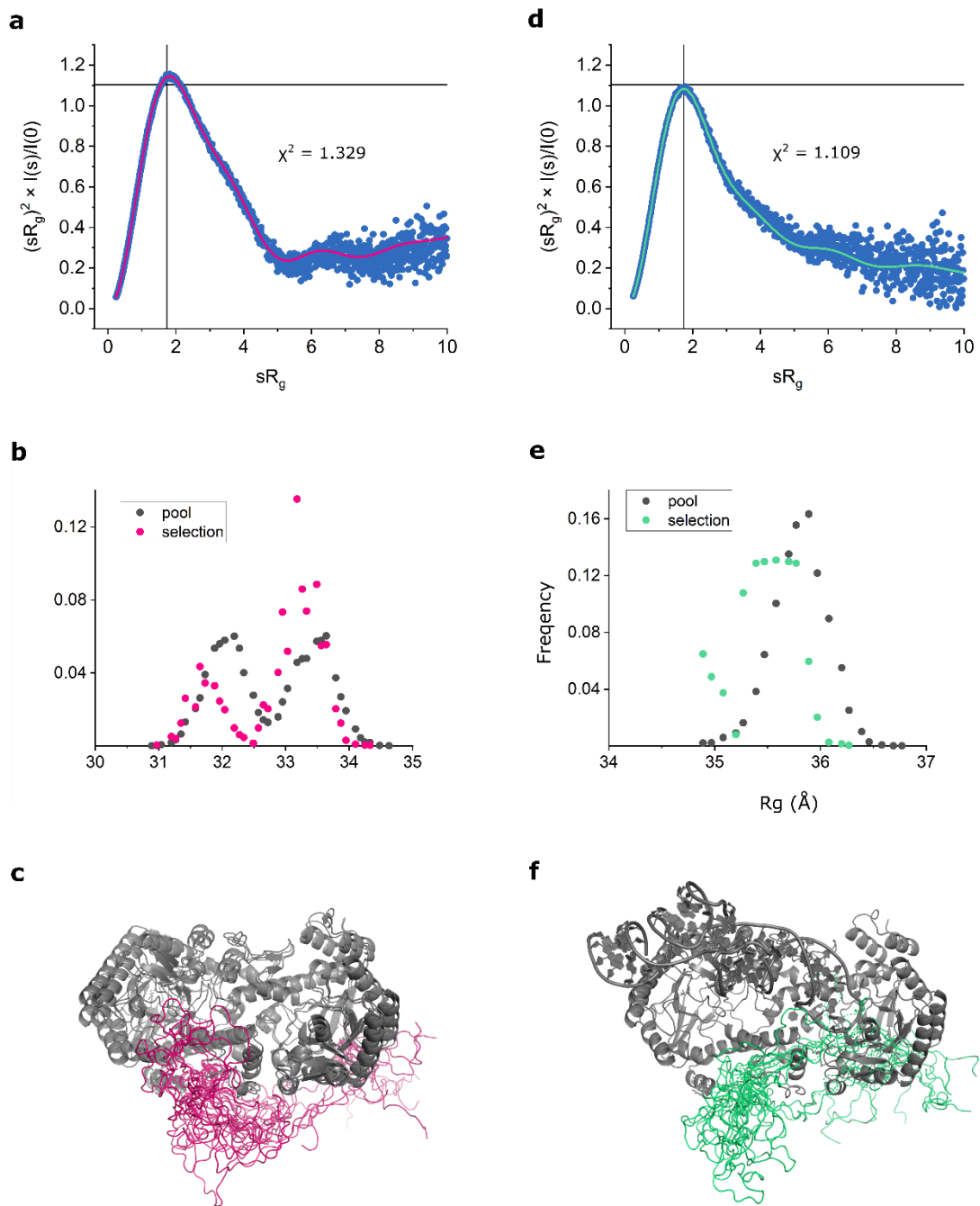
Figure 6: SAXS-based ensemble analysis of TGT and TGT·tRNA complex

a) Dimensionless Kratky-plot of TGT SAXS data, with theoretical scattering of an optimized ensemble that was selected from a mixed pool of structures based either on the cryo-EM structure reported in this work or a TGT crystal structure (PDB-ID: 7NQ4). The fit against the experimental data is expressed as χ^2. The crosshair marks $sR_g = \sqrt{3}$ and $(sR_g)^2 \times I(s)/I(0) = 3e^{-1}$. b) Distribution of the radii of gyration (R_g) of TGT structures in the mixed pool and the optimized ensemble selected from it. c) Ensemble structures selected from mixed pool. Domains modelled as a rigid body are shown in grey, disordered regions modelled as random chains are shown in magenta. d) Like a) but showing SAXS data of TGT·tRNA complex and the theoretical scattering of an optimized ensemble that was selected from a pool of structures based on the cryo-EM structure reported in this work. e) like b) but for TGT·tRNA complex. f) Like c) but for TGT·tRNA complex. Disordered regions modelled as random chains are shown in green.

3.3.5 tRNA binding sites are conserved among eukaryotes

Asking which of the structural elements discussed above are of general functional importance, we revisited sequence conservation using the ConSurf method[59]. Based on 150 homologous sequences evenly sampling the conservational spread, conservation scores were calculated for each amino acid position. In QTRT1, conserved residues are located mainly at the central $(\alpha\beta)_8$ barrel bearing the active site. Thus, amino acid conservation in QTRT1 is very similar to that of bacterial TGT (Figure 7b+d and Figure S7). Of the numerous insertions, helices αA (108-112) and αB (282-289) are particularly notable as both appear to be highly conserved. Helix αA bears active site residue P109 and closes off the active site during catalysis, while helix αB is the primary resting point for the anticodon loop, engaging in several intricate interactions with that particular part of the tRNA substrate. In contrast, K303, K304 and H335, which in the presented cryo-EM structure form hydrogen bonds to the backbone of the anticodon stem, are all poorly conserved.

Unlike QTRT1 and bacTGT, QTRT2 is characterized by a comparatively poorly conserved β-barrel core (Figure 7a). Highly conserved areas primarily involve the dimerization interface formed by its zinc-binding domain and selected residues of the tRNA binding motifs discussed above: Within the βEβF sheet, S114, G120 and R121 have the highest conservation scores. S114 is likely of structural importance, while G120 and R121 directly interact with the tRNA backbone. Among the several positively charged residues found within helix α4, only some are tightly conserved. K158, R157, K162 and R166, which point towards or directly interact with the tRNA's acceptor stem backbone in the reported cryo-EM structure, all have high to extremely high conservation scores, while R161, which points away, is conserved poorly. S156 and the short turn spanning residues 109-111, which were also observed to from hydrogen bonds to the tRNA backbone, are conserved at a medium level.

In contrast, regions that are not conserved include the disordered βGβH loop spanning QTRT2 residues 292-330. Inspection of the underlying multiple sequence alignment (supplied in supplement) reveals that this loop, while present in the vast majority of QTRT2 sequences, is not only variable in terms of amino acid composition but also varies dramatically in length, making it the most variable element of the subunit.
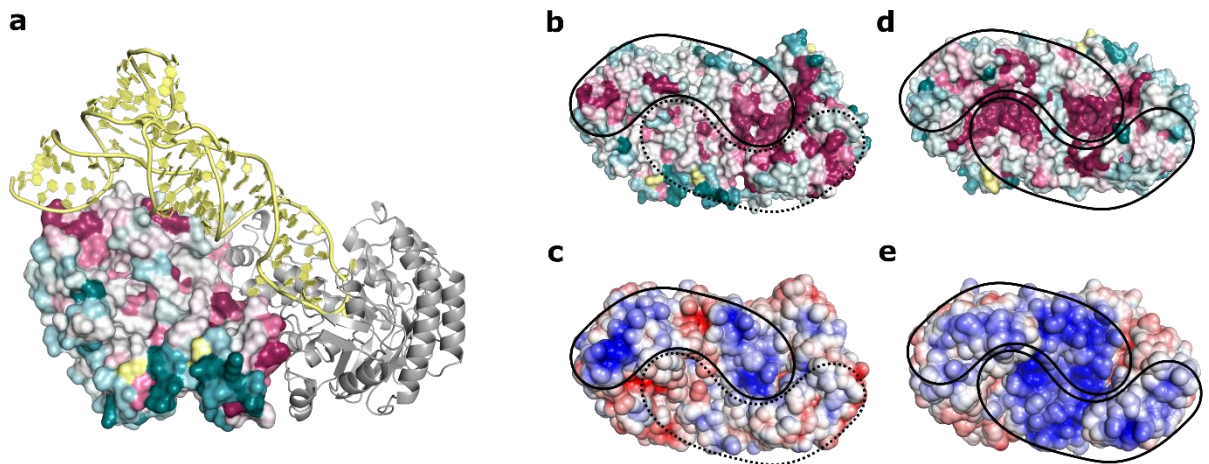
Figure 7: Amino acid conservation and surface electrostatics in TGT

a) Amino acid conservation of QTRT2, mapped onto the structure of human TGT in complex with tRNA. QTRT2 is shown in surface representation colored by conservation score (green: low conservation, pink: high conservation, yellow: insufficient data). b) Amino acid conservation of eukaryotic QTRT1 and QTRT2, mapped onto the structure of human TGT. Color key as in a). The functional (solid line) and degenerate (dotted) tRNA binding sites are outlined. c) Surface electrostatics of human TGT (blue: positive charge, red: negative charge). Binding site outlines as in b) d) Amino acid conservation of bacterial TGT, mapped onto the structure of Z. mobilis TGT (PDB-ID: 1Q2R). Color key as in a). The two alternative tRNA binding sites, inferred from the structure of human TGT·tRNA, are outlined. e) Surface electrostatics of Z. mobilis TGT (PDB-ID: 1Q2R), color key as in c). Binding site outlines as in d).

With the complete tRNA binding site of TGT finally known, we compared its surface electrostatics on eukaryotic and bacterial TGT, to better understand the adaptation of eukaryotic TGT to its heterodimeric architecture.

The overall appearance of surface charge is dominated by the differential constitution of eukaryotic and bacterial TGT: Due to it being a homodimer, the surface electrostatics of *Z. mobilis* TGT is characterized by 2-fold rotational symmetry, providing two identical, alternative tRNA binding orientations (Figure 7e and Figure S 8b). In contrast, human TGT is a heterodimer and its surface electrostatics are distinctly asymmetric: While the functional tRNA binding site features an overall positive charge, the degenerate would-be alternative is more neutrally charged and even has isolated patches of conserved negative charge (Figure 7c and Figure S8a).

The charge distribution within the effective binding site also varies between eukaryotic and bacterial TGT: The human binding site is clearly bipartite, featuring predominantly

positively charged patches around the QTRT1 active site and the acceptor stem binding site comprised mainly of QTRT2 helix α4. In *Z. mobilis* TGT, positive charge is continuous from the active site to the supporting subunit, but the positively charged area binding the tRNA body is limited largely to the 3-stranded βDβEβF motif.

3.4 Discussion

In this work we show that the TGT non-catalytic subunit QTRT2 supports substrate binding by direct interaction with the tRNA. These interactions are formed by three main binding motifs: The βEβF sheet (residues 112-125) which binds the tRNA core by the base of its D-arm, as well as the adjacent β3βE turn (109-111) and the N-terminal half of helix α4 (156-177) which both form hydrogen bonds with the 3' strand of the tRNA's acceptor stem. Both regions have previously been suspected to support tRNA binding, but structural information was lacking[42,57]. In addition to these main binding motifs, further hydrogen bonds were also found involving QTRT1 residues K303, K304 and H335.

The cryo-EM structure presented in this work reveals that the TGT·tRNA complex is based on extensive shape complementarity between TGT and its tRNA substrate. The buried interface between protein and RNA is 1874 Å² large and allows for more than 30 hydrogen bonds to form. The interaction between QTRT1 and tRNA anticodon stem loop is virtually identical to previous crystal structures of TGT and a stem loop RNA[42,47]. The additional contacts between tRNA and QTRT2 appear to be made possible by minor conformational changes of both TGT and tRNA: While the TGT-bound tRNA molecule features a different angle between its acceptor and anticodon arm than what is found in a tRNA[Asp] crystal structure (PDB-ID: 2TRA), the TGT has a larger diameter (97 Å) than what was previously observed of the free or stem loop-bound protein (92 Å). However, all previous information is based on crystal structures, making it unclear whether the difference in size is caused by tRNA binding or whether the more compact conformation in previous TGT crystal structures is due to crystal packing or dehydration effects. We collected SAXS data of free TGT in solution and found that a structure ensemble based predominantly or exclusively on the extended cryo-EM structure is more consistent with the data. Combining this information with the observed protein flexibility in the cryo-EM dataset and the subtle differences in the subunit-to-subunit arrangement in known TGT crystal structures, it can

be assumed that free TGT exists in an equilibrium of conformations which on average is significantly larger than its compacted crystal structures. Upon tRNA binding, an extended conformation is stabilized by the extensive contacts between tRNA and several regions of the protein. Of these contacts, those formed between tRNA and the QTRT2 βEβF sheet and adjacent β3βE turn appear to be mostly rigid. However, 3D Variability Analysis of the cryo-EM dataset had revealed that that the tRNA acceptor stem is surprisingly mobile despite the additional hydrogen bonds formed with positively charged residues of helix α4. This suggests that these contacts are itself loose or variable enough to not restrict this movement and may exist in several variations.

The contribution to free binding energy through both buried surface and hydrogen bonding suggested that the interface formed between QTRT2 and the tRNA body primarily serves to increase affinity between TGT and its tRNA substrates. We were able to confirm this experimentally by showing a significant difference in the equilibrium dissociation constant K_D and the Michaelis-Menten Constant K_M between a complete tRNA and stem loop RNA. In addition, we showed that full-length tRNA increases TGT thermostability more than stem loop RNA does, also suggesting the additional interface has a stabilizing effect on the complex formed. This is in contrast to a previous publication on eukTGT which reported no differences between the level of Q-incorporation into either tRNA or tRNA ASL[60]. However, while the authors used similar concentrations of both enzyme and RNA, they only measured endpoint values after 90 minutes and were thus unable to extract information on initial reaction velocities. Nevertheless, their data agrees with our observation and previous data on bacterial TGT in confirming that stem loop RNA featuring the correct $Y_{32}U_{33}G_{34}U_{35}$ recognition sequence is a viable substrate for TGT *in vitro*[52–54,60]. For this reason, several groups have looked for non-tRNA targets of Q-modification *in vivo*, but found that Q-modification is specific to tRNAs under cellular conditions[60,61]. It is very likely that the extensive contacts with the tRNA body ensure that $G_{34}U_{35}N_{36}$ tRNAs are the only RNAs being Q-modified. In this context it is also worth mentioning that TGT is a fairly slow enzyme (converting roughly 1 RNA molecule per minute): Although TGT is able to modify non-tRNA substrates at artificially high concentrations, this likely does not occur *in vivo*, simply because its affinity for non-tRNA substrates is too low. This makes TGT a highly specific enzyme, which is notable because

Q-incorporation is irreversible and no "eraser" or proofreading enzymes able to excise an erroneously incorporated queuine are known.

Extensive binding outside of the TGT active side might also be relevant because the tRNA anticodon stem loop has to adopt a very different conformation upon TGT binding compared to free tRNA and to deeply bury itself into the active site. It is possible that the QTRT2 contacts serve to loosely hold the tRNA in place while these conformational rearrangements occur. In this case, flexibility as observed in the cryo-EM data might be beneficial and even necessary for the anticodon stem loop to insert itself correctly into the active site.

The major contact sites between tRNA and QTRT2 (βEβF sheet and N-terminal half of α4 helix) are highly conserved among eukaryotes. Thus, the distribution of conserved residues in QTRT2 is very different from both QTRT1 and bacTGT, in which each subunit acts as both catalytic and non-catalytic subunit. In these proteins, conservation centers around the active site, which suggests that for the original, single gene product bacTGT, the pressure to conserve the active site region is the main driver of TGT evolution. In heterodimeric TGT, enzymatic activity and binding of the tRNA body are uncoupled to two separate genes, leaving both, and especially QTRT2 to specialize accordingly. Such specialization is also reflected in the respective charge distributions of bacTGT and eukTGT: While bacTGT (as a homodimer) has a 2-fold rotationally symmetric surface charge featuring two identical, positively charged tRNA binding sites, this is not the case for eukTGT. The original second, non-functional binding site features a more neutral to negative charge. This is likely to be very important, because, despite the degenerate active site of the QTRT2 subunits, the tertiary structures of both halves of the heterodimer are still very similar. If eukTGT did not evolve negative specificity elements, erroneous "reverse" binding would be inhibiting the enzyme: It is well known that only a single tRNA can bind to TGT at the same time. Therefore, tRNA bound to the degenerate binding site would block the second true binding site by steric hindrance, but unlike in bacTGT where the binding orientation does not matter because both subunits are catalytically active, such binding would be unproductive.

Another element that sets QTRT2 apart from its homologs is the insertion of a loop between βG and βH which appears to be intrinsically disordered. The sequence alignment of 150 representative sequences reveals many insertions at various locations, but only the βGβH

loop is present in almost all QTRT2 sequences, while occurring in neither QTRT1 nor bacTGT. Despite this, the actual sequence of this loop is not conserved and varies significantly between sequences, even in its length. An early idea regarding a potential function of this conspicuous loop was that it might adopt an ordered conformation upon tRNA binding and thus contribute to the interaction[41]. Now that a structure of the tRNA-bound TGT complex is available it is finally possible to rule out this possibility with certainty, as the βGβH loop is still largely disordered in the reported cryo-EM map. A second idea was that the presence of the loop might be related to the known mitochondrial association of eukTGT, possibly by an interaction with other surface-bound proteins. However, this idea likewise represented mere speculation and the very low degree of sequence-conservation makes a conserved, specific interaction fairly unlikely. The low sequence conservation might be an indication that that loop does not have a function at all, and that its presence is a coincidence rooting in its original insertion not being detrimental to eukTGT function. There is a fourth possibility however: Using ensemble optimization based on experimental SAXS data, we showed that the loop likely adopts many conformations of medium extension, occasionally flipping to the top site of the protein, where tRNA is bound. However, even these most extended structures strictly occupy the space of the degenerate, "reverse" binding site, not the true functional site on the opposite side of the protein. Perhaps, similar to the altered charge distribution and the flexible stretch (97-104) blocking the QTRT2 degenerate active site, the presence of a disordered loop is another negative specificity element which prevents binding of a tRNA to the wrong site of the TGT heterodimer. Such a function would be consistent with the structural ensemble and could explain why the presence of the loop is conserved but not its sequence, as the latter would be largely irrelevant.

In summary, we showed that tRNA is bound through multiple contact sites with both eukTGT subunits and interacts intimately with the non-catalytic subunit QTRT2. We uncovered two strongly conserved tRNA binding motifs interacting with different parts of the tRNA body. Their function is likely to raise the total affinity between TGT and tRNA to cross the threshold that makes the Q-incorporation reaction possible, not only in theory but also under *in vivo* conditions. Apart from adaptations to support tRNA binding and

increase binding affinity, we show that eukTGT is also equipped with negative specificity elements to prevent erroneous tRNA binding.

3.5 Methods

3.5.1 Protein purification

Human TGT heterodimer (QTRT1 and QTRT2) was co-expressed and purified as described previously[42]. Purified TGT was concentrated to 6-10 mg/mL, flash frozen in liquid nitrogen and stored at −80°C. For structural biology experiments, freshly purified protein, stored on ice for <24h, was used.

3.5.2 RNA constructs

Human tRNA[Asp] was transcribed *in vitro* as a sequence-modified construct optimized for transcription with T7 RNA polymerase (Table 4). Complimentary DNA templates were annealed to serve as a transcription template, the reverse complement strand carrying two 5' 2'-O-methyl RNA nucleotides for improved 3' homogeneity[62]. Large-scale (2×5 mL) *in vitro* transcription was carried out at 37 °C in 30 mM HEPES pH 8.0, 2 mM spermidine, 10 mM DTT, 40 mM MgCl$_2$, 4 mM rNTPs using 30 ng/µL template and 1 µM T7 polymerase.

The tRNA transcript was purified by gel-extraction from a 10% polyacrylamide gel containing 7M urea. The band containing the full-length tRNA transcript was cut from the gel, the gel slice crushed and the tRNA extracted to 10 mM HEPES pH 8.0, 1 mM EDTA, 300 mM NaCl by passive diffusion. RNA was precipitated with 70% (v/v) ethanol, centrifuged and re-dissolved in 10 mM HEPES pH 8.0, 1mM EDTA, 10 mM MgCl$_2$. The refolded tRNA was further purified by size exclusion chromatography in 20 mM HEPES pH 7.5, 100 mM NaCl using a S75 (600/16) column. Fractions containing correctly folded tRNA were pooled, concentrated to 3.5 mg/mL using a 3 kDa MWCO Amicon device (Merck) and flash-frozen in liquid nitrogen. RNA was stored at -80 °C until further use.

Alternatively, tRNA[Asp] was produced as described previously[42].

Stem loop RNAs mimicking the anticodon stem Loop of tRNA[Asp] and tRNA[Tyr] as well as a 20-mer polyadenine RNA were ordered as chemically synthesized RNAs (Axolabs, Kulmbach, Germany).

Table 4: RNA constructs used in this work

Name	Description	Sequence
*hs*tRNA^{Asp}	tRNA sequence based on human tRNA^{Asp}, bases 1-3, 69-71 modified for optimized *in vitro* transcription	AGGUCGUUAGUAUAGUGGUGAGUAUC CCCGCCUGUCACGCGGGAGACCGGGG UUCGAUUCCCCGACGGCCUGCCA
GGG-*hs*tRNA^{Asp}	tRNA^{Asp} with three additional G bases for optimized *in vitro* transcription	GGGUCCUCGUUAGUAUAGUGGUGAGU AUCCCGCCUGUCACGCGGGAGACCG GGGUUCGAUUCCCCGACGGGGAGCCA
*hs*tRNA^{Asp} ASL	Anticodon stem loop (bases 27-43) of *hs*tRNA^{Asp}, plus additional terminal G-C pair for optimized stem loop stability, chemically synthesized	GCCCGCCUGUCACGCGGGC
tRNA^{Tyr} ASL	anticodon stem loop (bases 26-43) based on tRNA^{Tyr}, stem sequence optimized for stability[47], chemically synthesized	AGCACGGCUGUAAACCGUGC
A20	Adenine 20-mer RNA, chemically synthesized	AAAAAAAAAAAAAAAAAAAA

3.5.3   Cryo-EM of hTGT·tRNA^{Asp} complex

For complex preparation, 32 μM TGT was mixed with 32 μM tRNA^{Asp} and 326 μM 9-deazaguanine in 20 mM HEPES pH 7.5, 100 mM NaCl. The mixture was incubated on ice for 20 h. The formed complex was concentrated to 5.6 mg/mL using a 30 kDa MWCO Amicon device and purified from its free constituents by size exclusion chromatography in 20 mM HEPES pH 7.5, 100 mM NaCl using a S200 3.2/300 Increase column at 4 °C.

Peak fractions were collected and 3 μl of TGT·tRNA^{Asp} complex (1 μg/μL) were applied onto freshly glow-discharged gold grids (UltrAuFoil R1.2/1.3) and plunge-frozen in liquid ethane using a Vitrobot Mark IV (Thermo Fisher Scientific). Micrographs of TGT·tRNA^{Asp} were recorded automatically (EPU) on a 200-kV Thermo Scientific Glacios cryo-transmission electron microscope (cryo-TEM) in electron counting mode with a Falcon 3EC direct electron detector (Thermo Scientific) at a nominal magnification of ×190,000 corresponding to a calibrated pixel size of 0.78 Å. Dose-fractionated movies were acquired at an electron flux of 0.8 e⁻ per pixel per s over 44.46 s distributed over 48 frames, corresponding to a total electron dose of ~62 e⁻ Å⁻². Movies were recorded in the defocus range from −1.0 to –2.0 μm (Supplementary table 1).

All image processing was done using cryoSPARC v 4.0 – 4.1 (Structura Biotechnology Inc.)[63]. Two datasets encompassing 680 and 706 (1,386 in total) movies were used for analysis. All movies were motion corrected using the patch motion correction as implemented in cryoSPARC. The contrast transfer function (CTF) was estimated using the patch CTF estimation method in cryoSPARC. Micrographs were manually curated and micrographs with unusually low CTF fit or high ice thickness were rejected, leaving 656 and 383 micrographs for the two datasets. Initial particles were picked from a 50-micrograph subset of dataset 1 using a blob picker (80-150 Å diameter). Particles were extracted at a box size of 256 px and subjected to 2D classification. Representative 2D class averages were chosen and used as inputs for templated particle picking from the complete dataset 1. Particles were extracted (256 px box) and cleaned by two rounds of 2D classification. An initial map was obtained from the cleaned particle stack using 3 class *ab initio* reconstruction, resulting in two "junk" maps and one "good" map. The initial maps were refined by hetero-refinement.

The refined correct map was used to generate 20 evenly spaced projections that were used as templates to pick particles from both datasets. Particles (656,321 and 387,323) were extracted at a box size of 64 px. Particles were cleaned separately by multiple rounds of 2D classification, leaving 354,373 and 162,276 particles. Particles were re-extracted at a box size of 256 px and cleaned further by 2D classification, leaving 324,311 and 154,241 particles. Particles from both datasets were combined and subjected to final cleaning by 2D classification, leaving a cleaned stack of 463,140 particles. Dataset 2 contained only particles of a single orientation, thus an initial map was obtained from the cleaned particles of dataset 1 only, using 3 class ab initio reconstruction. The initial maps were refined using hetero-refinement and the correct map was refined with all particles of both datasets, also using hetero-refinement. The map was further refined using homo-refinement and non-uniform refinement. FSC resolution was estimated using the final refined but not auto-tightened mask. Local resolution was estimated using the same mask. For model-building, the map was sharpened.

The final particle stack was analyzed using the 3D Variability Analysis (3DVA) in CryoSPARC[64]. For this, the particle stack was low-pass filtered to 8 Å to facilitate analysis of global and mid-range movement. Intermediates across each latent dimensions were

reconstructed and low pass filtered to 6 Å for visual analysis. Initial models for docking were obtained as follows: For the TGT protein, a crystal structure of human TGT (PDB-ID: 7NQ4) was used. A model of TGT-bound tRNA was built by combining the TGT-bound stem loop of the above crystal structure (PDB-ID: 7NQ4) and a model of yeast tRNA[Asp] (PDB-ID: 2TRA) and manually adjusting the resulting model's nucleotide sequence in Coot[65]. The two subunits of the TGT protein and the tRNA were separately fit into an initial low-resolution cryo-EM map using Chimera[66]. The model was refined against the final 3DFlex-reconstructed map by PHENIX real-space refinement and manual adjustment in Coot[65,67].

3.5.4   SAXS experiments

For SAXS experiments with TGT alone, freshly purified protein, stored on ice for 18h was used. For the complex, TGT was mixed with tRNA (*hs*tRNA or GGG-*hs*tRNA), stabilized with

9-deazaguanine and incubated on ice for 18h. SEC-SAXS data was collected at the P12 beamline operated by EMBL c/o DESY in Hamburg, Germany. Samples were separated in-line by size exclusion chromatography (Superdex 200 16/60 Increase) in 20 mM HEPES pH 7.5, 100 mM NaCl, 3% (w/v) glycerol, with the column outflow passed to the irradiation chamber of the beamline. The raw data was rotationally averaged, suitable sample frames were chosen and buffer-subtracted using data of the column flow-through. Primary data analysis was performed using the ATSAS software suite[68].

Pools of 5000 random-chain structures was generated using RANCH[69]. Structures were based on the TGT cryo-EM structure presented in this work or a previously published crystal structure (PDB-ID: 7NQ4). In both cases, QTRT1 residues 16-403 and QTRT2 residues 2-286, 332-414 were treated as rigid bodies and the remaining residues were modelled as random chains. For the TGT·tRNA complex, the cryo-EM derived model was adjusted to reflect the complete GGG-tRNA construct used and a structure pool was generated by again treating QTRT1 residues 16-403, QTRT2 residues 2-286 as well as 332-414 as rigid bodies and modeling the remaining regions as random chains. Iterative ensemble selection and optimization against SAXS data was achieved using GAJOE[69].

3.5.5 *Fluorescence polarization affinity test*

Fluorescein-labelled tRNA[Asp] was produced as described previously[40,42]. Several short RNAs (Table 4) were purchased from Axolabs (Kulmbach, Germany) and fluorescein-labelled by the same method.

The binding of fluorescein-labelled RNA constructs to TGT was measured by fluorescence polarization spectroscopy. For each RNA construct, 20 nM fluorescein-RNA was mixed with up to 120 µM TGT in 20 mM HEPES pH 7.5, 100 mM NaCl and incubated for 5 minutes at room temperature. The final sample volume was 50 µL. Fluorescence polarization was measured using a VICTOR Nivo Multimode Microplate Reader (PerkinElmer). The excitation wavelength was 480 nm (30 nm slit), and the emission was detected at wavelength 530 nm (30 nm slit) for 500 ms. Each experiment was performed in triplicates.

The function of measured polarization versus total protein concentration was fitted by non-linear regression with an asymmetric dose-response equation (5-parameter logistic fit) using the software OriginPro:

$$y = A_{min} + \frac{A_{max} - A_{min}}{\left(1 + \left(\frac{x}{x_0}\right)^{-h}\right)^s}$$

where

y = measured polarization

A_{min} = lower asymtote

A_{max} = upper asymptote

x = protein concentration

x_0 = inflection point

h = Hill slope

s = control factor

EC50 was calculated as x, where $y = \frac{A_{max}}{2}$

For data visualization purposes, each curve was normalized by setting A_{max} to 100 and A_{min} to 0:

$$y_{norm} = 100 \left(\frac{y - A_{min}}{A_{max}} \right)$$

Curves depicting the raw (not normalized) data and curve fits are supplied in Figure S4.

3.5.6 Thermal shift assay

Different RNA constructs were examined for their effect on TGT thermostability using a thermal shift assay. For each RNA construct, 2.64 µM RNA were mixed with 1.32 µM TGT in 20 mM HEPES pH 7.5, 100 mM NaCl, 200 mM dithiothreitol and incubated on ice for 30 min. Protein incubated with buffer only was used as a control. Each sample was prepared in triplicates. 2× SYPRO orange (diluted from a 5000x preparation by ThermoFisher Scientific), was added to each sample, giving a final sample volume of 20 µL. Samples were transferred to 96-microplate wells and subjected to thermal denaturation in a real time PCR cycler equipped with a CFX96 optical reaction module (Bio-Rad) by applying a temperature gradient from 20-95 °C and a rate of 1°C/min. The fluorescence of the SYPRO orange probe was determined every minute using an excitation wavelength of 492 nm and an emission wavelength of 526 nm.

The measured fluorescence emission was plotted as a function of temperature, fitted and normalized using a method described previously[70]. The T_M of each sample was estimated as the inflection point of its melting curve. For each sample type, the average and standard deviation was calculated from three triplicates.

3.5.7 Acrylamidophenylboronic acid gel-based activity tests and kinetics

The TGT-catalyzed incorporation of queuine into either hstRNA[Asp] or hstRNA[Asp] ASL was measured using a gel-based activity test. For both RNA constructs, RNA (various concentrations) was mixed with 7.2 mM queuine and 0.29 µM TGT in 16 mM HEPES pH 7.5, 80 mM NaCl, 5 mM DTT. Each 50 µL reaction was incubated at 37 °C. The reactions were sampled after 1, 2, 3, 5, 10, 20 and 30 min reaction time and each 5 µL sample was immediately mixed with 2x RNA loading dye (New England Biolabs) containing 47.5 % formamide.

Samples were stored at -20 °C until further use. Q-modified RNA was detected by separating each sample along a 10% polyacrylamide gel supplemented with 7M urea and 5 mg/mL 3-(acrylamide)phenylboronic acid before polymerization[71].

For each lane, the retarded Q-RNA band, as well as total RNA were quantified using the GelAnalyzer software [72]. The raw intensities of the Q-RNA bands were converted to fractions:

$$Q = \frac{I_{QRNA}}{I_{RNAtotal}}$$

where

I_{QRNA} = raw intensity Q-RNA band

$I_{RNAtotal}$ = raw intensity total RNA

For each reaction and time point, the concentration of Q-RNA in the sample was calculated using the initial RNA concentration:

$$C_{QRNA} = C_{initial} \times Q$$

where

$C_{initial}$ = initial concentration of substrate RNA

The concentration of Q-RNA was plotted as a function of reaction time to yield time course (progress) curves for each reaction. For each curve, the initial velocity was determined by performing a linear fit of the initial data points. Initial velocities were plotted as functions of initial RNA substrate concentrations and fitted with the Michaelis-Menten equation using non-linear regression (OriginPro software):

$$V = \frac{V_{max} \times [S]}{K_M + [S]}$$

where

V = reaction rate

V_{max}= maximum reaction speed

$[S]$ = substrae concentration

K_M= Michaelis constant

V_{max} was divided by the enzyme concentration (1 active site per dimer) to obtain the turnover number k_{cat}.

3.5.8   Calculation of conservation scores

Amino acid conservation scores of human and *Z. mobilis* TGT were used using the ConSurf web server[59]. Homologous sequences were selected from the UNIREF-90 data base using HMMER[73,74] as implemented on the ConSurf web server. For each search, the E-value cut-off was chosen to clearly differentiate between the homologous sequences of QTRT1 (E=1×10[-110]), QTRT2 (E=1×10^{-42}) and bacterial TGT (E=1×10[-100]). 150 sequences were automatically selected to sample the list of homologs using the standard parameters implemented on the ConSurf web server. From the selected sequences, a multiple sequence alignment (MSA) was built using MAFFT-L-INS-I [75]. Evolutionary conservation scores were calculated using the standard Bayesian method implemented on the ConSurf web server. Conservation scores were mapped onto the cryo-EM structure of human TGT presented in this work, or the previously published crystal structure of *Z. mobilis* TGT (PDB-ID: 1Q2R) and visualized as a color gradient using PyMol[76].

3.5.9   Calculation of surface electrostatics

Surface electrostatics were calculated using the Adaptive Poisson-Boltzmann method (APBS) as implemented within PyMOL[77].

3.6   Acknowledgements

3.7 Declaration of interests

The authors declare no competing interests.

3.8 Data and availability

The density map and model of the TGT·tRNA^{Asp} complex have been deposited at EMDB (ID: EMD-16976) and PDB (ID: 8OMR) and are publicly available as of the date of publication. Small angle X-ray scattering data, models and fits of apo TGT and the TGT·tRNA^{Asp} complex have been deposited at SASDB (IDs: SASDRB8 and SASDRC8) and are publicly available as of the date of publication. The results of 3D Variability Analysis are supplied as supplementary videos. Gel images used for Q-incorporation reaction kinetics, fitted raw fluorescence polarization curves, multiple sequence alignments and ConSurf results are supplied as supplementary figures and items. Any additional information or raw data required to re-analyze the data reported in this paper is available from the corresponding author upon request.

3.9 References

1. Harada, F., and Nishimura, S. (1972). Possible anticodon sequences of tRNAHis, tRNAAsn, and tRNAAsp from Escherichia coli. Universal presence of nucleoside Q in the first position of the anticodons of these transfer ribonucleic acid. Biochemistry *11*, 301–308. 10.1021/bi00752a024.

2. Meier, F., Suter, B., Grosjean, H., Keith, G., and Kubli, E. (1985). Queuosine modification of the wobble base in tRNAHis influences 'in vivo' decoding properties. EMBO J. *4*, 823–827. 10.1002/j.1460-2075.1985.tb03704.x.

3. Zaborske, J.M., DuMont, V.L.B., Wallace, E.W.J., Pan, T., Aquadro, C.F., and Drummond, D.A. (2014). A Nutrient-Driven tRNA Modification Alters Translational Fidelity and Genome-wide Protein Coding across an Animal Genus. PLOS Biol. *12*, e1002015. 10.1371/journal.pbio.1002015.

4. Tuorto, F., Legrand, C., Cirzi, C., Federico, G., Liebers, R., Müller, M., Ehrenhofer-Murray, A.E., Dittmar, G., Gröne, H.-J., and Lyko, F. (2018). Queuosine-modified tRNAs confer nutritional control of protein translation. EMBO J. *37*, e99777. 10.15252/embj.201899777.

5. Müller, M., Legrand, C., Tuorto, F., Kelly, V.P., Atlasi, Y., Lyko, F., and Ehrenhofer-Murray, A.E. (2019). Queuine links translational control in eukaryotes to a micronutrient from bacteria. Nucleic Acids Res. *47*, 3711–3727. 10.1093/nar/gkz063.

6. Dixit, S., Kessler, A.C., Henderson, J., Pan, X., Zhao, R., D'Almeida, G.S., Kulkarni, S., Rubio, M.A.T., Hegedűsová, E., Ross, R.L., et al. (2021). Dynamic queuosine changes in tRNA couple nutrient levels to codon choice in Trypanosoma brucei. Nucleic Acids Res. *49*, 12986–12999. 10.1093/nar/gkab1204.

7. Manickam, N., Joshi, K., Bhatt, M.J., and Farabaugh, P.J. (2016). Effects of tRNA modification on translational accuracy depend on intrinsic codon–anticodon strength. Nucleic Acids Res. *44*, 1871–1881.

8. Kulkarni, S., Rubio, M.A.T., Hegedűsová, E., Ross, R.L., Limbach, P.A., Alfonzo, J.D., and Paris, Z. (2021). Preferential import of queuosine-modified tRNAs into Trypanosoma brucei mitochondrion is critical for organellar protein synthesis. Nucleic Acids Res. *49*, 8247–8260. 10.1093/nar/gkab567.

9. Hayes, P., Fergus, C., Ghanim, M., Cirzi, C., Burtnyak, L., McGrenaghan, C.J., Tuorto, F., Nolan, D.P., and Kelly, V.P. (2020). Queuine Micronutrient Deficiency Promotes Warburg Metabolism and Reversal of the Mitochondrial ATP Synthase in Hela Cells. Nutrients *12*, 871. 10.3390/nu12030871.

10. Marks, T., and Farkas, W.R. (1997). Effects of a Diet Deficient in Tyrosine and Queuine on Germfree Mice. Biochem. Biophys. Res. Commun. *230*, 233–237. 10.1006/bbrc.1996.5768.

11. Rakovich, T., Boland, C., Bernstein, I., Chikwana, V.M., Iwata-Reuyl, D., and Kelly, V.P. (2011). Queuosine Deficiency in Eukaryotes Compromises Tyrosine Production through Increased Tetrahydrobiopterin Oxidation. J. Biol. Chem. *286*, 19354–19363. 10.1074/jbc.M111.219576.

12. Müller, M., Hartmann, M., Schuster, I., Bender, S., Thüring, K.L., Helm, M., Katze, J.R., Nellen, W., Lyko, F., and Ehrenhofer-Murray, A.E. (2015). Dynamic modulation of Dnmt2-dependent tRNA methylation by the micronutrient queuine. Nucleic Acids Res. *43*, 10952–10962. 10.1093/nar/gkv980.

13. Ehrenhofer-Murray, A.E. (2017). Cross-Talk between Dnmt2-Dependent tRNA Methylation and Queuosine Modification. Biomolecules *7*, 14. 10.3390/biom7010014.

14. Johannsson, S., Neumann, P., Wulf, A., Welp, L.M., Gerber, H.-D., Krull, M., Diederichsen, U., Urlaub, H., and Ficner, R. (2018). Structural insights into the stimulation of S. pombe Dnmt2 catalytic efficiency by the tRNA nucleoside queuosine. Sci. Rep. *8*, 8880. 10.1038/s41598-018-27118-5.

15. Wang, X., Matuszek, Z., Huang, Y., Parisien, M., Dai, Q., Clark, W., Schwartz, M.H., and Pan, T. (2018). Queuosine modification protects cognate tRNAs against ribonuclease cleavage. RNA *24*, 1305–1313. 10.1261/rna.067033.118.

16. Durand, J.M., Okada, N., Tobe, T., Watarai, M., Fukuda, I., Suzuki, T., Nakata, N., Komatsu, K., Yoshikawa, M., and Sasakawa, C. (1994). vacC, a virulence-associated chromosomal locus of Shigella flexneri, is homologous to tgt, a gene encoding tRNA-

guanine transglycosylase (Tgt) of Escherichia coli K-12. J. Bacteriol. *176*, 4627–4634. 10.1128/jb.176.15.4627-4634.1994.

17. Durand, J.M.B., Dagberg, B., Uhlin, B.E., and Björk, G.R. (2000). Transfer RNA modification, temperature and DNA superhelicity have a common target in the regulatory network of the virulence of Shigella flexneri: the expression of the virF gene. Mol. Microbiol. *35*, 924–935. 10.1046/j.1365-2958.2000.01767.x.

18. Kasai, H., Ohashi, Z., Harada, F., Nishimura, S., Oppenheimer, N.J., Crain, P.F., Liehr, J.G., Von Minden, D.L., and McCloskey, J.A. (1975). Structure of the modified nucleoside Q isolated from Escherichia coli transfer ribonucleic acid. 7-(4,5-cis-Dihydroxy-1-cyclopenten-3-ylaminomethyl)-7-deazaguanosine. Biochemistry *14*, 4198–4208. 10.1021/bi00690a008.

19. Yokoyama, S., Miyazawa, T., Iitaka, Y., Yamaizumi, Z., Kasai, H., and Nishimura, S. (1979). Three-dimensional structure of hyper-modified nucleoside Q located in the wobbling position of tRNA. Nature *282*, 107–109. 10.1038/282107a0.

20. Fergus, C., Barnes, D., Alqasem, M.A., and Kelly, V.P. (2015). The Queuine Micronutrient: Charting a Course from Microbe to Man. Nutrients *7*, 2897–2929. 10.3390/nu7042897.

21. Chikwana, V.M., Stec, B., Lee, B.W.K., Crécy-Lagard, V. de, Iwata-Reuyl, D., and Swairjo, M.A. (2012). Structural Basis of Biological Nitrile Reduction. J. Biol. Chem. *287*, 30560–30570. 10.1074/jbc.M112.388538.

22. Dowling, D.P., Bruender, N.A., Young, A.P., McCarty, R.M., Bandarian, V., and Drennan, C.L. (2014). Radical SAM enzyme QueE defines a new minimal core fold and metal-dependent mechanism. Nat. Chem. Biol. *10*, 106–112. 10.1038/nchembio.1426.

23. Lee, B.W.K., Van Lanen, S.G., and Iwata-Reuyl, D. (2007). Mechanistic Studies of Bacillus subtilis QueF, the Nitrile Oxidoreductase Involved in Queuosine Biosynthesis. Biochemistry *46*, 12844–12854. 10.1021/bi701265r.

24. McCarty, R.M., Somogyi, Á., and Bandarian, V. (2009). *Escherichia coli* QueD Is a 6-Carboxy-5,6,7,8-tetrahydropterin Synthase. Biochemistry *48*, 2301–2303. 10.1021/bi9001437.

25. McCarty, R.M., Somogyi, Á., Lin, G., Jacobsen, N.E., and Bandarian, V. (2009). The Deazapurine Biosynthetic Pathway Revealed: In Vitro Enzymatic Synthesis of PreQ0 from Guanosine 5′-Triphosphate in Four Steps. Biochemistry *48*, 3847–3852. 10.1021/bi900400e.

26. Phillips, G., El Yacoubi, B., Lyons, B., Alvarez, S., Iwata-Reuyl, D., and de Crécy-Lagard, V. (2008). Biosynthesis of 7-Deazaguanosine-Modified tRNA Nucleosides: a New Role for GTP Cyclohydrolase I. J. Bacteriol. *190*, 7876–7884. 10.1128/JB.00874-08.

27. Van Lanen, S.G., Reader, J.S., Swairjo, M.A., de Crécy-Lagard, V., Lee, B., and Iwata-Reuyl, D. (2005). From cyclohydrolase to oxidoreductase: Discovery of nitrile reductase activity in a common fold. Proc. Natl. Acad. Sci. *102*, 4264–4269. 10.1073/pnas.0408056102.

28. Okada, N., Noguchi, S., Kasai, H., Shindo-Okada, N., Ohgi, T., Goto, T., and Nishimura, S. (1979). Novel mechanism of post-transcriptional modification of tRNA. Insertion of bases of Q precursors into tRNA by a specific tRNA transglycosylase reaction. J. Biol. Chem. *254*, 3067–3073. 10.1016/S0021-9258(17)30183-7.

29. Dowling, D.P., Miles, Z.D., Köhrer, C., Maiocco, S.J., Elliott, S.J., Bandarian, V., and Drennan, C.L. (2016). Molecular basis of cobalamin-dependent RNA modification. Nucleic Acids Res., gkw806. 10.1093/nar/gkw806.

30. Frey, B., McCloskey, J., Kersten, W., and Kersten, H. (1988). New function of vitamin B12: cobamide-dependent reduction of epoxyqueuosine to queuosine in tRNAs of Escherichia coli and Salmonella typhimurium. J. Bacteriol. *170*, 2078–2082. 10.1128/jb.170.5.2078-2082.1988.

31. Grimm, C., Ficner, R., Sgraja, T., Haebel, P., Klebe, G., and Reuter, K. (2006). Crystal structure of Bacillus subtilis S-adenosylmethionine:tRNA ribosyltransferase-isomerase. Biochem. Biophys. Res. Commun. *351*, 695–701. 10.1016/j.bbrc.2006.10.096.

32. Mathews, I., Schwarzenbacher, R., McMullan, D., Abdubek, P., Ambing, E., Axelrod, H., Biorac, T., Canaves, J.M., Chiu, H.-J., Deacon, A.M., et al. (2005). Crystal structure of S-adenosylmethionine:tRNA ribosyltransferase-isomerase (QueA) from Thermotoga maritima at 2.0 Å resolution reveals a new fold. Proteins Struct. Funct. Bioinforma. *59*, 869–874. 10.1002/prot.20419.

33. Miles, Z.D., McCarty, R.M., Molnar, G., and Bandarian, V. (2011). Discovery of epoxyqueuosine (oQ) reductase reveals parallels between halorespiration and tRNA modification. Proc. Natl. Acad. Sci. *108*, 7368–7372. 10.1073/pnas.1018636108.

34. Payne, K.A.P., Fisher, K., Sjuts, H., Dunstan, M.S., Bellina, B., Johannissen, L., Barran, P., Hay, S., Rigby, S.E.J., and Leys, D. (2015). Epoxyqueuosine Reductase Structure Suggests a Mechanism for Cobalamin-dependent tRNA Modification. J. Biol. Chem. *290*, 27572–27581. 10.1074/jbc.M115.685693.

35. Slany, R.K., Bösl, M., and Kersten, H. (1994). Transfer and isomerization of the ribose moiety of AdoMet during the biosynthesis of queuosine tRNAs, a new unique reaction catalyzed by the QueA protein from Escherichia coli. Biochimie *76*, 389–393. 10.1016/0300-9084(94)90113-9.

36. Van Lanen, S.G., and Iwata-Reuyl, D. (2003). Kinetic Mechanism of the tRNA-Modifying Enzyme S-Adenosylmethionine:tRNA Ribosyltransferase-Isomerase (QueA). Biochemistry *42*, 5312–5320. 10.1021/bi034197u.

37. Patel, B.I., Heiss, M., Samel-Pommerencke, A., Carell, T., and Ehrenhofer-Murray, A.E. (2022). Queuosine salvage in fission yeast by Qng1-mediated hydrolysis to queuine. Biochem. Biophys. Res. Commun. *624*, 146–150. 10.1016/j.bbrc.2022.07.104.

38. Sarid, L., Sun, J., Chittrakanwong, J., Trebicz-Geffen, M., Ye, J., Dedon, P.C., and Ankri, S. (2022). Queuine Salvaging in the Human Parasite Entamoeba histolytica. Cells *11*, 2509. 10.3390/cells11162509.

39. Hung, S.-H., Elliott, G.I., Ramkumar, T.R., Burtnyak, L., McGrenaghan, C.J., Alkuzweny, S., Quaiyum, S., Iwata-Reuyl, D., Pan, X., Green, B.D., et al. (2023). Structural basis of Qng1-mediated salvage of the micronutrient queuine from queuosine-5'-monophosphate as the biological substrate. Nucleic Acids Res. *51*, 935–951. 10.1093/nar/gkac1231.

40. Johannsson, S., Neumann, P., and Ficner, R. (2018). Crystal Structure of the Human tRNA Guanine Transglycosylase Catalytic Subunit QTRT1. Biomolecules *8*, 81. 10.3390/biom8030081.

41. Behrens, C., Biela, I., Petiot-Bécard, S., Botzanowski, T., Cianférani, S., Sager, C.P., Klebe, G., Heine, A., and Reuter, K. (2018). Homodimer Architecture of QTRT2, the Noncatalytic Subunit of the Eukaryotic tRNA-Guanine Transglycosylase. Biochemistry *57*, 3953–3965. 10.1021/acs.biochem.8b00294.

42. Sievers, K., Welp, L., Urlaub, H., and Ficner, R. (2021). Structural and functional insights into human tRNA guanine transgylcosylase. RNA Biol. *18*, 382–396. 10.1080/15476286.2021.1950980.

43. Ishitani, R., Nureki, O., Nameki, N., Okada, N., Nishimura, S., and Yokoyama, S. (2003). Alternative Tertiary Structure of tRNA for Recognition by a Posttranscriptional Modification Enzyme. Cell *113*, 383–394. 10.1016/S0092-8674(03)00280-0.

44. Ishitani, R., Nureki, O., Fukai, S., Kijimoto, T., Nameki, N., Watanabe, M., Kondo, H., Sekine, M., Okada, N., Nishimura, S., et al. (2002). Crystal Structure of Archaeosine tRNA-guanine Transglycosylase. J. Mol. Biol. *318*, 665–677. 10.1016/S0022-2836(02)00090-6.

45. Ritschel, T., Atmanene, C., Reuter, K., Van Dorsselaer, A., Sanglier-Cianferani, S., and Klebe, G. (2009). An Integrative Approach Combining Noncovalent Mass Spectrometry, Enzyme Kinetics and X-ray Crystallography to Decipher Tgt Protein-Protein and Protein-RNA Interaction. J. Mol. Biol. *393*, 833–847. 10.1016/j.jmb.2009.07.040.

46. Chen, Y.-C., Kelly, V.P., Stachura, S.V., and Garcia, G.A. (2010). Characterization of the human tRNA-guanine transglycosylase: Confirmation of the heterodimeric subunit structure. RNA *16*, 958–968. 10.1261/rna.1997610.

47. Xie, W., Liu, X., and Huang, R.H. (2003). Chemical trapping and crystal structure of a catalytic tRNA guanine transglycosylase covalent intermediate. Nat. Struct. Mol. Biol. *10*, 781–788. 10.1038/nsb976.

48. Goodenough-Lashua, D.M., and Garcia, G.A. (2003). tRNA–guanine transglycosylase from E. coli: a ping-pong kinetic mechanism is consistent with nucleophilic catalysis. Bioorganic Chem. *31*, 331–344. 10.1016/S0045-2068(03)00069-5.

49. Farkas, W.R., Jacobson, K.B., and Katze, J.R. (1984). Substrate and inhibitor specificity of tRNA-guanine ribosyltransferase. Biochim. Biophys. Acta BBA - Gene Struct. Expr. *781*, 64–75. 10.1016/0167-4781(84)90124-6.

50. Sebastiani, M., Behrens, C., Dörr, S., Gerber, H.-D., Benazza, R., Hernandez-Alba, O., Cianférani, S., Klebe, G., Heine, A., and Reuter, K. (2022). Structural and Biochemical Investigation of the Heterodimeric Murine tRNA-Guanine Transglycosylase. ACS Chem. Biol. *17*, 2229–2247. 10.1021/acschembio.2c00368.

51. Boland, C., Hayes, P., Santa-Maria, I., Nishimura, S., and Kelly, V.P. (2009). Queuosine Formation in Eukaryotic tRNA Occurs via a Mitochondria-localized Heteromeric Transglycosylase*. J. Biol. Chem. *284*, 18218–18227. 10.1074/jbc.M109.002477.

52. Curnow, A.W., Kung, F.L., Koch, K.A., and Garcia, G.A. (1993). tRNA-guanine transglycosylase from Escherichia coli: Gross tRNA structural requirements for recognition. Biochemistry *32*, 5239–5246. 10.1021/bi00070a036.

53. Curnow, A.W., and Garcia, G.A. (1995). tRNA-guanine Transglycosylase from Escherichia coli: MINIMAL tRNA STRUCTURE AND SEQUENCE REQUIREMENTS FOR RECOGNITION *. J. Biol. Chem. *270*, 17264–17267. 10.1074/jbc.270.29.17264.

54. Nakanishi, S., Ueda, T., Hori, H., Yamazaki, N., Okada, N., and Watanabe, K. (1994). A UGU sequence in the anticodon loop is a minimum requirement for recognition by Escherichia coli tRNA-guanine transglycosylase. J. Biol. Chem. *269*, 32221–32225. 10.1016/S0021-9258(18)31624-7.

55. Hurt, J.K., Olgen, S., and Garcia, G.A. (2007). Site-specific modification of Shigella flexneri virF mRNA by tRNA-guanine transglycosylase in vitro. Nucleic Acids Res. *35*, 4905–4913. 10.1093/nar/gkm473.

56. Grosjean, H., Edqvist, J., Stråby, K.B., and Giegé, R. (1996). Enzymatic Formation of Modified Nucleosides in tRNA: Dependence on tRNA Architecture. J. Mol. Biol. *255*, 67–85. 10.1006/jmbi.1996.0007.

57. Stengl, B., Meyer, E.A., Heine, A., Brenk, R., Diederich, F., and Klebe, G. (2007). Crystal Structures of tRNA-guanine Transglycosylase (TGT) in Complex with Novel and Potent Inhibitors Unravel Pronounced Induced-fit Adaptations and Suggest Dimer Formation Upon Substrate Binding. J. Mol. Biol. *370*, 492–511. 10.1016/j.jmb.2007.04.008.

58. Krissinel, E., and Henrick, K. (2007). Inference of macromolecular assemblies from crystalline state. J. Mol. Biol. *372*, 774–797. 10.1016/j.jmb.2007.05.022.

59. Ashkenazy, H., Abadi, S., Martz, E., Chay, O., Mayrose, I., Pupko, T., and Ben-Tal, N. (2016). ConSurf 2016: an improved methodology to estimate and visualize evolutionary conservation in macromolecules. Nucleic Acids Res. *44*, W344–W350. 10.1093/nar/gkw408.

60. Fergus, C., Al-qasem, M., Cotter, M., McDonnell, C.M., Sorrentino, E., Chevot, F., Hokamp, K., Senge, M.O., Southern, J.M., Connon, S.J., et al. (2021). The human tRNA-guanine transglycosylase displays promiscuous nucleobase preference but strict tRNA specificity. Nucleic Acids Res. *49*, 4877–4890. 10.1093/nar/gkab289.

61. Bessler, L., Kaur, N., Vogt, L.-M., Flemmich, L., Siebenaller, C., Winz, M.-L., Tuorto, F., Micura, R., Ehrenhofer-Murray, A.E., and Helm, M. (2022). Functional integration of a semi-synthetic azido-queuosine derivative into translation and a tRNA modification circuit. Nucleic Acids Res. *50*, 10785–10800. 10.1093/nar/gkac822.

62. Turunen, J.J., Pavlova, L.V., Hengesbach, M., Helm, M., Müller, S., Hartmann, R.K., and Frilander, M.J. (2014). Generating Homogeneous Acceptor 3'-Ends for Ligation. In Handbook of RNA Biochemistry. Second, Completely Revised and Enlarged Edition (Wiley-VCH Verlag GmbH & Co.), pp. 53–54.

63. Punjani, A., Rubinstein, J.L., Fleet, D.J., and Brubaker, M.A. (2017). cryoSPARC: algorithms for rapid unsupervised cryo-EM structure determination. Nat. Methods *14*, 290–296. 10.1038/nmeth.4169.

64. Punjani, A., and Fleet, D.J. (2021). 3D variability analysis: Resolving continuous flexibility and discrete heterogeneity from single particle cryo-EM. J. Struct. Biol. *213*, 107702. 10.1016/j.jsb.2021.107702.

65. Emsley, P., Lohkamp, B., Scott, W.G., and Cowtan, K. (2010). Features and development of *Coot*. Acta Crystallogr. D Biol. Crystallogr. *66*, 486–501. 10.1107/S0907444910007493.

66. Pettersen, E.F., Goddard, T.D., Huang, C.C., Couch, G.S., Greenblatt, D.M., Meng, E.C., and Ferrin, T.E. (2004). UCSF Chimera--a visualization system for exploratory research and analysis. J. Comput. Chem. *25*, 1605–1612. 10.1002/jcc.20084.

67. Afonine, P.V., Poon, B.K., Read, R.J., Sobolev, O.V., Terwilliger, T.C., Urzhumtsev, A., and Adams, P.D. (2018). Real-space refinement in PHENIX for cryo-EM and crystallography. Acta Crystallogr. Sect. Struct. Biol. *74*, 531–544. 10.1107/S2059798318006551.

68. Manalastas-Cantos, K., Konarev, P.V., Hajizadeh, N.R., Kikhney, A.G., Petoukhov, M.V., Molodenskiy, D.S., Panjkovich, A., Mertens, H.D.T., Gruzinov, A., Borges, C., et al. (2021). ATSAS 3.0: expanded functionality and new tools for small-angle scattering data analysis. J. Appl. Crystallogr. *54*, 343–355. 10.1107/S1600576720013412.

69. Tria, G., Mertens, H.D.T., Kachala, M., and Svergun, D.I. (2015). Advanced ensemble modelling of flexible macromolecules using X-ray solution scattering. IUCrJ *2*, 207–217. 10.1107/S205225251500202X.

70. Chari, A., Haselbach, D., Kirves, J.-M., Ohmer, J., Paknia, E., Fischer, N., Ganichkin, O., Möller, V., Frye, J.J., Petzold, G., et al. (2015). ProteoPlex: stability optimization of macromolecular complexes by sparse-matrix screening of chemical space. Nat. Methods *12*, 859–865. 10.1038/nmeth.3493.

71. Igloi, G.L., and Kössel, H. (1985). Affinity electrophoresis for monitoring terminal phosphorylation and the presence of queuosine in RNA. Application of polyacrylamide containing a covalently bound boronic acid. Nucleic Acids Res. *13*, 6881–6898. 10.1093/nar/13.19.6881.

72. Lazar, I.J., and Lazar, I.S. (2019). GelAnalyzer.

73. Finn, R.D., Clements, J., and Eddy, S.R. (2011). HMMER web server: interactive sequence similarity searching. Nucleic Acids Res. *39*, W29–W37. 10.1093/nar/gkr367.

74. Suzek, B.E., Wang, Y., Huang, H., McGarvey, P.B., Wu, C.H., and the UniProt Consortium (2015). UniRef clusters: a comprehensive and scalable alternative for improving sequence similarity searches. Bioinformatics *31*, 926–932. 10.1093/bioinformatics/btu739.

75. Katoh, K., Rozewicki, J., and Yamada, K.D. (2019). MAFFT online service: multiple sequence alignment, interactive sequence choice and visualization. Brief. Bioinform. *20*, 1160–1166. 10.1093/bib/bbx108.

76. DeLano, W.L. The PyMOL Molecular Graphics System.

77. Jurrus, E., Engel, D., Star, K., Monson, K., Brandi, J., Felberg, L.E., Brookes, D.H., Wilson, L., Chen, J., Liles, K., et al. (2018). Improvements to the APBS biomolecular solvation software suite. Protein Sci. *27*, 112–128. 10.1002/pro.3280.

78. Blanchet, C.E., Spilotros, A., Schwemmer, F., Graewert, M.A., Kikhney, A., Jeffries, C.M., Franke, D., Mark, D., Zengerle, R., Cipriani, F., et al. (2015). Versatile sample environments and automation for biological solution X-ray scattering experiments at the P12 beamline (PETRA III, DESY). J. Appl. Crystallogr. *48*, 431–443. 10.1107/S160057671500254X.

79. Franke, D., Kikhney, A.G., and Svergun, D.I. (2012). Automated acquisition and analysis of small angle X-ray scattering data. Nucl. Instrum. Methods Phys. Res. Sect. Accel. Spectrometers Detect. Assoc. Equip. *689*, 52–59. 10.1016/j.nima.2012.06.008.

3.10 Supplementary figures and tables
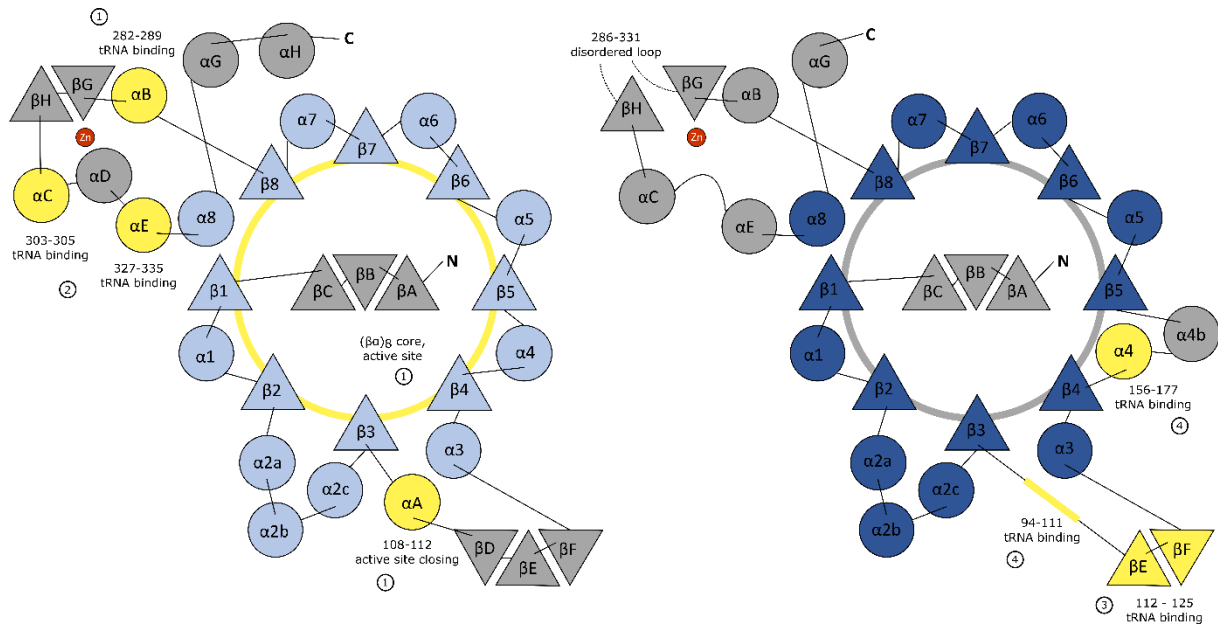
Figure S1: *Secondary structure elements of human TGT*

Secondary structure elements of human QTRT1 (left) and QTRT2 (right) are shown. Elements and residue numbers named in the main text are labelled. Blue elements form the central (βα)₈ core of each domain. Insertions to the (βα)8 core are depicted in grey. Elements discussed as tRNA binding motifs in the main text are highlighted in yellow and labelled according to Figure 1b.
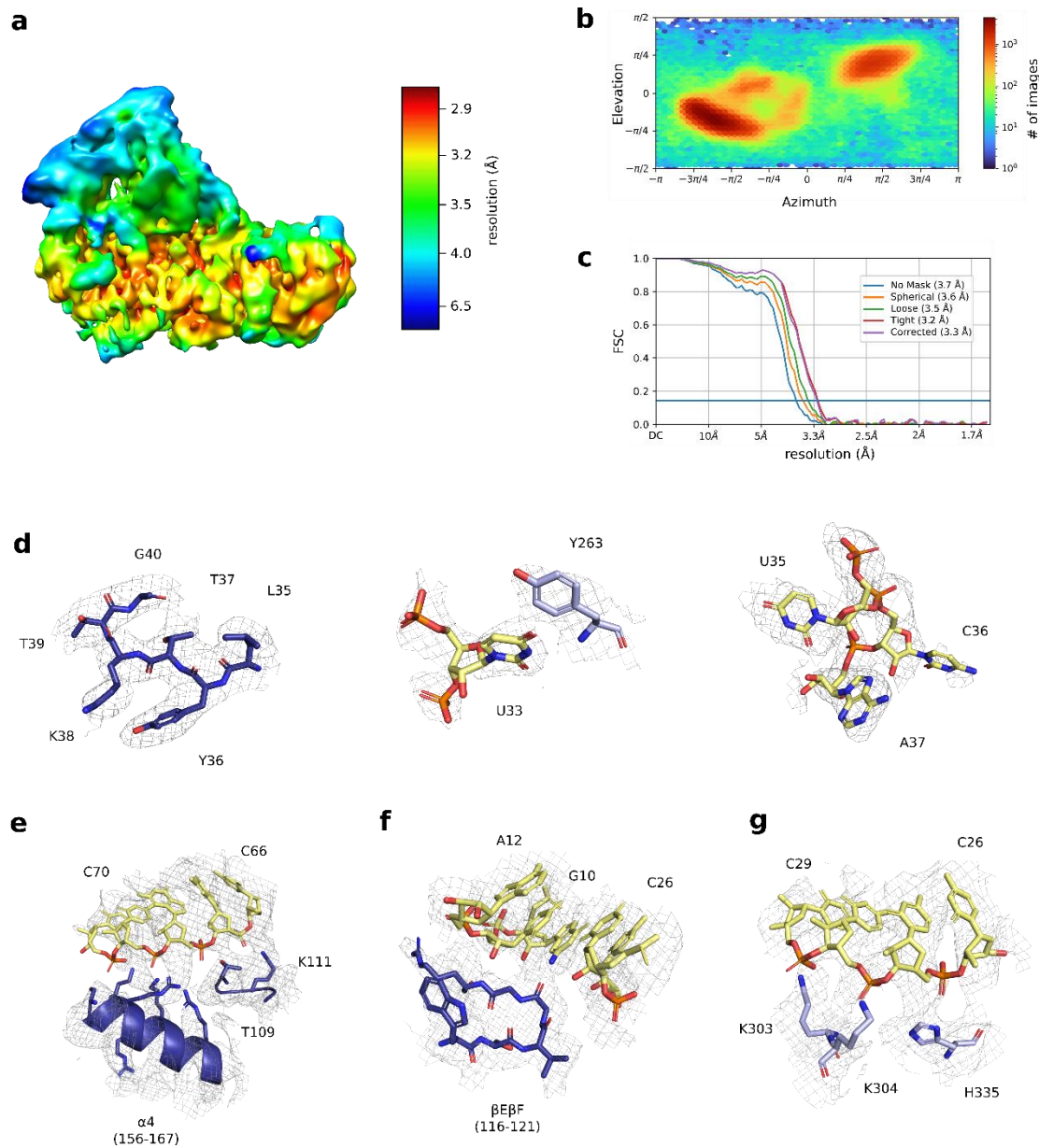
Figure S2: *Overview of cryo-EM map quality and model fit*

a) *Cryo-EM map of TGT·tRNA complex, low-pass filtered to FSC resolution (3.3Å) and colored by local resolution.*
b) *Azimuth plot showing distribution of viewing orientations.* *c)* *Fourier-shell correlation curves of cryo-EM half maps.*
d) *Cryo-EM map and TGT·tRNA model in three distinct orientations.* *e)* *Representative examples of map quality at different regions of the TGT·tRNA complex.* *f-h)* *Map quality at different RNA-binding sites.*

a

b

d

TGT-tRNA^Asp dataset 1
(680 micrographs)

TGT-tRNA^Asp dataset 2
(706 micrographs)

e

c

Motion correction
CTF estimation
Micrograph curation

Motion correction
CTF estimation
Micrograph curation

656 micrographs

383 micrographs

Particle picking (blob)
Particle extraction
2D classification

particle picking (template)
particle extraction

2D classification
(2 rounds)

3 class ab initio reconstruction
heterorefinement

template volume

template generation

particle picking (templates)
particle extraction (64px)

particle picking (templates)
particle extraction (64px)

656,321 particles

387,323 particles

2D classification
(6 rounds)

2D classification
(5 rounds)

354,374 particles

162,276 particles

particle re-extraction (256px)
2D classification
(6 rounds)

particle re-extraction (256px)
2D classification
(2 rounds, see d)

324,311 particles

154,241 particles

3 class ab initio reconstruction
heterorefinement (see f)

2D classification
(4 rounds, see e)

selected volume

463,140 particles

Heterorefinement (1 class)
Homorefinement
Non-uniform refinement (see g)

Final map

f

19.8%

33.5%

46.8%

g

FSC = 3.3 Å

Figure S3: *Processing of cryo-EM data*

a) *CTF fit histogram and representative micrograph from dataset 1.* **b)** *CTF fit histogram and representative micrograph from dataset 2.* **c)** *Flow-chart summarizing data processing, details in methods.* **d)** *Representative 2D class averages for dataset 1.* **e)** *Representative 2D class averages for all particles.* **f)** *Ab initio reconstructions and heatmap showing particle orientation.* **g)** *Final map, filtered to FSC resolution (3.3 Å).*
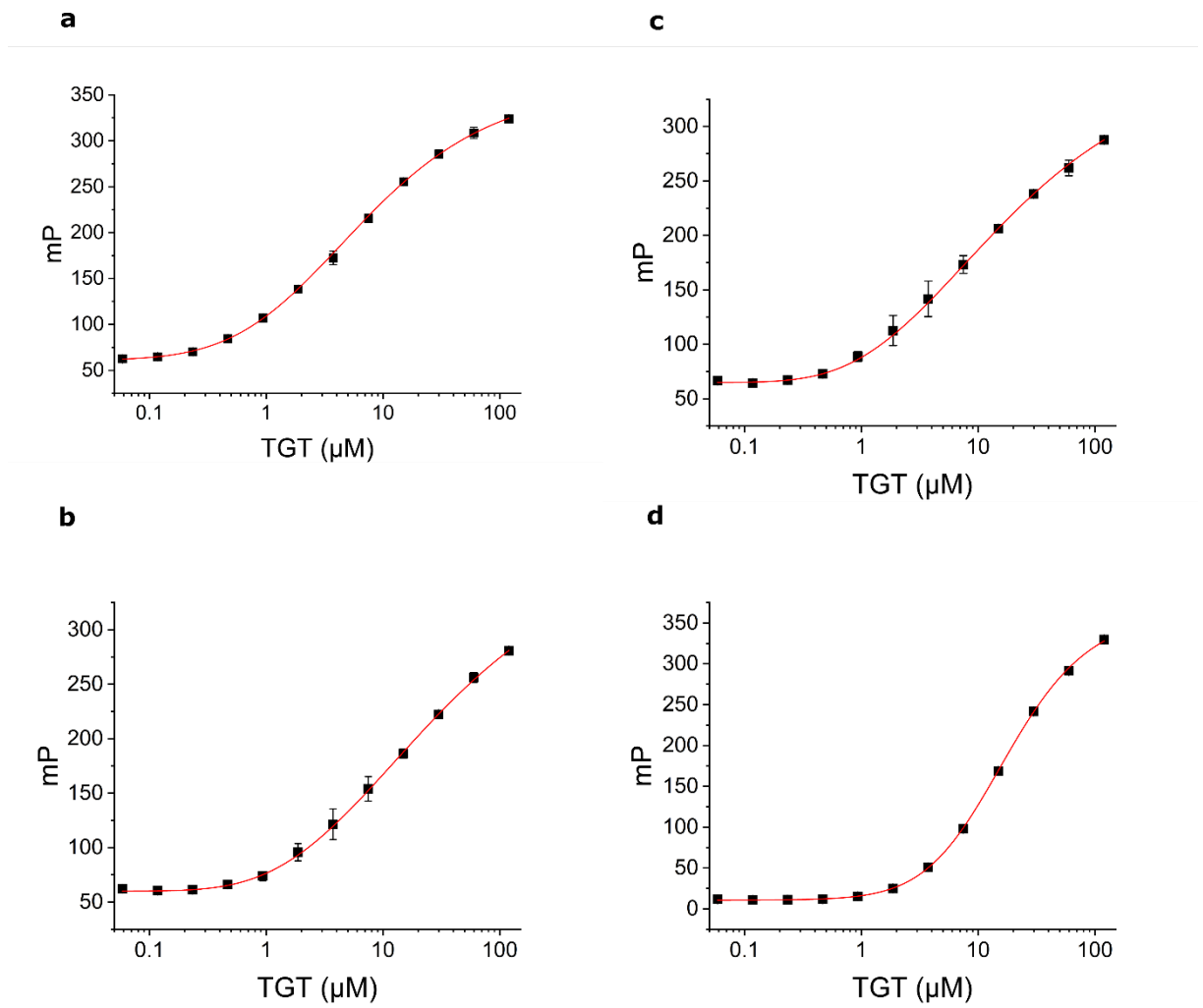
Figure S4: Raw fluorescence polarization data and curve fits

Fluorescence polarization data obtained for varying concentrations of TGT and four fluorescently labelled RNA constructs: a) hstRNA^{Asp}, b) hstRNA^{Asp} ASL, c) tRNA^{Tyr} ASL and d) A20 RNA. For each experiment, the average and standard deviation of three triplicates as well as the fitted curve (red) is shown. Data is not normalized.

a

g

b

h

c

i

d

j

e

k

f

l
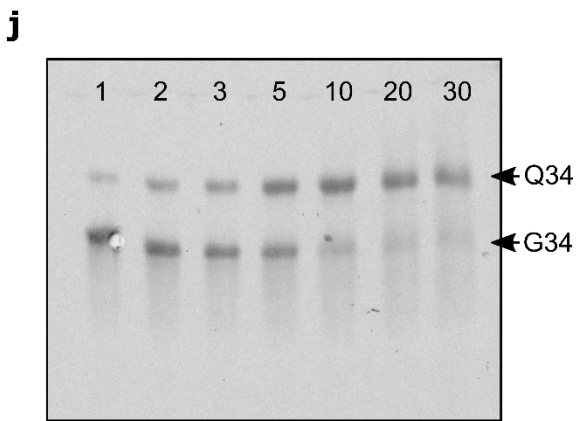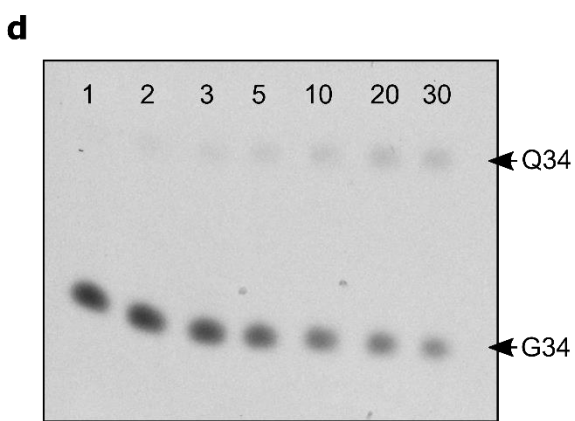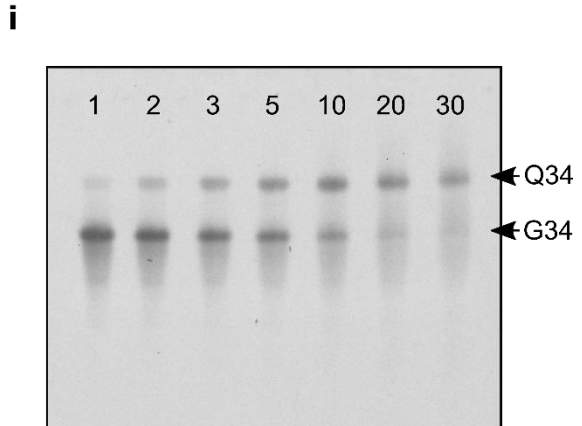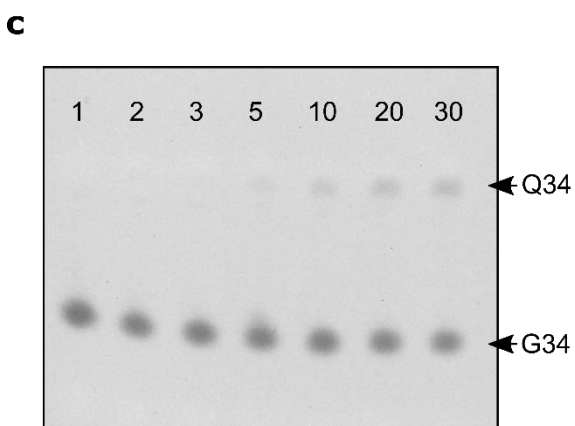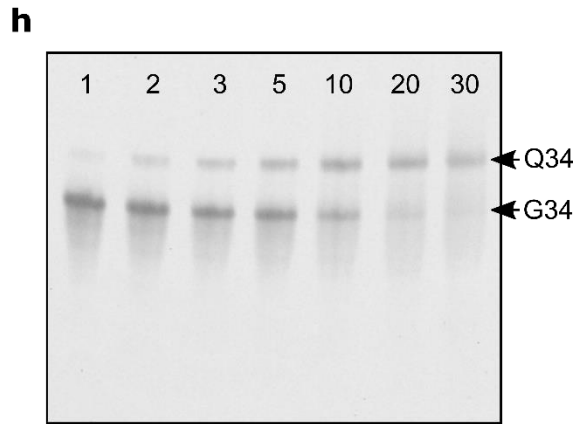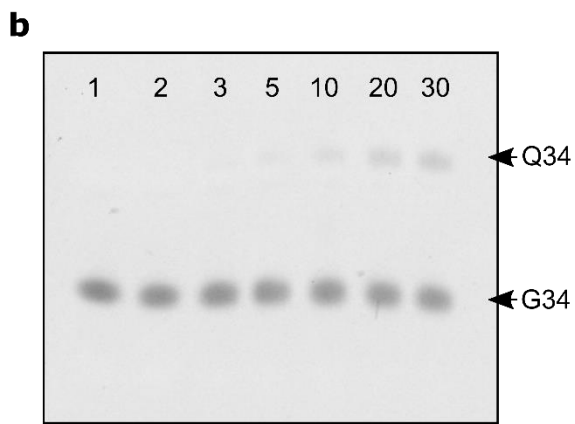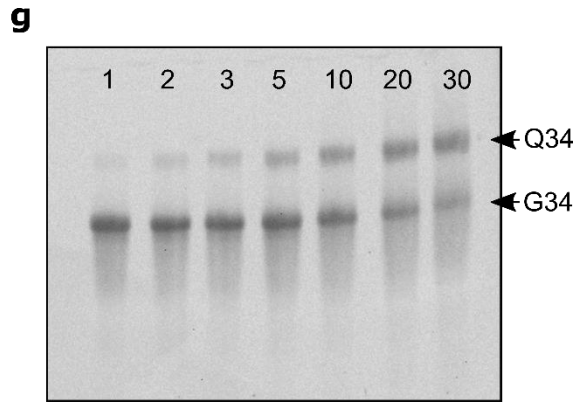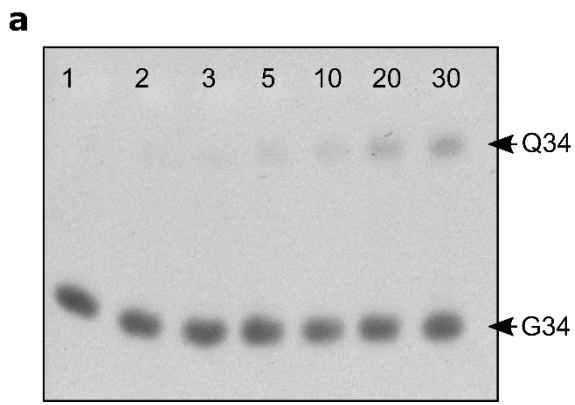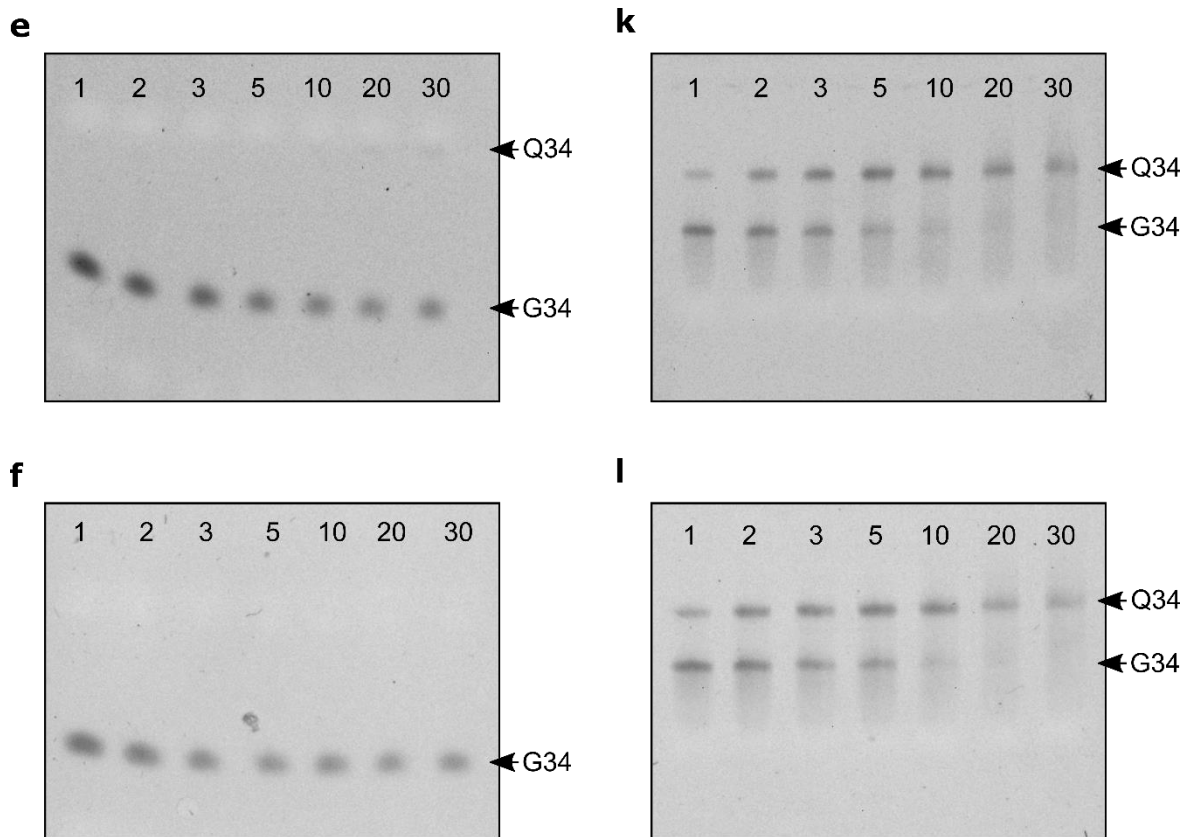
Figure S5: Gel images used for Q-incorporation activity test

Each gel image shows the separated samples taken from a Q-incorporation reaction (contrast linearly increased). Lanes 1-7 correspond to samples taken after 2, 3, 5, 10, 20 and 30 minutes. Lower bands are comprised of unmodified RNA, upper bands represent Q-modified RNA. Q-incorporation reactions were carried out with varying RNA substrate concentrations: ***a)*** *17.7 µM tRNA^{Asp} ASL* ***b)*** *8.8 µM tRNA^{Asp} ASL* ***c)*** *5.9 µM tRNA^{Asp} ASL* ***d)*** *3.5 µM tRNA^{Asp} ASL* ***e)*** *1.8 µM tRNA^{Asp} ASL* ***f)*** *0.9 µM tRNA^{Asp} ASL* ***g)*** *14.0 µM tRNA^{Asp}* ***h)*** *7.0 µM tRNA^{Asp}* ***i)*** *4.7 µM tRNA^{Asp}* ***j)*** *2.8 µM tRNA^{Asp}* ***k)*** *1.4 µM tRNA^{Asp}* ***l)*** *0.7 µM tRNA^{Asp}.*

Figure S 6: *Ensemble optimization with structure pool based on TGT cryo-EM or crystal structure*

a) *Dimensionless Kratky-plot of TGT SAXS data (see S6a), with theoretical scattering of an optimized ensemble that was selected from structures based on the cryo-EM TGT structure presented in this work. The fit against the experimental data is expressed as χ^2. The crosshair marks $sR_g = \sqrt{3}$ and $(sR_g)^2 \times I(s)/I(0) = 3e^{-1}$. **b)** Distribution of the radii of gyration (R_g) of structures in pool and the optimized ensemble. **c)** Structures in the ensemble. Domains modelled as a rigid body are shown in grey, disordered regions modelled as random chains are shown in cyan. **d)** Like a) but with theoretical scattering of an ensemble that was selected from structures based on a TGT crystal structure (PDB-ID: 7NQ4) **e)** like b) but for data shown in d). **f)** Like c) but for data shown in d). Disordered regions modelled as random chains are shown in yellow.*
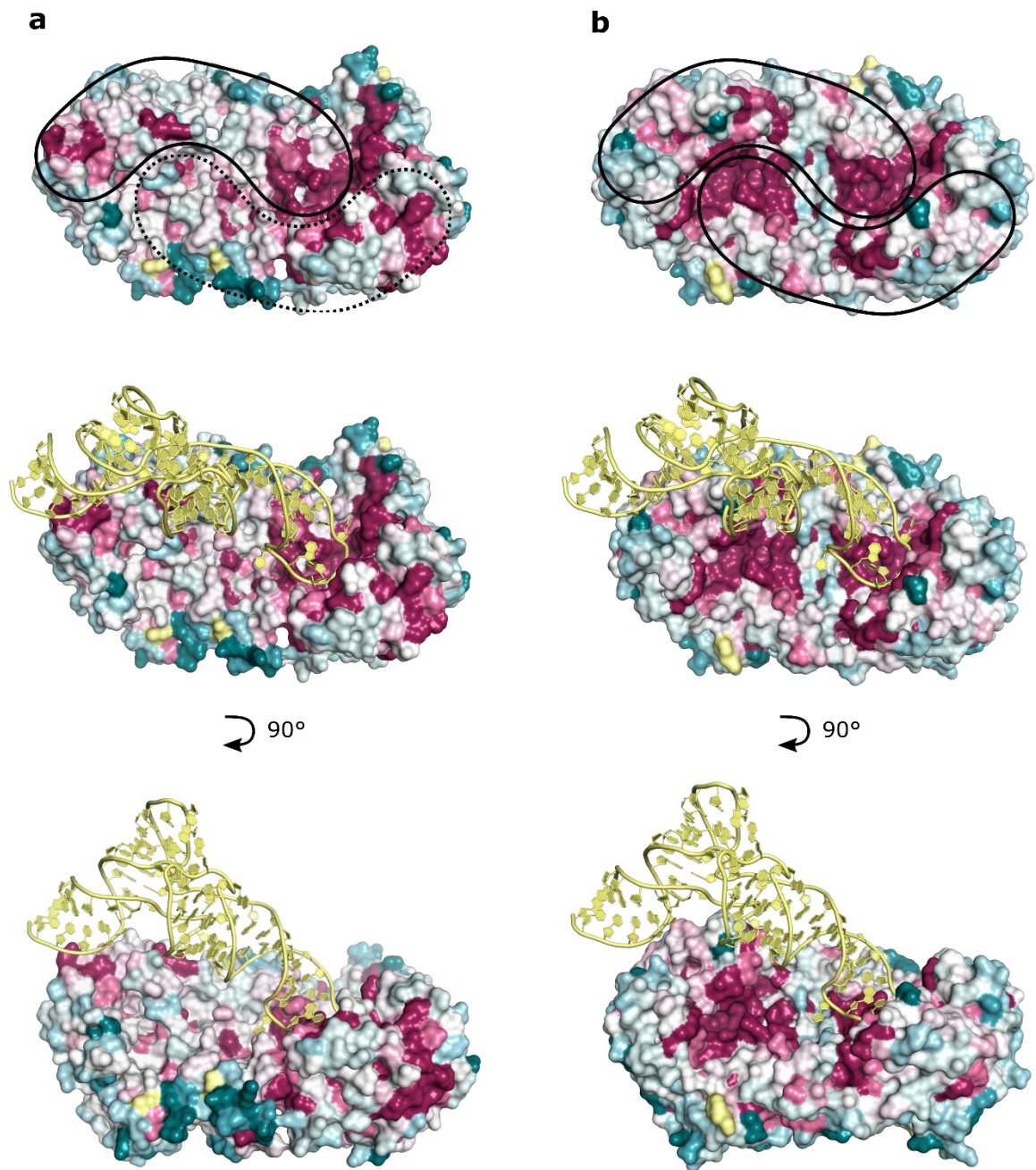
Figure S 7: *Amino acid conservation of eukaryotic and bacterial TGT*

a) Amino acid conservation in eukaryotic TGT mapped onto the surface of human TGT. In the top figure, the functional and non-functional degenerate tRNA binding sites are highlighted by a solid and dotted outline respectively. The middle and bottom figures show the bound tRNA as observed by cryo-EM of the human TGT·tRNA complex from two different perspectives. b) Amino acid conservation in bacterial TGT mapped onto the surface of Z. mobilis TGT (PDB-ID: 1Q2R). In the top figure, the two tRNA binding sites, inferred from the cryo-EM structure of the human TGT·tRNA complex, are outlined. The middle and bottom figures show a tRNA superimposed from the structure of the human TGT·tRNA complex from two different perspectives.

a

b
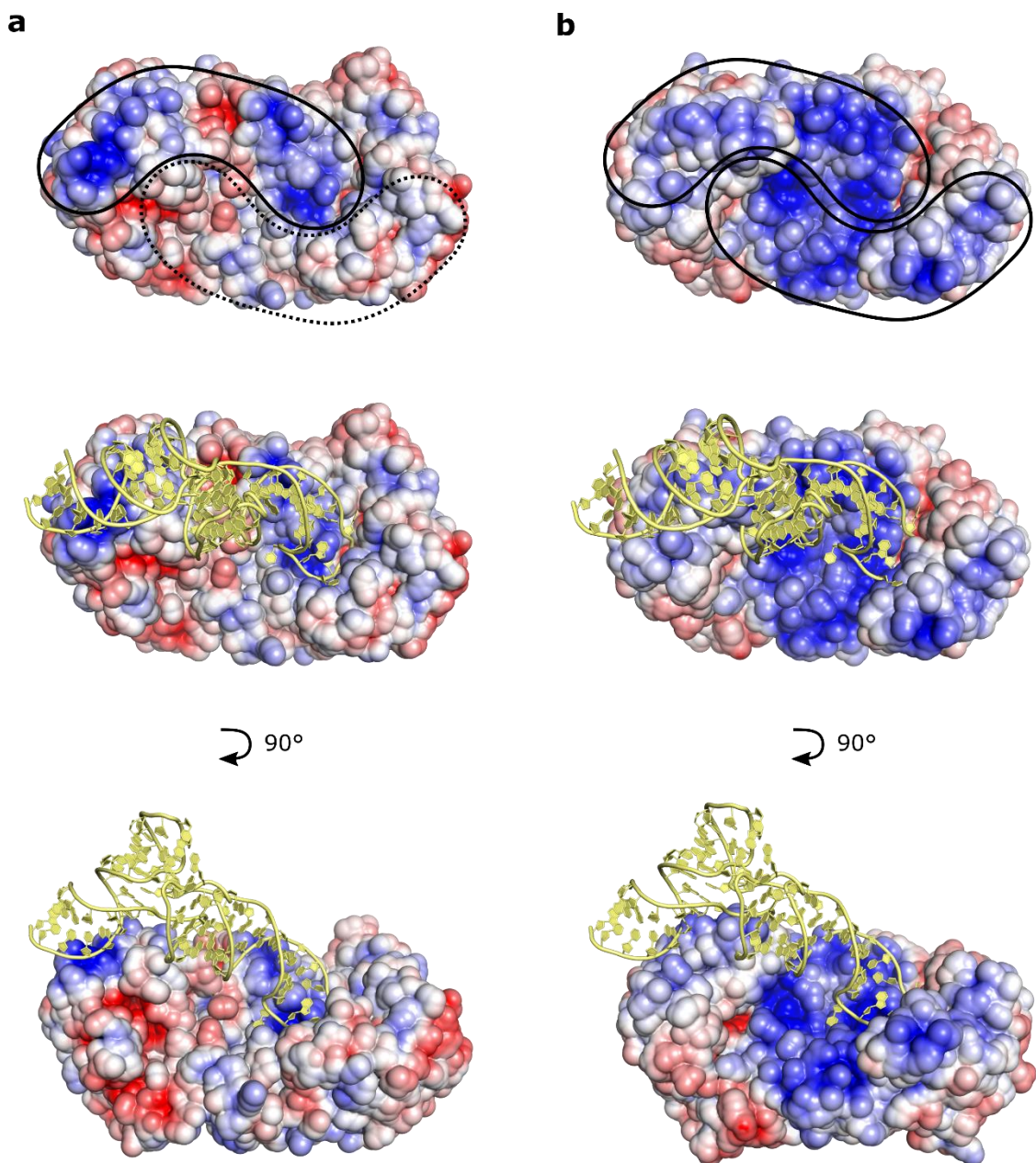
Figure S 8: *Surface electrostatics of eukaryotic and bacterial TGT*

a) Surface electrostatics of human TGT. In the top figure, the functional and non-functional degenerate tRNA binding sites are highlighted by a solid and dotted outline respectively. The middle and bottom figures show the bound tRNA as observed by cryo-EM of the human TGT·tRNA complex from two different perspectives. b) Surface electrostatics of Z. mobilis TGT (PDB-ID: 1Q2R). In the top figure, the two tRNA binding sites, inferred from the cryo-EM structure of the human TGT·tRNA complex, are outlined. The middle and bottom figures show a tRNA superimposed from the structure of the human TGT·tRNA complex from two different perspectives.

Supplementary table 1: Cryo electron microscopy data collection, data processing and refinement statistics

Data collection and processing	TGT·tRNA complex
Microscope	Thermo Scientific Glacios
Magnification (×)	190,000
Voltage (kV)	200
Dose rate (e$^-$ pixel^{-1} s^{-1})	0.8
Total electron exposure (e$^-$ Å^{-2})	62
Defocus range (µm)	−1.0 to −2.0
Camera	Falcon 3EC direct electron detector
Pixel size (Å)	0.78
Number of frames per movie	48
Number of movies	1,386
Data processing software	CryoSPARC[63]
Initial particle images	1.043.644
Final particle images	463140
Map resolution (Å)	3.3
FSC threshold	0.143
Map resolution range (Å)	1.664 – 41.59
Map sharpening B factor (Å^2)	-162.4

Refinement	
Initial models used (PDB codes)	7NQ4, 2TRA
Model composition	
Non-hydrogen atoms	7520
Residues (protein)	768
Residues (RNA)	72
Model to map fit	
CCmask	0.1645
CCvolume	0.1754
CCpeaks	0.1012
R.m.s. deviations	
Bond lengths (Å)	0.008
Bond angles (°)	0.835
Ramachandran plot	
Favored (%)	96
Allowed (%)	4
Disallowed (%)	0
Validation	
All-atom clashscore	16.35
Rotamer outliers (%)	2

Accession codes	
EMDB	EMD-16976
PDB	8OMR

Supplementary table 2: Details of SAXS data collection and primary data analysis

Sample details	TGT	TGT·tRNA complex
Scattering particle composition	QTRT1, QTRT2	QTRT1, QTRT2, GGG-hstRNA
Buffer composition	20 mM HEPES pH 7.5, 100 mM NaCl, 3 % (w/v) glycerol	
Temperature (°C)	4 ˚C (storage), 20 ˚C (measurement)	
Size Exclusion Chromatography (SEC-SAXS)		
Sample injection concentration (µg/µL)	10.0	4.5
Sample injection volume (µL)	75	75
SEC column type	S200 300/10 increase	
SEC flowrate (mL/min)	0.5	0.7
Online MALS-RI		
Molecular mass, theoretical (kDa)	90.9	116.3
Molecular mass, MALS-RI (kDa)	93 ± 5	111.8 ± 1.3

SAXS data collection

	TGT	TGT·tRNA complex
In-beam sample cell	1-mm quartz capillary	
Radiation source	Synchrotron (Petra III, beamline P12, EMBL Hamburg)[78]	
Wavelength (Å)	1.23980	
Detector	Pilatus 6M	
Measured s-range (Å^{-1})	2.23×10^{-3} - 7.31×10^{-1}	2.43×10^{-3} - 7.37×10^{-1}
Data acquisition/reduction software	SASFLOW[79]	
Exposure time/frame (s)	0.995000	
Number of frames	3600	2160
Sample frames used for averaging	34	38
Solvent blank	Column flow-through	

SAXS-derived structural parameters

	TGT	TGT·tRNA complex
Methods/Software	PRIMUS, GNOM[68]	
Guinier Analysis		
$R_g \pm \sigma$ (Å)	32.8 ± 0.0	34.8 ± 0.0
$min < sR_g < max$ limit	0.33 - 1.27	0.23 - 1.27
Linear fit assessment (Fidelity)	0.41	0.34
PDDF/P(r) analysis		
R_g (Å)	33.2	35.2
R_{max} (Å)	114	109
s-range (Å^{-1})	$1.00 \times 10^{-3} - 2.44 \times 10^{-1}$	$0.66 \times 10^{-3} - 2.29 \times 10^{-1}$
Volume estimates		
Porod volume (Å^3)	125095	159665
Molecular weight estimates		
Bayesian Inference Credibility Interval (kDa), (probability)	67.9 - 90.0, (92.98)	92.7 - 106.9, (90.49)

Modelling

Methods/Software	Ensemble optimization method (RANCH, GAJOE)[69]	
s-range for fit (Å^{-1})	$7.25 \times 10^{-3} - 5.00 \times 10^{-1}$	$7.14 \times 10^{-3} - 5.00 \times 10^{-1}$
Ensemble name	"mixed" (cryo-EM, crystal structure-based)	Cryo-EM structure-based
Atomic structure (PDB-ID)	8OMR, 7NQ4	8OMR[a]
residues	QTRT1 16-403, QTRT2 2-286, 332-414	QTRT1 16-303, QTRT2 2-286, 332-414, tRNA 1-75
Loop modelling	random	random
residues	QTRT1 (-2)-15, QTRT2 1, QTRT2 287-331, QTRT2 415	QTRT1 (-2)-15, QTRT2 1, QTRT2 287-331, QTRT2 415
Number of models in ensemble	18	15
χ^2	1.329	1.109
Ensemble name	Cryo-EM structure-based	
Atomic structure (PDB-ID)	8OMR	
Residues	QTRT1 16-305, QTRT2 2-286, 332-414	
Loop modelling	random	
Residues	QTRT1 (-2)-15, QTRT2 1, QTRT2 287-331, QTRT2 415	
Number of models in ensemble	15	
χ^2	1.371	
Ensemble name	Crystal structure-based	
Atomic structure (PDB-ID)	7NQ4	
Residues	QTRT1 16-305, QTRT2 2-286, 332-414	
Loop modelling	random	
Residues	QTRT1 (-2)-15, QTRT2 1, QTRT2 287-331, QTRT2 415	
Number of models in ensemble	15	
χ^2	2.910	

Accession codes

SASDB	SASDRB8	SASDRC8

[a] sequence adjusted and 5' GGG residues added manually in Coot

4   DISCUSSION

4.1   Towards a model of tRNA-binding by eukTGT

The combined structural data presented in this thesis gives a thorough account on how the human TGT heterodimer functions as a binding platform for its tRNA substrate. Prior to this work, the association of the two subunits into the functional eukTGT heterodimer was not yet known. The crystal structure of human TGT presented in chapter 2 clearly shows that the eukTGT heterodimer assembles in close homology to the bacTGT homodimer. This suggests that tRNA binding builds on very similar structural foundations in both bacterial and eukaryotic TGT. While this first structure did not allow to analyze tRNA binding beyond the tRNA anticodon loop, its accompanying mutagenesis work and cross-linking data did provide clues that specific elements of the non-catalytic subunit might be additional tRNA-binding motifs. The involvement of the QTRT2 subunit in tRNA-binding was proven by the second structure of this thesis (chapter 3), which was obtained by means of single particle cryo-EM and is the first structural account of tRNA binding by a bacterial/eukaryotic-type TGT.

However, while the TGT·tRNA cryo-EM structure confirmed a close association between tRNA and QTRT2 subunit, it revealed that tRNA engages with the tRNA-binding motifs in a different orientation than initially expected. The preliminary TGT·tRNA model presented in chapter 2 (Ch. 2, Figure 6) was generated by superposition of a tRNA structure and was primarily based on the orientation of the crystallized anticodon stem-like helix. This model was supported by crosslinking data, a prominent pattern in surface electrostatics and mutagenesis of positively charged residues. It suggested a "diagonal" tRNA binding site, stretching from the QTRT1 active site diagonally across the QTRT2 subunit to allow contact with charged residues of both the $\alpha 4$ helix and its preceding loop (Figure 1). The TGT·tRNA cryo-EM structure later revealed this to be incorrect, as the tRNA is bound exclusively by one site of the QTRT2 subunit, coming in close contact with the N-terminal half of helix $\alpha 4$, but not the preceding loop containing QTRT2 residue K152 (Figure 1). In the earlier TGT·RNA crystal structure, this residue is located in close proximity to the positively charged residues of $\alpha 4$, initially giving the appearance of a

continued positively charged binding surface. This region of the crystal structure, including K152, is further affected by contacts with a symmetry mate RNA (Ch. 2, S5), causing it to adopt a conformation that was likely different from both free TGT and the tRNA-bound complex. The additional information presented in chapter 3 clearly proves that K152 is not part of the tRNA binding interface. The TGT·tRNA cryo-EM structure is actually better suited to explain results obtained in chapter 2 (Ch. 2, Figure 8B): While double mutants of K158 and R161, two residues later shown to actually be in close vicinity of the tRNA acceptor stem, had decreased tRNA affinity compared to the wild type TGT, the binding affinity of triple mutants, containing an additional K152 mutation, was not decreased further, fully in line with it not contributing to tRNA binding.
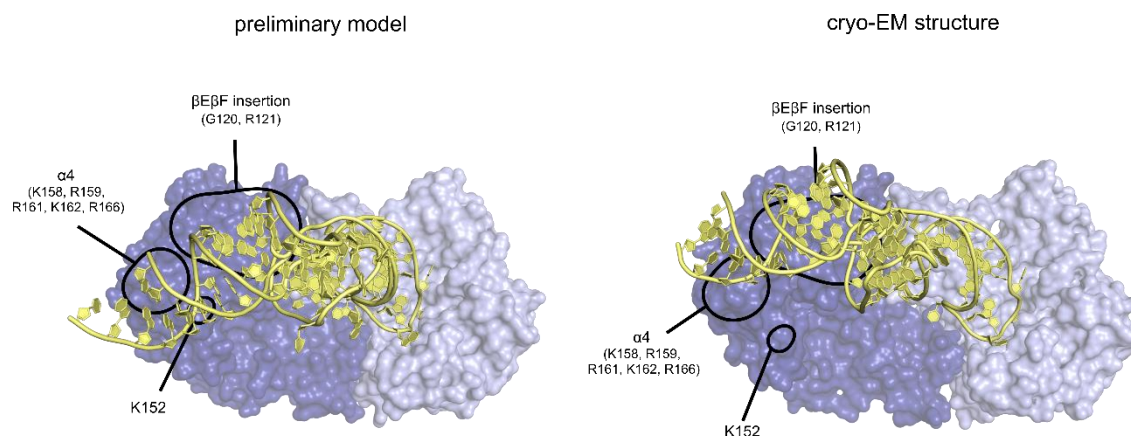
Figure 1: Comparison of preliminary TGT·tRNA model with final cryo-EM structure

Comparison of the preliminary TGT·tRNA model (Ch. 2), which was based on the orientation of a crystallized anticodon stem and supported by crosslinking data and mutagenesis, with the final cryo-EM structure (Ch. 3). Elements of interest are labelled.

The preliminary model was based on a crystal structure of yeast tRNA^{Asp} (PDB-ID: 2TRA) which was treated as a rigid body; thus, the superposed model inherited a tRNA conformation that was the direct product of specific crystallization conditions. While it was suspected that the tRNA was likely to adopt a somewhat different conformation in the context of a TGT·tRNA complex (Ch. 2, Discussion), the nature of such a conformational

change was not known. The TGT·tRNA cryo-EM structure later revealed that the innate flexibility of the tRNA elbow region allows for the tRNA to bend towards the QTRT2 half that contains the βEβF insertion and the α4 binding site.

Thus, the tRNA-binding site of eukaryotic TGT, now finally known, stretches from the active site and QTRT1 helix αB, which supports binding of the anticodon loop, along the QTRT1 zinc binding domain, which makes minor contacts with the anticodon stem. From there it is continued on the QTRT2 subunit by the βEβF insertion, binding both the base of the D-arm and the acceptor arm, and finally the N-terminal half of helix α4, contributing five charged residues to bind the tRNA backbone.

The contribution of each of these binding motifs was described in detail in chapters 2 and 3 and their conservation among eukaryotes was analyzed (Ch 3, Figure 7a+b), revealing residues G120 and R121 as well as the positively charged α4 patch to be highly conserved. The reason for this is easily apparent: A glycine at position 120 of the βEβF insertion ensures close contact with the ribose of nucleotide 11, an interaction that would be obstructed by the presence of an amino acid side chain. The adjacent R121 supports binding of the tRNA D-stem through interactions with both its aliphatic linker and guanidino group. The positively charged residues of the α4 N-terminus form salt bridges or hydrogen bonds that strictly require a lysine or arginine at their individual positions.

However, tRNA-binding by TGT is also clearly dependent on the secondary structure and three-dimensional shape of its binding motifs, which can be conserved even at low overall sequence similarity[180]. The βEβF insertion, one of three TGT-specific insertions to the basic $(\beta\alpha)_8$ barrel (Ch. 1, Figure 9), is an example of this: Its two-sided interaction with both the tRNA D-arm (via the turn connecting βE and βF) and the acceptor arm (via the turn preceding βE) recognizes the tRNA bend by its specific shape and orientation in space (Ch. 3, Figure 1).

In summary, TGT appears to recognize its substrate tRNA at three levels: First on the electrostatic level: Positively charged areas will unspecifically draw in molecules of opposing negative charge, which is the likely reason for binding of unstructured A20 RNA (Ch 3, Figure 3a). Secondly, shape complementarity provided by the different tRNA binding motifs arranged on a 3-dimensional surface will strongly select for the

characteristic tRNA L-form of a tRNA. This is supported by the finding that TGT only modifies tRNAs *in vivo*, despite its ability to modify other RNAs at artificially high concentrations *in vitro*[165,170]. Thirdly, specific base-recognition within the active site discriminates $G_{34}U_{35}N_{36}$-tRNA from other tRNAs. The combination of these three features on a single protein works as a molecular implementation of a logic AND ($\wedge$) gate, allowing to define the TGT substrate tRNA pool among the entirety of cellular molecules (Figure 2).
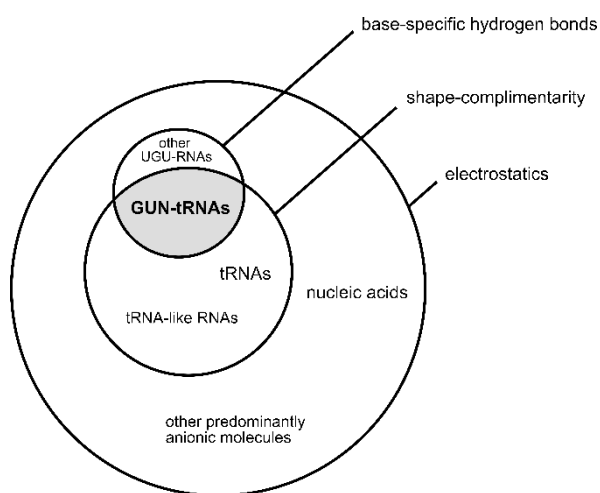
Figure 2: Logic of TGT substrate identification

Logic model of TGT substrate recognition: The three elements of substrate recognition are shown as circles enclosing sets of cellular molecules with particular characteristics. Because they are connected by a logic AND, only those molecules that combine all three types of characteristics are recognized as substrates. All molecules fulfilling the base-specific hydrogen bond and shape-complementarity requirements are already a subset of electrostatically selected anionic molecules, making electrostatics in essence a pre-filter rather than a third independent requirement.

4.2   Comparison to tRNA binding in bacterial and archaeal TGT

4.2.1   Comparison to tRNA-binding in bacterial TGT

To date, no structure of bacterial TGT bound to a complete tRNA is available for a direct comparison to tRNA-binding by eukTGT. However, the available pieces of information, namely the strong similarities of the dimeric binding platform, the conservation of critical elements such as the (βD)βEβF insertion and the virtually identical binding mode of a stem

loop RNA, strongly suggest that tRNA binding by bacterial TGT will be very similar to that by eukaryotic TGT. In chapter 3, some differences between eukTGT and bacTGT were addressed already, focusing mainly on the direct consequences of heterodimeric and homodimeric composition. Here, bacterial TGT is discussed in detail to infer details of its tRNA binding.

Superposition of the tRNA from the cryo-EM TGT·tRNA structure onto a crystal structure of *Z. mobilis* TGT revealed the likely tRNA binding site (Ch 3, Figures S7+S9). However, such a simple superposition causes a clash of the βDβEβF insertion with tRNA nucleotides 10-12. The reason for this is likely two-fold: Firstly, the βDβEβF insertion of bacterial TGT, while somewhat flexible, is consistently oriented in a steeper angle than its QTRT2 counterpart[151,152,157]. Thus, the βEβF turn that is expected to make contact with the tRNA ends roughly 6 Å further from the center of the subunit than the equivalent element in eukaryotic TGT (Figure 3). Secondly, eukaryotic TGT appears to adopt a more extended conformation in solution, certainly upon tRNA binding (chapter 3). To date, all structural information on bacterial TGT is based on crystal structures depicting a compact conformation, leaving it unclear how and to what extent bacterial TGT may adjust upon tRNA binding. It seems highly likely that conformational readjustment could mitigate the observed clash of the superposed model. However, the 6 Å difference in outreach between the QTRT2 and bacTGT insertions is likely too great to accommodate identical tRNA binding geometry.

In eukaryotic QTRT2, G120 is among the most highly conserved residues, strictly required to make a close contact to nucleotide 11 (Ch. 3, Figure 1e). In bacterial TGT, the equivalent residue, G130, is also strongly conserved, suggesting it might fulfill a similar role. The steep angle of the βDβEβF sheet is a direct consequence of it being propped up by the presence of the preceding helix αA, which is of central importance to the catalytic subunit. In QTRT2, αA is not needed and both αA and βD are replaced by a more flexible linker, which both blocks the degenerate active site[157] and allows the remaining βEβF sheet to pack more closely against the $(\beta\alpha)_8$ barrel core of its subunit[157]. In consequence, it is likely that the orientation of the bacterial αA-βF insertion creates a steeper angle between the active site and the βEβF turn expected to come in contact with the tRNA D-arm base. Interestingly, a comparison (Ch. 2) of the two crystal structures of bacterial and human TGT in complex

with a stem loop RNA had previously revealed that the anticodon stem is also angled more steeply against the catalytic subunit in the bacterial structure. Although alternative causes are possible (discussed in Ch 2), this might be a direct consequence of the differential position of the βEβF turn in each structure with which the RNA stem makes contact. Manual repositioning of the tRNA structure to follow the steeper angle of nucleotides 25-31 significantly reduces the clash with the βEβF sheet in the bacterial model (Figure 3b).
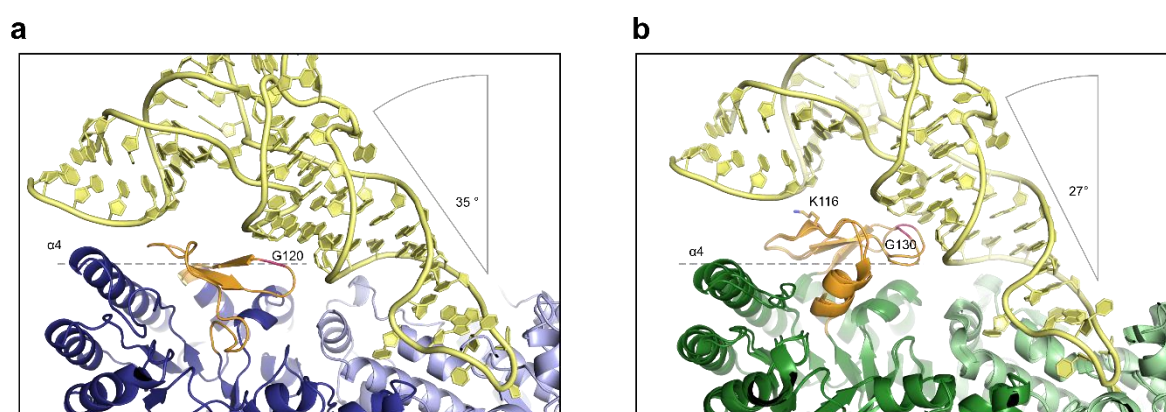
Figure 3: Comparison of tRNA binding in eukTGT and bacTGT

a) Cryo-EM structure of human TGT·tRNA complex. b) Two crystal structures of Z. mobilis TGT (PDB-IDs: 1Q2R, 1PUD) with manually superposed tRNA model. The tRNA model is derived from the cryo-EM structure of human TGT·tRNA but was manually repositioned to reduce clashing and the interstem angle was manually reduced by 6°. Both structures are shown in the same orientation, a dashed line is drawn at identical positions for comparison. The tRNA angle is indicated in both figures. The αA-ϐF/ϐEϐF insertion is highlighted in orange, elements and residues of interest are labelled.

The manually realigned model puts conserved G130 of the protein in close proximity with nucleotide 11 of the tRNA, its inferred interaction partner. Two positively charged residues, K125 and R132 that have long been suspected to support tRNA binding[177], are equally in a location in which they might form backbone contacts. However, both of these residues are specific to *Z. mobilis* TGT and not conserved among bacteria. Another lysine, K116 is much more conserved. Its position suggests that rather than interacting with the tRNA D-arm, it might support binding of the tRNA acceptor arm (Figure 3b). However, the steeper tRNA binding angle increases the distance between TGT and tRNA acceptor arm. Disregarding potential conformational changes on the protein side, contact with K116 would require an approximate 6° tightening of the tRNA interstem angle. A steeper tRNA binding angle also greatly increases the distance to the N-terminal half of helix α4, a conserved electrostatic

binding motif in eukaryotic TGT. In *Z. mobilis* TGT, this region is positively charged, albeit not as strongly as in human TGT (Ch 3, Figure 7c+e). However, this feature is not at all conserved among bacteria (Ch 3, Figure 7d), suggesting that it is much less significant in bacterial TGT, possibly because a steeper tRNA binding angle makes this area less likely to come in contact with the tRNA acceptor stem.

In summary, tRNA binding is likely very similar in both eukaryotic and bacterial TGT, preserving key binding elements, such as the presence of a βEβF sheet and a conserved glycine at position 120/130. Yet, there appear to be some key differences: In the bacterial homodimer, active site helix αA is present in both subunits, limiting the angular range of the αA-βF insertion. This likely causes a steeper tRNA binding angle in comparison to the human TGT·tRNA complex, which might be the underlying reason why bacterial TGT lacks an equivalent of the conserved electrostatic α4 binding batch that is found in eukaryotic TGT.

4.2.2   *Comparison to tRNA-binding in archaeal TGT*

Phylogenetically, arcTGT and bacTGT represent fully separated sister groups which share a common ancestor[181]. In contrast, eukTGT is a more recent branch diverging from the bacTGT tree[181]. Thus, human TGT and arcTGT, such as *Pyrococcus horikoshii* TGT (*ph*TGT), are separated by great evolutionary distance within the TGT superfamily. Specifically, subunit and domain re-organization that occurred in the history of both eukTGT and arcTGT evolution created fundamental differences. Yet, functional principles are surprisingly similar among the three TGT subfamilies. Evolution and adaptation of their active site regions is well understood[181,182], and has been summarized in chapter 1. In contrast, functional comparison of tRNA binding was long hindered by the absence of a complete tRNA-bound structure of bac/euk-type TGT. With such a structure now being available, the principles of tRNA binding by eukTGT and arcTGT can be compared in detail.

As summarized in chapter 1.4.2, arcTGT has acquired three additional C-terminal PUA domains that support tRNA-binding. Specifically, these domains provide a large patch of continuous positive charge that binds the substrate tRNA by its acceptor arm (Figure 18a), while the anticodon arm is wedged between the PUA domains and the catalytic $(\beta\alpha)_8$

domain[160]. This mode of binding of the acceptor arm in particular stabilizes the substrate tRNA and positions it correctly near the arcTGT active site. In that way, the PUA domains can be seen as a functional equivalent of the bacterial/eukaryotic αA-βF insertion as both support tRNA binding and stabilization via shape complementarity (creating buried surface area) and opposing charge. In eukaryotic TGT, the positively charged binding area is extended by cationic residues of helix α4. The need for a functional replacement in arcTGT arises from its divergent dimer association and nucleotide position modified, which requires a different tRNA orientation during catalysis. Consequently, arcTGT only contains an equivalent of the active site helix αA, while an equivalent of the tRNA-binding bacterial βDβEβF sheet is missing and would serve no function in arcTGT[159].

As arcTGT modifies position 15, which is deeply buried in the tRNA core, a base exchange at this position requires partial tRNA unfolding. In particular, a hairpin structure (K465-T467 in *ph*TGT) destabilizes the L-form conformation of the tRNA D-arm and forces it to adopt an alternative conformation (Figure 4b). This alternative conformation, referred to as the tRNA λ-form, allows the D-arm loop to reach into the arcTGT active site[160]. The conformal change required of tRNA upon binding bac/euk-type TGT is modest by comparison, and only involves re-arrangement of the anticodon loop and no hydrogen bond breakage[152], an event that can be expected to be thermodynamically much less challenging than the transition from L-form-to λ-form. In each TGT complex, the productive tRNA conformation is stabilized by the tRNA-TGT interface. Notably, in arcTGT this interface is much larger and energetically even more favorable than in bac/euk-type TGT (Table 1), an adaptation that might help to drive a thermodynamically challenging tRNA refolding event.

Finally, superposition of a free tRNA onto the human TGT·tRNA complex reveals that helix αB causes a clash with the free-form tRNA anticodon loop which is resolved in the reorganized "zig-zag" conformation (Figure 4d), confirming a previous observation[152]. Thus, this helix fulfills a similar function as the archaeal hairpin as both cause the destabilization of the native tRNA conformation, enforcing a conformational change. However, it is important to note that αB is also present in arcTGT, as it stabilizes the RNA stretch within the active sites of both enzymes.
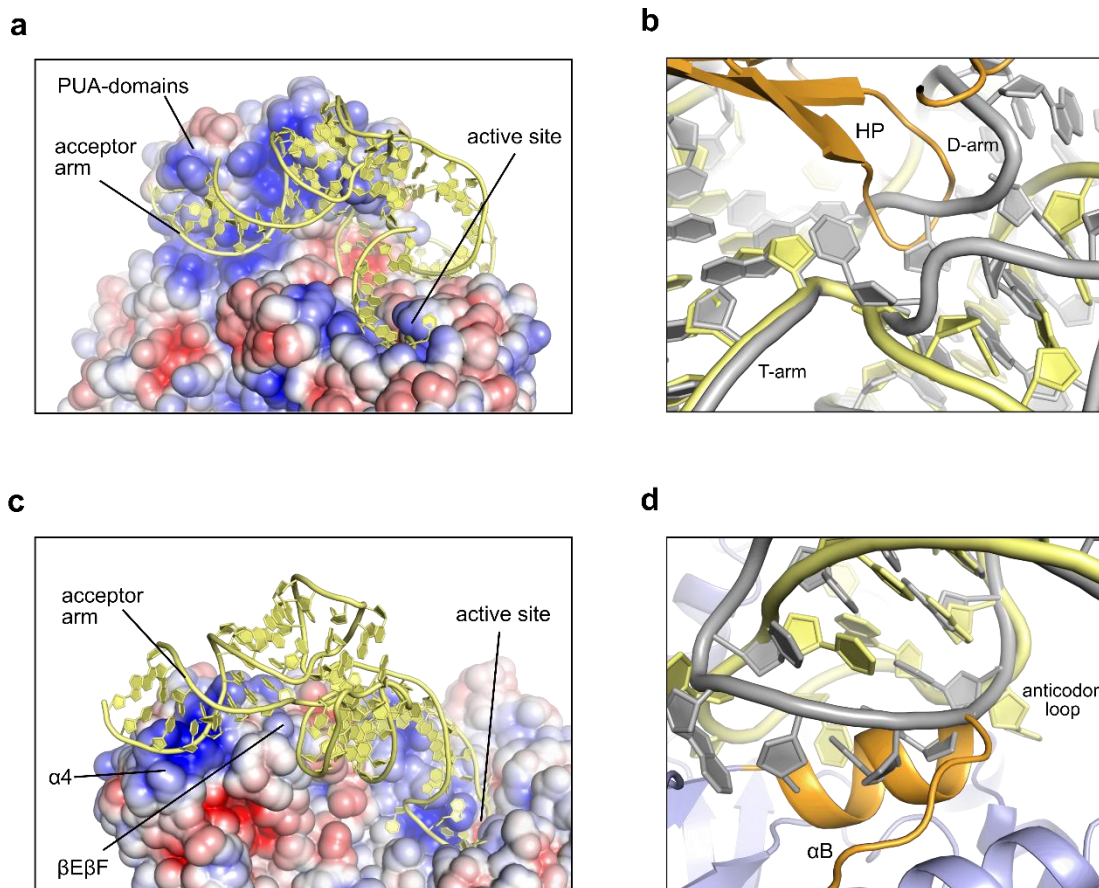
Figure 4: Functional homology of eukaryotic and archaeal TGT

Functional elements of tRNA binding in Pyrococcus horikoshii TGT (PDB-ID: 1J2B) and H. sapiens TGT. a) Surface electrostatics of phTGT at the tRNA binding site. b) D-arm destabilization by phTGT hairpin (HP, orange) motif. TGT-bound λ-form tRNA is shown in yellow, superposed L-form tRNA^{Val} (PDB-ID: 7EQJ) is shown in grey for comparison. c) Surface electrostatics of hsTGT at the tRNA binding site. d) Anticodon loop of superposed free tRNA^{Asp} (PDB-ID: 2TRA, grey) clashes with helix αB (orange). TGT-bound tRNA ("zig-zag" conformation) is shown in yellow.

In summary, eukTGT and arcTGT share an evolutionary origin and basic functional principles. However, due to the individual properties of each TGT subfamily, these functions are partly reassigned to divergent components of each protein. In addition, arcTGT requires partial tRNA refolding and its tRNA interface is considerably larger than it is in bac/euk-type TGT.

Table 1: Comparative PISA[183] analysis of TGT-tRNA interfaces in three domains of life

TGT	Interface	Interface area (Å²)	Δ^{i}G (kcal/mol)[1]	Reference
*hs*TGT	QTRT1-RNA (crystal)	1311	-18.4	This work
	QTRT1-tRNA (EM)	1358	-22.3	This work
	QTRT2-tRNA (EM)	515	-7.6	This work
	Total tRNA interface	**1850 ± 33**	**-28.0 ± 2.8**	
*zm*TGT	cat. SU-RNA (crystal)[2]	1208, 1213	-10.4, -8.1	[152]
	cat. SU-tRNA (model)[3]	1157	-15.8	This work
	non-cat.-tRNA (model)[3]	402	-6.8	This work
	Total tRNA interface	**1595 ± 31**	**-18.2 ± 4.0**	
*ph*TGT	cat. Domain-tRNA[2]	1714, 1641	-21.5, -21.9	[160]
	PUA-tRNA[2]	1804, 1790	-28.9, -25.0	[160]
	Total tRNA interface	**3475 ± 62**	**-48.7 ± 2.5**	

[1] Δ^{i}G[1] indicates the solvation free energy gain upon formation of the interface without the contribution of satisfied hydrogen bonds. [2] Comma-separated values refer to two copies/asymmetric unit. [3] Estimates derived from superposed model are listed.

4.3 Adaptation of eukTGT

Having compared human TGT to TGT enzymes from other domains of life allowed to pinpoint its idiosyncrasies, which in the following will be put into a broader evolutionary context. In brief, differences between TGT subfamilies can be traced back to two different root-causes: Firstly, diverging base substrate preferences, caused by divergent metabolic strategies and availability of nutrients, led to differences in the TGT active site composition. In particular, this is the reason why eukTGT, but also bacTGT of certain pathogenic bacteria[128], are characterized by active site adaptations that allow to accommodate a bulky queuine base. Secondly, divergent subunit composition or association influence the relative geometry of TGT and bound tRNA, driving the differential adaptation of tRNA-binding motifs. In arcTGT, tRNA orientation is determined by a divergent tRNA modification site, which required the co-evolution of new tRNA-binding motifs.

Eukaryotes are unique in typically maintaining two TGT genes, encoding a dedicated catalytic and non-catalytic subunit. As summarized in chapter 1, the two subunits are paralogs, making the non-catalytic subunit QTRT2 the likely result of gene duplication and divergent evolution. However, not all eukaryotic genomes contain both genes: While some

organisms, such as *Arabidopsis thaliana* or *Saccharomyces cerevisiae*, known to be Q-deficient, lack both genes, a significantly sized (30%), polyphyletic group of eukaryotes encode a QTRT1 ortholog but not a QTRT2 ortholog[132]. The reverse case, genomes encoding only QTRT2, is much rarer (4%)[132], making it unlikely that QTRT1-only genomes are the result of random gene loss in which QTRT1 is without function. Thus, in organisms with such genomes, "single" QTRT1 might have retained or re-acquired the ability to form functional homodimers similar to bacterial TGT. This idea is supported by the example of *Triticum aestivum* (wheat), a species appearing to lack a QTRT2 ortholog[132] but which was experimentally proven to Q-modify its tRNA[184], suggesting that its QTRT1 ortholog is fully functional. Consequently, an early study reported the purification of functional TGT from wheat and had found it to be homodimeric[52].

In eukaryotes that produce the typical combination of both QTRT1 and QTRT2, the heterodimeric composition represents the uncoupling of evolutionary pressure on catalytic activity and binding of the tRNA body. The secondary loss of active site helix αA in catalytically inactive QTRT2 is likely to be a direct result of this, and its absence enables closer tRNA binding and the formation of several additional hydrogen bonds or salt bridges. As outlined in chapter 3, eukTGT is also clearly asymmetric and its degenerate second tRNA binding site is less conserved, differentially charged and also de-rigidified in comparison to the functional binding sites of eukTGT or bacTGT.

The cost of maintaining a second gene suggests that eukaryotes must benefit from a more specialized, "better" non-catalytic subunit, an idea that is partly supported by the observed adaptations of eukTGT. In contrast, available kinetic data does not suggest that eukaryotic TGT has improved tRNA affinity or functionality compared to bacterial TGT (Table 2). However, all of the kinetic data available to date was generated by separate studies, in part by using different methods and conditions, which need to be considered: In particular, high salinity can be expected to interfere with ionic binding, thus reducing tRNA affinity. Although physiological, the addition of 20 mM $MgCl_2$ was found to noticeably lower the Q incorporation reaction speed (data not shown), severely reducing the applicability of a gel-based activity assay. In this work, the buffer conditions of queuine incorporation assays were kept consistent with cryo-EM and SAXS experiments. Consequently, the kinetic

parameters recorded in these conditions suggest a lower tRNA affinity (K_M) but higher reaction velocity (k_{cat}) than those previously reported for eukTGT.

Table 2: Kinetic parameters of TGT from different species

TGT species	K_M tRNA (μM)	K_{cat} (s^{-1})	Salinity, pH, Temperature	Method	Reference
H. sapiens	3.0 ± 0.2	2.8×10^{-2}	100 mM NaCl, pH 7.5, 37˚C	APB-gel (Q inc.)	This work
H. sapiens	0.3 ± 0.4	$5.6 \pm 0.1 \times 10^{-3}$	20 mM MgCl$_2$, pH 7.3, 37 ˚C	[^{14}C]-guanine inc.	[154]
M. musculus	2.0 ± 0.4	$7.5 \pm 0.2 \times 10^{-3}$	20 mM MgCl$_2$, pH 7.3, 37 ˚C	[^{3}H]-guanine inc.	[157]
M. musculus	0.4 ± 0.1	$6.5 \pm 0.3 \times 10^{-3}$	20 mM MgCl$_2$, pH 7.3, 37 ˚C	[^{3}H]-guanine inc.	[164]
Z. mobilis	0.9 ± 0.2	$5.4 \pm 0.1 \times 10^{-2}$	20 mM MgCl$_2$, pH 7.3, 37 ˚C	[^{3}H]-guanine inc.	[185]
Z. mobilis	2.17	1.1×10^{-2}	20 mM MgCl$_2$, pH 7.3, 37 ˚C	[^{3}H]-guanine inc.	[153]

In a broader sense, TGT is only one of many examples where proteins that require a single gene product in bacteria are comprised of distinct subunits in eukaryotes: Five enzymes that fit this category are involved in yeast tRNA modification alone, most notably TAD2/3 (an A34 deaminase) and Trm61/6 (a methyltransferase) which like QTRT1/QTRT2 have arisen by gene duplication and divergence[186].

It is possible that the explanation for this shared phenomenon simply lies in the different genome sizes of bacteria and eukaryotes: A typical bacterial genome is comprised of 5 million base pairs and encodes approximately 5,000 proteins[187]. In contrast, eukaryotic genomes are on average much larger, although spanning a size range that encompasses four orders of magnitude[188]. The human nuclear genome is comprised of 3 billion base pairs, encoding 60,000 genes, of which 20,000 are predicted to be protein coding[189]. It is easy to see how such an elaborate genomic environment is much more favorable to retain heterodimeric compositions. Interestingly, fungi and "protists" (unrelated groups of predominantly unicellular eukaryotes), among which QTRT1-only genomes were most commonly found[132] also tend to have the smallest genomes among eukaryotes[188].

5 SYNOPSIS

In this thesis, two novel structures were presented, jointly illuminating dimerization and tRNA binding by human TGT. A first structure, obtained by X-ray crystallography, allowed to give a thorough account of the atomic details of the heterodimeric interface as well as active site recognition of the substrate RNA. The second structure, obtained by single particle cryo-EM, is the first to show complete tRNA binding by a TGT enzyme of the bacterial/eukaryotic type, revealing that both TGT subunits are intimately involved in tRNA binding. Together, these two structures close several knowledge gaps that remained in the understanding of eukaryotic TGT and the broader TGT family.

Furthermore, insights on TGT flexibility yielded by cryo-EM dataset were expanded on by solution small-angle X-ray scattering, allowing to move beyond the previously rigid, crystal-based view on TGT. The structural data of this thesis was further accompanied by biochemical characterization, focusing on tRNA binding and the association between tRNA body and non-catalytic subunit. This integrative approach yielded a new understanding of eukTGT function which, by careful comparison with bacterial and archaeal TGT, was finally placed in an evolutionary context.

In consequence, the structural biology of eukaryotic TGT and its tRNA complex is now well characterized. In contrast, TGT subcellular location, regulation and potential transport are all largely unknown. It remains to be hoped that complimentary approaches will shed light on these issues in the future and thus grant a full understanding of eukaryotic TGT in its cellular context.

BIBLIOGRAPHY

1. Dahm, R. (2008). Discovering DNA: Friedrich Miescher and the early years of nucleic acid research. Hum. Genet. *122*, 565–581. 10.1007/s00439-007-0433-0.

2. Avery, O.T., MacLeod, C.M., and McCarty, M. (1944). Studies on the nature of the substance inducing transformation of pneumococcal types. Induction of transformation by a desoxyribonucleic acid fraction isolated from Pneumococcus Type III. J. Exp. Med., 137–158.

3. Watson, J.D., and Crick, F.H.C. (1953). Molecular Structure of Nucleic Acids: A Structure for Deoxyribose Nucleic Acid. Nature *171*, 737–738. 10.1038/171737a0.

4. Crick, F.H.C., Barnett, L., Brenner, S., and Watts-Tobin, R.J. (1961). General Nature of the Genetic Code for Proteins. Nature *192*, 1227–1232. 10.1038/1921227a0.

5. Crick, F. (1970). Central Dogma of Molecular Biology. Nature *227*, 561–563. 10.1038/227561a0.

6. Gilbert, W. (1986). Origin of life: The RNA world. Nature *319*, 618–618. 10.1038/319618a0.

7. Jarrous, N., Mani, D., and Ramanathan, A. (2022). Coordination of transcription and processing of tRNA. FEBS J. *289*, 3630–3641. 10.1111/febs.15904.

8. Betat, H., Rammelt, C., and Mörl, M. (2010). tRNA nucleotidyltransferases: ancient catalysts with an unusual mechanism of polymerization. Cell. Mol. Life Sci. *67*, 1447–1463. 10.1007/s00018-010-0271-4.

9. Gomez, M.A.R., and Ibba, M. (2023). Aminoacyl-tRNA synthetases. RNA, 910–936.

10. Paushkin, S.V., Patel, M., Furia, B.S., Peltz, S.W., and Trotta, C.R. (2004). Identification of a Human Endonuclease Complex Reveals a Link between tRNA Splicing and Pre-mRNA 3' End Formation. Cell *117*, 311–321. 10.1016/S0092-8674(04)00342-3.

11. HSPC117 Is the Essential Subunit of a Human tRNA Splicing Ligase Complex https://www.science.org/doi/epdf/10.1126/science.1197847.

12. Boccaletto, P., Stefaniak, F., Ray, A., Cappannini, A., Mukherjee, S., Purta, E., Kurkowska, M., Shirvanizadeh, N., Destefanis, E., Groza, P., et al. (2022). MODOMICS: a database of RNA modification pathways. 2021 update. Nucleic Acids Res. *50*, D231–D235. 10.1093/nar/gkab1083.

13. Cantara, W.A., Crain, P.F., Rozenski, J., McCloskey, J.A., Harris, K.A., Zhang, X., Vendeix, F.A.P., Fabris, D., and Agris, P.F. (2011). The RNA Modification Database, RNAMDB: 2011 update. Nucleic Acids Res. *39*, D195-201. 10.1093/nar/gkq1028.

14. Lei, H.-T., Wang, Z.-H., Li, B., Sun, Y., Mei, S.-Q., Yang, J.-H., Qu, L.-H., and Zheng, L.-L. (2023). tModBase: deciphering the landscape of tRNA modifications and their dynamic changes from epitranscriptome data. Nucleic Acids Res. *51*, D315–D327. 10.1093/nar/gkac1087.

15. Pan, T. (2018). Modifications and functional genomics of human transfer RNA. Cell Res. *28*, 395–404. 10.1038/s41422-018-0013-y.

16. Suzuki, T. (2021). The expanding world of tRNA modifications and their disease relevance. Nat. Rev. Mol. Cell Biol. *22*, 375–392. 10.1038/s41580-021-00342-0.

17. Helm, M., Giegé, R., and Florentz, C. (1999). A Watson–Crick Base-Pair-Disrupting Methyl Group (m1A9) Is Sufficient for Cloverleaf Folding of Human Mitochondrial tRNALys. Biochemistry *38*, 13338–13346. 10.1021/bi991061g.

18. Voigts-Hoffmann, F., Hengesbach, M., Kobitski, A.Yu., van Aerschot, A., Herdewijn, P., Nienhaus, G.U., and Helm, M. (2007). A Methyl Group Controls Conformational Equilibrium in Human Mitochondrial tRNALys. J. Am. Chem. Soc. *129*, 13382–13383. 10.1021/ja075520+.

19. Sissler, M., Helm, M., Frugier, M., Giegé, R., and Florentz, C. (2004). Aminoacylation properties of pathology-related human mitochondrial tRNALys variants. RNA *10*, 841–853. 10.1261/rna.5267604.

20. Helm, M., and Attardi, G. (2004). Nuclear Control of Cloverleaf Structure of Human Mitochondrial tRNALys. J. Mol. Biol. *337*, 545–560. 10.1016/j.jmb.2004.01.036.

21. Pütz, J., Dupuis, B., Sissler, M., and Florentz, C. (2007). Mamit-tRNA, a database of mammalian mitochondrial tRNA primary and secondary structures. RNA *13*, 1184–1190. 10.1261/rna.588407.

22. Helm, M. (2006). Post-transcriptional nucleotide modification and alternative folding of RNA. Nucleic Acids Res. *34*, 721–733. 10.1093/nar/gkj471.

23. Davis, D.R. (2014). Biophysical and Conformational Properties of Modified Nucleosides in RNA (Nuclear Magnetic Resonance Studies). In Modification and Editing of RNA, H. Grosjean and R. Benne, eds. (ASM Press), pp. 85–102. 10.1128/9781555818296.ch5.

24. Chen, Y., Sierzputowska-Gracz, H., Guenther, R., Everett, K., and Agris, P.F. (1993). 5-Methylcytidine is required for cooperative binding of Mg2+ and a conformational transition at the anticodon stem-loop of yeast phenylalanine tRNA. Biochemistry *32*, 10249–10253. 10.1021/bi00089a047.

25. Dao, V., Guenther, R.H., and Agris, P.F. (1992). The role of 5-methylcytidine in the anticodon arm of yeast tRNA(Phe): site-specific Mg2+ binding and coupled conformational transition in DNA analogs. Biochemistry *31*, 11012–11019. 10.1021/bi00160a010.

26. Motorin, Y., and Helm, M. (2010). tRNA Stabilization by Modified Nucleotides. Biochemistry *49*, 4934–4944. 10.1021/bi100408z.

27. Muramatsu, T., Nishikawa, K., Nemoto, F., Kuchino, Y., Nishimura, S., Miyazawa, T., and Yokoyama, S. (1988). Codon and amino-acid specificities of a transfer RNA are both converted by a single post-transcriptional modification. Nature *336*, 179–181. 10.1038/336179a0.

28. Sylvers, L.A., Rogers, K.C., Shimizu, M., Ohtsuka, E., and Soll, D. (1993). A 2-thiouridine derivative in tRNAGlu is a positive determinant for aminoacylation by Escherichia coli glutamyl-tRNA synthetase. Biochemistry *32*, 3836–3841. 10.1021/bi00066a002.

29. Senger, B., Auxilien, S., Englisch, U., Cramer, F., and Fasiolo, F. (1997). The Modified Wobble Base Inosine in Yeast tRNA [Ile] Is a Positive Determinant for Aminoacylation by Isoleucyl-tRNA Synthetase. Biochemistry *36*, 8269–8275. 10.1021/bi970206l.

30. Niimi, T., Nureki, O., Yokogawa, T., Hayashi, N., Nishikawa, K., Watanabe, K., and Yokoyama, S. (1994). Recognition of the Anticodon Loop of tRNAIle 1 by Isoleucyl-tRNA Synthetase from Escherichia coli. Nucleosides Nucleotides *13*, 1231–1237. 10.1080/15257779408012147.

31. Demeshkina, N., Jenner, L., Westhof, E., Yusupov, M., and Yusupova, G. (2012). A new understanding of the decoding principle on the ribosome. Nature *484*, 256–259. 10.1038/nature10913.

32. Rozov, A., Demeshkina, N., Westhof, E., Yusupov, M., and Yusupova, G. (2015). Structural insights into the translational infidelity mechanism. Nat. Commun. *6*, 7251. 10.1038/ncomms8251.

33. Crick, F. (1966). Codon–anticodon pairing: the wobble hypothesis. J. Mol. Biol., 548–555.

34. Lei, L., and Burton, Z.F. (2022). "Superwobbling" and tRNA-34 Wobble and tRNA-37 Anticodon Loop Modifications in Evolution and Devolution of the Genetic Code. Life *12*, 252. 10.3390/life12020252.

35. Rafels-Ybern, À., Torres, A.G., Grau-Bove, X., Ruiz-Trillo, I., and Ribas de Pouplana, L. (2018). Codon adaptation to tRNAs with Inosine modification at position 34 is widespread among Eukaryotes and present in two Bacterial phyla. RNA Biol. *15*, 500–507. 10.1080/15476286.2017.1358348.

36. Murphy, F.V., and Ramakrishnan, V. (2004). Structure of a purine-purine wobble base pair in the decoding center of the ribosome. Nat. Struct. Mol. Biol. *11*, 1251–1252. 10.1038/nsmb866.

37. Grosjean, H., and Westhof, E. (2016). An integrated, structure- and energy-based view of the genetic code. Nucleic Acids Res. *44*, 8020–8040. 10.1093/nar/gkw608.

38. Kasai, H., Ohashi, Z., Harada, F., Nishimura, S., Oppenheimer, N.J., Crain, P.F., Liehr, J.G., Von Minden, D.L., and McCloskey, J.A. (1975). Structure of the modified nucleoside Q isolated from Escherichia coli transfer ribonucleic acid. 7-(4,5-cis-Dihydroxy-1-cyclopenten-3-ylaminomethyl)-7-deazaguanosine. Biochemistry *14*, 4198–4208. 10.1021/bi00690a008.

39. Yokoyama, S., Miyazawa, T., Iitaka, Y., Yamaizumi, Z., Kasai, H., and Nishimura, S. (1979). Three-dimensional structure of hyper-modified nucleoside Q located in the wobbling position of tRNA. Nature *282*, 107–109. 10.1038/282107a0.

40. Harada, F., and Nishimura, S. (1972). Possible anticodon sequences of tRNAHis, tRNAAsn, and tRNAAsp from Escherichia coli. Universal presence of nucleoside Q in the first position of the anticodons of these transfer ribonucleic acid. Biochemistry *11*, 301–308. 10.1021/bi00752a024.

41. RajBhandary, U.L., Chang, S.H., Gross, H.J., Harada, F., Kimura, F., and Nishimura, S. (1969). Fed. Am. Soc. Exp. Biol. J. *28*.

42. Goodman, H.M., Abelson, J., Landy, A., Brenner, S., and Smith, J.D. (1968). Amber Suppression: a Nucleotide Change in the Anticodon of a Tyrosine Transfer RNA. Nature *217*, 1019–1024. 10.1038/2171019a0.

43. Goodman, H.M., Abelson, J.N., Landy, A., Zadrazil, S., and Smith, J.D. (1970). The Nucleotide Sequences of Tyrosine Transfer RNAs of Escherichia coli. Eur. J. Biochem. *13*, 461–483. 10.1111/j.1432-1033.1970.tb00950.x.

44. Doctor, B.P., Loebel, J.E., Sodd, M.A., and Winter, D.B. (1969). Nucleotide Sequence of *Escherichia coli* Tyrosine Transfer Ribonucleic Acid. Science *163*, 693–695. 10.1126/science.163.3868.693.

45. White, B.N., Teneb, G.M., Holden, J., and Suzuki, D.T. (1973). Activity of a transfer RNA modifying enzyme during the development of Drosophila and its relationship to the su(s) locus. J. Mol. Biol. *74*, 635–651. 10.1016/0022-2836(73)90054-5.

46. Kasai, H., Nakanishi, K., Macfarlane, R.D., Torgerson, D.F., Ohashi, Z., McCloskey, J.A., Gross, H.J., and Nishimura, S. (1976). The structure of Q* nucleoside isolated from rabbit liver transfer ribonucleic acid. J. Am. Chem. Soc. *98*, 5044–5046. 10.1021/ja00432a071.

47. Kasai, H., Kuchino, Y., Nihei, K., and Nishimura, S. (1975). Distribution of the modified nucleoside Q and its derivatives in animal and plant transfer RNA's. Nucleic Acids Res. *2*, 1931–1940. 10.1093/nar/2.10.1931.

48. Walden, T.L., Howes, N., and Farkas, W.R. (1982). Purification and properties of guanine, queuine-tRNA transglycosylase from wheat germ. J. Biol. Chem. *257*, 13218–13222. 10.1016/S0021-9258(18)33433-1.

49. Randerath, E., Agrawal, H.P., and Randerath, K. (1984). Specific Lack of the Hypermodified Nucleoside, Queuosine, in Hepatoma Mitochondria! Aspartate Transfer RNA and Its Possible Biological Significance. *44*.

50. Suzuki, T., Yashiro, Y., Kikuchi, I., Ishigami, Y., Saito, H., Matsuzawa, I., Okada, S., Mito, M., Iwasaki, S., Ma, D., et al. (2020). Complete chemical structures of human mitochondrial tRNAs. Nat. Commun. *11*, 4269. 10.1038/s41467-020-18068-6.

51. Suzuki, T., and Suzuki, T. (2014). A complete landscape of post-transcriptional modifications in mammalian mitochondrial tRNAs. Nucleic Acids Res. *42*, 7346–7357. 10.1093/nar/gku390.

52. Walden, T., Reyniers, J.P., Hiatt, V., and Farkas, W.R. (1982). Yeast Cells Cannot Incorporate Queuine into Their tRNA. Proc. Soc. Exp. Biol. Med. *170*, 328–332. 10.3181/00379727-170-41438.

53. Globisch, D., Pearson, D., Hienzsch, A., Brückl, T., Wagner, M., Thoma, I., Thumbs, P., Reiter, V., Kneuttinger, A.C., Müller, M., et al. (2011). Systems-Based Analysis of Modified tRNA Bases. Angew. Chem. Int. Ed. *50*, 9739–9742. 10.1002/anie.201103229.

54. Chen, P., Jäger, G., and Zheng, B. (2010). Transfer RNA modifications and genes for modifying enzymes in Arabidopsis thaliana. BMC Plant Biol. *10*, 201. 10.1186/1471-2229-10-201.

55. Eiler, S., Dock-Bregeon, A.-C., Moulinier, L., Thierry, J.-C., and Moras, D. (1999). Synthesis of aspartyl-tRNAAsp in Escherichia coli—a snapshot of the second step. EMBO J. *18*, 6532–6541. 10.1093/emboj/18.22.6532.

56. Briand, C., Poterszman, A., Eiler, S., Webster, G., Thierry, J.-C., and Moras, D. (2000). An intermediate step in the recognition of tRNAAsp by aspartyl-tRNA synthetase11Edited by J. Doudna. J. Mol. Biol. *299*, 1051–1060. 10.1006/jmbi.2000.3819.

57. Ruff, M., Krishnaswamy, S., Boeglin, M., Poterszman, A., Mitschler, A., Podjarny, A., Rees, B., Thierry, J.C., and Moras, D. (1991). Class II Aminoacyl Transfer Rna Synthetases: Crystal Structure of Yeast Aspartyl-trna Synthetase Complexed with tRNAAsp. Science *252*, 1682–1689. 10.1126/science.2047877.

58. Tian, Q., Wang, C., Liu, Y., and Xie, W. (2015). Structural basis for recognition of G-1-containing tRNA by histidyl-tRNA synthetase. Nucleic Acids Res. *43*, 2980. 10.1093/nar/gkv129.

59. Yaremchuk, A., Kriklivyi, I., Tukalo, M., and Cusack, S. (2002). Class I tyrosyl-tRNA synthetase has a class II mode of cognate tRNA recognition. EMBO J. *21*, 3829–3840. 10.1093/emboj/cdf373.

60. Curnow, A.W., Ibba, M., and Söll, D. (1996). tRNA-dependent asparagine formation. Nature *382*, 589–590. 10.1038/382589b0.

61. Suzuki, T., Nakamura, A., Kato, K., Söll, D., Tanaka, I., Sheppard, K., and Yao, M. (2015). Structure of the Pseudomonas aeruginosa transamidosome reveals unique aspects of bacterial tRNA-dependent asparagine biosynthesis. Proc. Natl. Acad. Sci. *112*, 382–387. 10.1073/pnas.1423314112.

62. McNamara, A.L., and Smith, D.W. (1978). The function of the histidine tRNA isoaccepting species in hemoglobin synthesis. J. Biol. Chem. *253*, 5964–5970.

63. Singhal, R.P., and Vakharia, V.N. (1983). The role of queuine in the aminoacylation of mammalian aspartate transfer RNAs. Nucleic Acids Res. *11*, 4257–4272. 10.1093/nar/11.12.4257.

64. Noguchi, S., Nishimura, Y., Hirota, Y., and Nishimura, S. (1982). Isolation and characterization of an Escherichia coli mutant lacking tRNA-guanine transglycosylase. Function and biosynthesis of queuosine in tRNA. J. Biol. Chem. *257*, 6544–6550. 10.1016/S0021-9258(20)65176-6.

65. Ramakrishnan, V. (2002). Ribosome Structure and the Mechanism of Translation. Cell *108*, 557–572. 10.1016/S0092-8674(02)00619-0.

66. Singhal, R.P. (1981). MODIFICATION OF GUANINE TO QUHUINE IN TRANSFER RNAs DURING DEVELOPMFXV AND AGING. Biochem. Biophys. Res. Commun. *99*.

67. Grosjean, H.J., de Henau, S., and Crothers, D.M. (1978). On the physical basis for ambiguity in genetic coding interactions. Proc. Natl. Acad. Sci. *75*, 610–614. 10.1073/pnas.75.2.610.

68. Meier, F., Suter, B., Grosjean, H., Keith, G., and Kubli, E. (1985). Queuosine modification of the wobble base in tRNAHis influences 'in vivo' decoding properties. EMBO J. *4*, 823–827. 10.1002/j.1460-2075.1985.tb03704.x.

69. Manickam, N., Joshi, K., Bhatt, M.J., and Farabaugh, P.J. (2016). Effects of tRNA modification on translational accuracy depend on intrinsic codon–anticodon strength. Nucleic Acids Res. *44*, 1871–1881.

70. Kulkarni, S., Rubio, M.A.T., Hegedűsová, E., Ross, R.L., Limbach, P.A., Alfonzo, J.D., and Paris, Z. (2021). Preferential import of queuosine-modified tRNAs into Trypanosoma brucei mitochondrion is critical for organellar protein synthesis. Nucleic Acids Res. *49*, 8247–8260. 10.1093/nar/gkab567.

71. Dixit, S., Kessler, A.C., Henderson, J., Pan, X., Zhao, R., D'Almeida, G.S., Kulkarni, S., Rubio, M.A.T., Hegedűsová, E., Ross, R.L., et al. (2021). Dynamic queuosine changes in tRNA couple nutrient levels to codon choice in Trypanosoma brucei. Nucleic Acids Res. *49*, 12986–12999. 10.1093/nar/gkab1204.

72. Urbonavičius, J., Qian, Q., Durand, J.M.B., Hagervall, T.G., and Björk, G.R. (2001). Improvement of reading frame maintenance is a common function for several tRNA modifications. EMBO J. *20*, 4863–4873. 10.1093/emboj/20.17.4863.

73. Tuorto, F., Legrand, C., Cirzi, C., Federico, G., Liebers, R., Müller, M., Ehrenhofer-Murray, A.E., Dittmar, G., Gröne, H.-J., and Lyko, F. (2018). Queuosine-modified tRNAs confer nutritional control of protein translation. EMBO J. *37*, e99777. 10.15252/embj.201899777.

74. Müller, M., Legrand, C., Tuorto, F., Kelly, V.P., Atlasi, Y., Lyko, F., and Ehrenhofer-Murray, A.E. (2019). Queuine links translational control in eukaryotes to a micronutrient from bacteria. Nucleic Acids Res. *47*, 3711–3727. 10.1093/nar/gkz063.

75. Zaborske, J.M., DuMont, V.L.B., Wallace, E.W.J., Pan, T., Aquadro, C.F., and Drummond, D.A. (2014). A Nutrient-Driven tRNA Modification Alters Translational Fidelity and Genome-wide Protein Coding across an Animal Genus. PLOS Biol. *12*, e1002015. 10.1371/journal.pbio.1002015.

76. Hurt, J.K. (2010). MODULATION OF EXPRESSION AND ANTIBACTERIAL TARGETING OF SHIGELLA FLEXNERI VIRF.

77. Durand, J.M.B., Dagberg, B., Uhlin, B.E., and Björk, G.R. (2000). Transfer RNA modification, temperature and DNA superhelicity have a common target in the regulatory network of the virulence of Shigella flexneri: the expression of the virF gene. Mol. Microbiol. *35*, 924–935. 10.1046/j.1365-2958.2000.01767.x.

78. Durand, J.M., Okada, N., Tobe, T., Watarai, M., Fukuda, I., Suzuki, T., Nakata, N., Komatsu, K., Yoshikawa, M., and Sasakawa, C. (1994). vacC, a virulence-associated chromosomal locus of Shigella flexneri, is homologous to tgt, a gene encoding tRNA-guanine transglycosylase (Tgt) of Escherichia coli K-12. J. Bacteriol. *176*, 4627–4634. 10.1128/jb.176.15.4627-4634.1994.

79. Sokołowski, M., Klassen, R., Bruch, A., Schaffrath, R., and Glatt, S. (2018). Cooperativity between different tRNA modifications and their modification pathways. Biochim. Biophys. Acta BBA - Gene Regul. Mech. *1861*, 409–418. 10.1016/j.bbagrm.2017.12.003.

80. Müller, M., Hartmann, M., Schuster, I., Bender, S., Thüring, K.L., Helm, M., Katze, J.R., Nellen, W., Lyko, F., and Ehrenhofer-Murray, A.E. (2015). Dynamic modulation of Dnmt2-dependent tRNA methylation by the micronutrient queuine. Nucleic Acids Res. *43*, 10952–10962. 10.1093/nar/gkv980.

81. Johannsson, S., Neumann, P., Wulf, A., Welp, L.M., Gerber, H.-D., Krull, M., Diederichsen, U., Urlaub, H., and Ficner, R. (2018). Structural insights into the stimulation of S. pombe Dnmt2 catalytic efficiency by the tRNA nucleoside queuosine. Sci. Rep. *8*, 8880. 10.1038/s41598-018-27118-5.

82. Schaefer, M., Pollex, T., Hanna, K., Tuorto, F., Meusburger, M., Helm, M., and Lyko, F. (2010). RNA methylation by Dnmt2 protects transfer RNAs against stress-induced cleavage. Genes Dev. *24*, 1590–1595. 10.1101/gad.586710.

83. Wang, X., Matuszek, Z., Huang, Y., Parisien, M., Dai, Q., Clark, W., Schwartz, M.H., and Pan, T. (2018). Queuosine modification protects cognate tRNAs against ribonuclease cleavage. RNA *24*, 1305–1313. 10.1261/rna.067033.118.

84. Pichot, F., Hogg, M.C., Marchand, V., Bourguignon, V., Jirström, E., Farrell, C., Gibriel, H.A., Prehn, J.H.M., Motorin, Y., and Helm, M. (2023). Quantification of substoichiometric modification reveals global tsRNA hypomodification, preferences for angiogenin-mediated tRNA cleavage, and idiosyncratic epitranscriptomes of human neuronal cell-lines. Comput. Struct. Biotechnol. J. *21*, 401–417. 10.1016/j.csbj.2022.12.020.

85. Frazer, J.M., and Yang, W.-K. (1972). Isoaccepting transfer ribonucleic acids in liver and brain of young and old BC3F1 mice. Arch. Biochem. Biophys. *153*, 610–618. 10.1016/0003-9861(72)90380-3.

86. Shindo-Okada, N., Terada, M., and Nishimura, S. (1981). Changes in amount of hypo-modified tRNA having guanine in place of queuine during erythroid differentiation of murine erythroleukemia cells. Eur. J. Biochem. *115*, 423–428. 10.1111/j.1432-1033.1981.tb05254.x.

87. Lin, V.K., Farkas, W.R., and Agris, P.F. (1980). Specific changes in Q-ribonucleoside containing transfer RNA species during Friend leukemia cell erythroid differentiation. Nucleic Acids Res. *8*, 3481–3489. 10.1093/nar/8.15.3481.

88. Chen, Y.L., and Wu, R.T. (1994). Altered queuine modification of transfer RNA involved in the differentiation of human K562 erythroleukemia cells in the presence of distinct differentiation inducers. Cancer Res. *54*, 2192–2198.

89. Owenby, R.K., Stulberg, M.P., and Jacobson, K.B. (1979). Alteration of the Q family of transfer RNAs in adult Drosophila melanogaster as a function of age, nutrition, and genotype. Mech. Ageing Dev. *11*, 91–103.

90. White, B.N., and Lassam, N.J. (1979). An analysis of Q and Q∗ containing tRNAs during the development of Lucilia sericata, Musca domestica and Tenebrio molitor. Insect Biochem. *9*, 375–378. 10.1016/0020-1790(79)90085-4.

91. Kirtland, G.M., Morris, T.D., Moore, P.H., O'Brian, J.J., Edmonds, C.G., McCloskey, J.A., and Katze, J.R. (1988). Novel salvage of queuine from queuosine and absence of queuine synthesis in Chlorella pyrenoidosa and Chlamydomonas reinhardtii. J. Bacteriol. *170*, 5633–5641. 10.1128/jb.170.12.5633-5641.1988.

92. Gaur, R., Björk, G.R., Tuck, S., and Varshney, U. (2007). Diet-dependent depletion of queuosine in tRNAs in Caenorhabditis elegans does not lead to a developmental block. J. Biosci. *32*, 747–754. 10.1007/s12038-007-0074-4.

93. Szabo, L., Nishimura, S., and Farkas, W.R. (1988). Possible involvement of queuine in oxidative metabolism. BioFactors Oxf. Engl. *1*, 241–244.

94. Reisser, T., Langgut, W., and Kersten, H. (1994). The nutrient factor queuine protects HeLa cells from hypoxic stress and improves metabolic adaptation to oxygen availability. Eur. J. Biochem. *221*, 979–986. 10.1111/j.1432-1033.1994.tb18814.x.

95. Pathak, C., and Vinayak, M. (2005). Modulation of Lactate Dehydrogenase Isozymes by Modified Base Queuine. Mol. Biol. Rep. *32*, 191–196. 10.1007/s11033-004-6941-2.

96. Schachner, E., Aschhoff, H.J., and Kersten, H. (1984). Specific changes in lactate levels, lactate dehydrogenase patterns and cytochrome b559 in Dictyostelium discoideum caused by queuine. Eur. J. Biochem. *139*, 481–487. 10.1111/j.1432-1033.1984.tb08031.x.

97. Hayes, P., Fergus, C., Ghanim, M., Cirzi, C., Burtnyak, L., McGrenaghan, C.J., Tuorto, F., Nolan, D.P., and Kelly, V.P. (2020). Queuine Micronutrient Deficiency Promotes Warburg Metabolism and Reversal of the Mitochondrial ATP Synthase in Hela Cells. Nutrients *12*, 871. 10.3390/nu12030871.

98. Farkas, W.R. (1980). Effect of diet on the queuosine family of tRNAs of germ-free mice. J. Biol. Chem. *255*, 6832–6835. 10.1016/S0021-9258(18)43648-4.

99. Rakovich, T., Boland, C., Bernstein, I., Chikwana, V.M., Iwata-Reuyl, D., and Kelly, V.P. (2011). Queuosine Deficiency in Eukaryotes Compromises Tyrosine Production through Increased Tetrahydrobiopterin Oxidation. J. Biol. Chem. *286*, 19354–19363. 10.1074/jbc.M111.219576.

100. Marks, T., and Farkas, W.R. (1997). Effects of a Diet Deficient in Tyrosine and Queuine on Germfree Mice. Biochem. Biophys. Res. Commun. *230*, 233–237. 10.1006/bbrc.1996.5768.

101. Dirheimer, G., Baranowski, W., and Keith, G. (1995). Variations in tRNA modifications, particularly of their queuine content in higher eukaryotes. Its relation to malignancy grading. Biochimie *77*, 99–103.

102. Emmerich, B., Zubrod, E., Weber, H., Maubach, P.A., Kersten, H., and Kersten, W. (1985). Relationship of queuine-lacking transfer RNA to the grade of malignancy in human leukemias and lymphomas. Cancer Res. *45*, 4308–4314.

103. Aytaç, U., and Gündüz, U. (1994). Q-modification of tRNAs in human brain tumors. Cancer Biochem. Biophys. *14*, 93–98.

104. Huang, B.S., Wu, R.T., and Chien, K.Y. (1992). Relationship of the queuine content of transfer ribonucleic acids to histopathological grading and survival in human lung cancer. Cancer Res. *52*, 4696–4700.

105. Baranowski, W., Dirheimer, G., Jakowicki, J.A., and Keith, G. (1994). Deficiency of queuine, a highly modified purine base, in transfer RNAs from primary and metastatic ovarian malignant tumors in women. Cancer Res. *54*, 4468–4471.

106. Phillips, G., El Yacoubi, B., Lyons, B., Alvarez, S., Iwata-Reuyl, D., and de Crécy-Lagard, V. (2008). Biosynthesis of 7-Deazaguanosine-Modified tRNA Nucleosides: a New Role for GTP Cyclohydrolase I. J. Bacteriol. *190*, 7876–7884. 10.1128/JB.00874-08.

107. Katzenmeier, G., Schmid, C., and Bacher, A. (1990). Cloning and expression of the putative gene coding for GTP cyclohydrolase I from *Escherichia coli*. FEMS Microbiol. Lett. *66*, 231–234. 10.1111/j.1574-6968.1990.tb04002.x.

108. Nar, H., Huber, R., Auerbach, G., Fischer, M., Hösl, C., Ritz, H., Bracher, A., Meining, W., Eberhardt, S., and Bacher, A. (1995). Active site topology and reaction mechanism of GTP cyclohydrolase I. Proc. Natl. Acad. Sci. *92*, 12120–12125. 10.1073/pnas.92.26.12120.

109. Yim, J.J., and Brown, G.M. (1976). Characteristics of guanosine triphosphate cyclohydrolase I purified from Escherichia coli. J. Biol. Chem. *251*, 5087–5094. 10.1016/S0021-9258(17)33222-2.

110. McCarty, R.M., Somogyi, Á., and Bandarian, V. (2009). *Escherichia coli* QueD Is a 6-Carboxy-5,6,7,8-tetrahydropterin Synthase. Biochemistry *48*, 2301–2303. 10.1021/bi9001437.

111. Miles, Z.D., Roberts, S.A., McCarty, R.M., and Bandarian, V. (2014). Biochemical and Structural Studies of 6-Carboxy-5,6,7,8-tetrahydropterin Synthase Reveal the Molecular Basis of Catalytic Promiscuity within the Tunnel-fold Superfamily *. J. Biol. Chem. *289*, 23641–23652. 10.1074/jbc.M114.555680.

112. Dowling, D.P., Bruender, N.A., Young, A.P., McCarty, R.M., Bandarian, V., and Drennan, C.L. (2014). Radical SAM enzyme QueE defines a new minimal core fold and metal-dependent mechanism. Nat. Chem. Biol. *10*, 106–112. 10.1038/nchembio.1426.

113. McCarty, R.M., Somogyi, Á., Lin, G., Jacobsen, N.E., and Bandarian, V. (2009). The Deazapurine Biosynthetic Pathway Revealed: In Vitro Enzymatic Synthesis of PreQ0 from Guanosine 5′-Triphosphate in Four Steps. Biochemistry *48*, 3847–3852. 10.1021/bi900400e.

114. Gaur, R., and Varshney, U. (2005). Genetic analysis identifies a function for the queC (ybaX) gene product at an initial step in the queuosine biosynthetic pathway in Escherichia coli. J. Bacteriol. *187*, 6893–6901. 10.1128/JB.187.20.6893-6901.2005.

115. Nelp, M.T., and Bandarian, V. (2015). A Single Enzyme Transforms a Carboxylic Acid into a Nitrile through an Amide Intermediate. Angew. Chem. Int. Ed. *54*, 10627–10629. 10.1002/anie.201504505.

116. Noguchi, S., Yamaizumi, Z., Ohgi, T., Goto, T., Nishimura, Y., Hirota, Y., and Nishimura, S. (1978). Isolation of Q nucleoside precursor present in tRNA of an E.coli mutant and its characterization as 7-(cyano)-7-deazaguanosine. Nucleic Acids Res. *5*, 4215–4224. 10.1093/nar/5.11.4215.

117. Van Lanen, S.G., Reader, J.S., Swairjo, M.A., de Crécy-Lagard, V., Lee, B., and Iwata-Reuyl, D. (2005). From cyclohydrolase to oxidoreductase: Discovery of nitrile reductase activity in a common fold. Proc. Natl. Acad. Sci. *102*, 4264–4269. 10.1073/pnas.0408056102.

118. Lee, B.W.K., Van Lanen, S.G., and Iwata-Reuyl, D. (2007). Mechanistic Studies of Bacillus subtilis QueF, the Nitrile Oxidoreductase Involved in Queuosine Biosynthesis. Biochemistry *46*, 12844–12854. 10.1021/bi701265r.

119. Okada, N., Noguchi, S., Nishimura, S., Ohgi, T., Goto, T., Crain, P.F., and McCloskey, J.A. (1978). Structure determination of a nucleoside Q precursor isolated from E. coli tRNA: 7-{aminomethyl)-7-deazaguanosine. Nucleic Acids Res. *5*, 2289–2296. 10.1093/nar/5.7.2289.

120. Slany, R.K., Boesl, M., Crain, P.F., and Kersten, H. (1993). A new function of S-adenosylmethionine: The ribosyl moiety of AdoMet is the precursor of the cyclopentenediol moiety of the tRNA wobble base queuine. Biochemistry *32*, 7811–7817. 10.1021/bi00081a028.

121. Slany, R.K., Bösl, M., and Kersten, H. (1994). Transfer and isomerization of the ribose moiety of AdoMet during the biosynthesis of queuosine tRNAs, a new unique reaction catalyzed by the QueA protein from Escherichia coli. Biochimie *76*, 389–393. 10.1016/0300-9084(94)90113-9.

122. Miles, Z.D., McCarty, R.M., Molnar, G., and Bandarian, V. (2011). Discovery of epoxyqueuosine (oQ) reductase reveals parallels between halorespiration and tRNA modification. Proc. Natl. Acad. Sci. *108*, 7368–7372. 10.1073/pnas.1018636108.

123. Zallot, R., Ross, R., Chen, W.-H., Bruner, S.D., Limbach, P.A., and de Crécy-Lagard, V. (2017). Identification of a Novel Epoxyqueuosine Reductase Family by Comparative Genomics. ACS Chem. Biol. *12*, 844–851. 10.1021/acschembio.6b01100.

124. Eitinger, T., Rodionov, D.A., Grote, M., and Schneider, E. (2011). Canonical and ECF-type ATP-binding cassette importers in prokaryotes: diversity in modular organization and cellular functions. FEMS Microbiol. Rev. *35*, 3–67. 10.1111/j.1574-6976.2010.00230.x.

125. Rodionov, D.A., Hebbeln, P., Eudes, A., ter Beek, J., Rodionova, I.A., Erkens, G.B., Slotboom, D.J., Gelfand, M.S., Osterman, A.L., Hanson, A.D., et al. (2009). A Novel Class of Modular Transporters for Vitamins in Prokaryotes. J. Bacteriol. *191*, 42–51. 10.1128/JB.01208-08.

126. Roth, A., Winkler, W.C., Regulski, E.E., Lee, B.W.K., Lim, J., Jona, I., Barrick, J.E., Ritwik, A., Kim, J.N., Welz, R., et al. (2007). A riboswitch selective for the queuosine precursor preQ1 contains an unusually small aptamer domain. Nat. Struct. Mol. Biol. *14*, 308–317. 10.1038/nsmb1224.

127. Meyer, M.M., Roth, A., Chervin, S.M., Garcia, G.A., and Breaker, R.R. (2008). Confirmation of a second natural preQ1 aptamer class in Streptococcaceae bacteria. RNA *14*, 685–695. 10.1261/rna.937308.

128. Yuan, Y., Zallot, R., Grove, T.L., Payan, D.J., Martin-Verstraete, I., Šepić, S., Balamkundu, S., Neelakandan, R., Gadi, V.K., Liu, C.-F., et al. (2019). Discovery of novel bacterial queuine salvage enzymes and pathways in human pathogens. Proc. Natl. Acad. Sci. *116*, 19126–19135. 10.1073/pnas.1909604116.

129. Thumbs, P., Ensfelder, T.T., Hillmeier, M., Wagner, M., Heiss, M., Scheel, C., Schön, A., Müller, M., Michalakis, S., Kellner, S., et al. (2020). Synthesis of Galactosyl-Queuosine and Distribution of Hypermodified Q-Nucleosides in Mouse Tissues. Angew. Chem. Int. Ed. *59*, 12352–12356. 10.1002/anie.202002295.

130. Elliott, M.S., Trewyn, R.W., and Katze, J.R. (1985). Inhibition of queuine uptake in cultured human fibroblasts by phorbol-12,13-didecanoate. Cancer Res. *45*, 1079–1085.

131. Hung, S.-H., Elliott, G.I., Ramkumar, T.R., Burtnyak, L., McGrenaghan, C.J., Alkuzweny, S., Quaiyum, S., Iwata-Reuyl, D., Pan, X., Green, B.D., et al. (2023). Structural basis of Qng1-mediated salvage of the micronutrient queuine from queuosine-5′-monophosphate as the biological substrate. Nucleic Acids Res. *51*, 935–951. 10.1093/nar/gkac1231.

132. Zallot, R., Brochier-Armanet, C., Gaston, K.W., Forouhar, F., Limbach, P.A., Hunt, J.F., and de Crécy-Lagard, V. (2014). Plant, Animal, and Fungal Micronutrient Queuosine Is Salvaged by Members of the DUF2419 Protein Family. ACS Chem. Biol. *9*, 1812–1825. 10.1021/cb500278k.

133. Patel, B.I., Heiss, M., Samel-Pommerencke, A., Carell, T., and Ehrenhofer-Murray, A.E. (2022). Queuosine salvage in fission yeast by Qng1-mediated hydrolysis to queuine. Biochem. Biophys. Res. Commun. *624*, 146–150. 10.1016/j.bbrc.2022.07.104.

134. Sarid, L., Sun, J., Chittrakanwong, J., Trebicz-Geffen, M., Ye, J., Dedon, P.C., and Ankri, S. (2022). Queuine Salvaging in the Human Parasite Entamoeba histolytica. Cells *11*, 2509. 10.3390/cells11162509.

135. Boland, C., Hayes, P., Santa-Maria, I., Nishimura, S., and Kelly, V.P. (2009). Queuosine Formation in Eukaryotic tRNA Occurs via a Mitochondria-localized Heteromeric Transglycosylase*. J. Biol. Chem. *284*, 18218–18227. 10.1074/jbc.M109.002477.

136. Rath, S., Sharma, R., Gupta, R., Ast, T., Chan, C., Durham, T.J., Goodman, R.P., Grabarek, Z., Haas, M.E., Hung, W.H.W., et al. (2021). MitoCarta3.0: an updated mitochondrial proteome now with sub-organelle localization and pathway annotations. Nucleic Acids Res. *49*, D1541–D1547. 10.1093/nar/gkaa1011.

137. Wiedemann, N., and Pfanner, N. (2017). Mitochondrial Machineries for Protein Import and Assembly. Annu. Rev. Biochem. *86*, 685–714. 10.1146/annurev-biochem-060815-014352.

138. Blaise, M., Becker, H.D., Keith, G., Cambillau, C., Lapointe, J., Giegé, R., and Kern, D. (2004). A minimalist glutamyl-tRNA synthetase dedicated to aminoacylation of the tRNAAsp QUC anticodon. Nucleic Acids Res. *32*, 2768–2775. 10.1093/nar/gkh608.

139. Salazar, J.C., Ambrogelly, A., Crain, P.F., McCloskey, J.A., and Söll, D. (2004). A truncated aminoacyl–tRNA synthetase modifies RNA. Proc. Natl. Acad. Sci. *101*, 7536–7541. 10.1073/pnas.0401982101.

140. Blaise, M., Olieric, V., Sauter, C., Lorber, B., Roy, B., Karmakar, S., Banerjee, R., Becker, H.D., and Kern, D. (2008). Crystal Structure of Glutamyl-Queuosine tRNAAsp Synthetase Complexed with l-Glutamate: Structural Elements Mediating tRNA-Independent Activation of Glutamate and Glutamylation of tRNAAsp Anticodon. J. Mol. Biol. *381*, 1224–1237. 10.1016/j.jmb.2008.06.053.

141. Hillmeier, M., Wagner, M., Ensfelder, T., Korytiakova, E., Thumbs, P., Müller, M., and Carell, T. (2021). Synthesis and structure elucidation of the human tRNA nucleoside mannosyl-queuosine. Nat. Commun. *12*, 7123. 10.1038/s41467-021-27371-9.

142. Kilpatrick, M.W., and Walker, R.T. (1982). The Nucleotide Sequence of the tRNA{ie} from the Archaebacterium Thermoplasma acidophilum. Zentralblatt Für Bakteriol. Mikrobiol. Hyg. Abt Orig. C Allg. Angew. Ökol. Mikrobiol. *3*, 79–89. 10.1016/S0721-9571(82)80056-2.

143. Edmonds, C.G., Crain, P.F., Gupta, R., Hashizume, T., Hocart, C.H., Kowalak, J.A., Pomerantz, S.C., Stetter, K.O., and McCloskey, J.A. (1991). Posttranscriptional modification of tRNA in thermophilic archaea (Archaebacteria). J. Bacteriol. *173*, 3138–3148. 10.1128/jb.173.10.3138-3148.1991.

144. Gregson, J.M., Crain, P.F., Edmonds, C.G., Gupta, R., Hashizume, T., Phillipson, D.W., and McCloskey, J.A. (1993). Structure of the archaeal transfer RNA nucleoside G*-15 (2-amino-4,7-dihydro- 4-oxo-7-beta-D-ribofuranosyl-1H-pyrrolo[2,3-d]pyrimidine-5-carboximi dam ide (archaeosine)). J. Biol. Chem. *268*, 10076–10086. 10.1016/S0021-9258(18)82174-3.

145. Watanabe, M., Matsuo, M., Tanaka, S., Akimoto, H., Asahi, S., Nishimura, S., Katze, J.R., Hashizume, T., Crain, P.F., McCloskey, J.A., et al. (1997). Biosynthesis of Archaeosine, a Novel Derivative of 7-Deazaguanosine Specific to Archaeal tRNA, Proceeds via a Pathway Involving Base Replacement on the tRNA Polynucleotide Chain *. J. Biol. Chem. *272*, 20146–20151. 10.1074/jbc.272.32.20146.

146. Phillips, G., Chikwana, V.M., Maxwell, A., El-Yacoubi, B., Swairjo, M.A., Iwata-Reuyl, D., and Crécy-Lagard, V. de (2010). Discovery and Characterization of an Amidinotransferase Involved in the Modification of Archaeal tRNA *♦. J. Biol. Chem. *285*, 12706–12713. 10.1074/jbc.M110.102236.

147. Bon Ramos, A., Bao, L., Turner, B., De Crécy-Lagard, V., and Iwata-Reuyl, D. (2017). QueF-Like, a Non-Homologous Archaeosine Synthase from the Crenarchaeota. Biomolecules *7*, 36. 10.3390/biom7020036.

148. Mei, X., Alvarez, J., Bon Ramos, A., Samanta, U., Iwata-Reuyl, D., and Swairjo, M.A. (2017). Crystal structure of the archaeosine synthase QueF-like—Insights into amidino transfer and tRNA recognition by the tunnel fold. Proteins Struct. Funct. Bioinforma. *85*, 103–116. 10.1002/prot.25202.

149. Phillips, G., Swairjo, M.A., Gaston, K.W., Bailly, M., Limbach, P.A., Iwata-Reuyl, D., and de Crécy-Lagard, V. (2012). Diversity of Archaeosine Synthesis in Crenarchaeota. ACS Chem. Biol. *7*, 300–305. 10.1021/cb200361w.

150. Susanto, A., Honberger, M., Murphy, R., Bayooz, S., Yi, S., and Swairjo, M.A. (2020). Overexpression, Purification, and Preliminary Crystallographic Analysis of the Archaeosine Synthase GAT-QueC. FASEB J. *34*, 1–1. 10.1096/fasebj.2020.34.s1.06647.

151. Romier, C., Reuter, K., Suck, D., and Ficner, R. (1996). Crystal structure of tRNA-guanine transglycosylase: RNA modification by base exchange. EMBO J. *15*, 2850–2857.

152. Xie, W., Liu, X., and Huang, R.H. (2003). Chemical trapping and crystal structure of a catalytic tRNA guanine transglycosylase covalent intermediate. Nat. Struct. Mol. Biol. *10*, 781–788. 10.1038/nsb976.

153. Ritschel, T., Atmanene, C., Reuter, K., Van Dorsselaer, A., Sanglier-Cianferani, S., and Klebe, G. (2009). An Integrative Approach Combining Noncovalent Mass Spectrometry, Enzyme Kinetics and X-ray Crystallography to Decipher Tgt Protein-Protein and Protein-RNA Interaction. J. Mol. Biol. *393*, 833–847. 10.1016/j.jmb.2009.07.040.

154. Chen, Y.-C., Kelly, V.P., Stachura, S.V., and Garcia, G.A. (2010). Characterization of the human tRNA-guanine transglycosylase: Confirmation of the heterodimeric subunit structure. RNA *16*, 958–968. 10.1261/rna.1997610.

155. Jakobi, S., Nguyen, P.T.X., Debaene, F., Cianférani, S., Reuter, K., and Klebe, G. (2015). What Glues a Homodimer Together: Systematic Analysis of the Stabilizing Effect of an Aromatic Hot Spot in the Protein–Protein Interface of the tRNA-Modifying Enzyme Tgt. ACS Chem. Biol. *10*, 1897–1907. 10.1021/acschembio.5b00028.

156. Jakobi, S., Nguyen, T.X.P., Debaene, F., Metz, A., Sanglier-Cianférani, S., Reuter, K., and Klebe, G. (2014). Hot-spot analysis to dissect the functional protein–protein interface of a tRNA-modifying enzyme. Proteins Struct. Funct. Bioinforma. *82*, 2713–2732. 10.1002/prot.24637.

157. Behrens, C., Biela, I., Petiot-Bécard, S., Botzanowski, T., Cianférani, S., Sager, C.P., Klebe, G., Heine, A., and Reuter, K. (2018). Homodimer Architecture of QTRT2, the Noncatalytic Subunit of the Eukaryotic tRNA-Guanine Transglycosylase. Biochemistry *57*, 3953–3965. 10.1021/acs.biochem.8b00294.

158. Johannsson, S., Neumann, P., and Ficner, R. (2018). Crystal Structure of the Human tRNA Guanine Transglycosylase Catalytic Subunit QTRT1. Biomolecules *8*, 81. 10.3390/biom8030081.

159. Ishitani, R., Nureki, O., Fukai, S., Kijimoto, T., Nameki, N., Watanabe, M., Kondo, H., Sekine, M., Okada, N., Nishimura, S., et al. (2002). Crystal Structure of Archaeosine tRNA-guanine Transglycosylase. J. Mol. Biol. *318*, 665–677. 10.1016/S0022-2836(02)00090-6.

160. Ishitani, R., Nureki, O., Nameki, N., Okada, N., Nishimura, S., and Yokoyama, S. (2003). Alternative Tertiary Structure of tRNA for Recognition by a Posttranscriptional Modification Enzyme. Cell *113*, 383–394. 10.1016/S0092-8674(03)00280-0.

161. Aravind, L., and Koonin, E.V. (1999). Novel Predicted RNA-Binding Domains Associated with the Translation Machinery. J. Mol. Evol. *48*, 291–302. 10.1007/PL00006472.

162. Tidten, N., Stengl, B., Heine, A., Garcia, G.A., Klebe, G., and Reuter, K. (2007). Glutamate versus glutamine exchange swaps substrate selectivity in tRNA-guanine transglycosylase: Insight into the regulation of substrate selectivity by kinetic and crystallographic studies. J. Mol. Biol. *374*, 764–776. 10.1016/j.jmb.2007.09.062.

163. Brenk, R., Stubbs, M.T., Heine, A., Reuter, K., and Klebe, G. (2003). Flexible Adaptations in the Structure of the tRNA-Modifying Enzyme tRNA–Guanine Transglycosylase and Their Implications for Substrate Selectivity, Reaction Mechanism and Structure-Based Drug Design. ChemBioChem *4*, 1066–1077. 10.1002/cbic.200300644.

164. Sebastiani, M., Behrens, C., Dörr, S., Gerber, H.-D., Benazza, R., Hernandez-Alba, O., Cianférani, S., Klebe, G., Heine, A., and Reuter, K. (2022). Structural and Biochemical Investigation of the Heterodimeric Murine tRNA-Guanine Transglycosylase. ACS Chem. Biol. *17*, 2229–2247. 10.1021/acschembio.2c00368.

165. Fergus, C., Al-qasem, M., Cotter, M., McDonnell, C.M., Sorrentino, E., Chevot, F., Hokamp, K., Senge, M.O., Southern, J.M., Connon, S.J., et al. (2021). The human tRNA-guanine transglycosylase displays promiscuous nucleobase preference but strict tRNA specificity. Nucleic Acids Res. *49*, 4877–4890. 10.1093/nar/gkab289.

166. Farkas, W.R., Jacobson, K.B., and Katze, J.R. (1984). Substrate and inhibitor specificity of tRNA-guanine ribosyltransferase. Biochim. Biophys. Acta BBA - Gene Struct. Expr. *781*, 64–75. 10.1016/0167-4781(84)90124-6.

167. Okada, N., Noguchi, S., Kasai, H., Shindo-Okada, N., Ohgi, T., Goto, T., and Nishimura, S. (1979). Novel mechanism of post-transcriptional modification of tRNA. Insertion of bases of Q precursors into tRNA by a specific tRNA transglycosylase reaction. J. Biol. Chem. *254*, 3067–3073. 10.1016/S0021-9258(17)30183-7.

168. Goodenough-Lashua, D.M., and Garcia, G.A. (2003). tRNA–guanine transglycosylase from E. coli: a ping-pong kinetic mechanism is consistent with nucleophilic catalysis. Bioorganic Chem. *31*, 331–344. 10.1016/S0045-2068(03)00069-5.

169. Alqasem, M.A., Fergus, C., Southern, J.M., Connon, S.J., and Kelly, V.P. (2020). The eukaryotic tRNA-guanine transglycosylase enzyme inserts queuine into tRNA via a sequential bi–bi mechanism. Chem. Commun. *56*, 3915–3918. 10.1039/C9CC09887A.

170. Bessler, L., Kaur, N., Vogt, L.-M., Flemmich, L., Siebenaller, C., Winz, M.-L., Tuorto, F., Micura, R., Ehrenhofer-Murray, A.E., and Helm, M. (2022). Functional integration of a semi-synthetic azido-queuosine derivative into translation and a tRNA modification circuit. Nucleic Acids Res. *50*, 10785–10800. 10.1093/nar/gkac822.

171. Alexander, S.C., Busby, K.N., Cole, C.M., Zhou, C.Y., and Devaraj, N.K. (2015). Site-Specific Covalent Labeling of RNA by Enzymatic Transglycosylation. J. Am. Chem. Soc. *137*, 12756–12759. 10.1021/jacs.5b07286.

172. Varghese, S., Cotter, M., Chevot, F., Fergus, C., Cunningham, C., Mills, K.H., Connon, S.J., Southern, J.M., and Kelly, V.P. (2017). In vivo modification of tRNA with an artificial nucleobase leads to full disease remission in an animal model of multiple sclerosis. Nucleic Acids Res. *45*, 2029–2039. 10.1093/nar/gkw847.

173. Zhang, D., Zhou, C.Y., Busby, K.N., Alexander, S.C., and Devaraj, N.K. (2018). Light-Activated Control of Translation by Enzymatic Covalent mRNA Labeling. Angew. Chem. Int. Ed. *57*, 2822–2826. 10.1002/anie.201710917.

174. Nakanishi, S., Ueda, T., Hori, H., Yamazaki, N., Okada, N., and Watanabe, K. (1994). A UGU sequence in the anticodon loop is a minimum requirement for recognition by Escherichia coli tRNA-guanine transglycosylase. J. Biol. Chem. *269*, 32221–32225. 10.1016/S0021-9258(18)31624-7.

175. Curnow, A.W., and Garcia, G.A. (1995). tRNA-guanine Transglycosylase from Escherichia coli: MINIMAL tRNA STRUCTURE AND SEQUENCE REQUIREMENTS FOR RECOGNITION *. J. Biol. Chem. *270*, 17264–17267. 10.1074/jbc.270.29.17264.

176. Curnow, A.W., Kung, F.L., Koch, K.A., and Garcia, G.A. (1993). tRNA-guanine transglycosylase from Escherichia coli: Gross tRNA structural requirements for recognition. Biochemistry *32*, 5239–5246. 10.1021/bi00070a036.

177. Stengl, B., Meyer, E.A., Heine, A., Brenk, R., Diederich, F., and Klebe, G. (2007). Crystal Structures of tRNA-guanine Transglycosylase (TGT) in Complex with Novel and Potent Inhibitors Unravel Pronounced Induced-fit Adaptations and Suggest Dimer Formation Upon Substrate Binding. J. Mol. Biol. *370*, 492–511. 10.1016/j.jmb.2007.04.008.

178. Grosjean, H., Edqvist, J., Stråby, K.B., and Giegé, R. (1996). Enzymatic Formation of Modified Nucleosides in tRNA: Dependence on tRNA Architecture. J. Mol. Biol. *255*, 67–85. 10.1006/jmbi.1996.0007.

179. Hurt, J.K., Olgen, S., and Garcia, G.A. (2007). Site-specific modification of Shigella flexneri virF mRNA by tRNA-guanine transglycosylase in vitro. Nucleic Acids Res. *35*, 4905–4913. 10.1093/nar/gkm473.

180. Chothia, C., and Lesk, A.M. (1986). The relation between the divergence of sequence and structure in proteins. EMBO J. *5*, 823–826. 10.1002/j.1460-2075.1986.tb04288.x.

181. Chen, Y.-C., Brooks, A.F., Goodenough-Lashua, D.M., Kittendorf, J.D., Showalter, H.D., and Garcia, G.A. (2011). Evolution of eukaryal tRNA-guanine transglycosylase: insight gained from the heterocyclic substrate recognition by the wild-type and mutant human and Escherichia coli tRNA-guanine transglycosylases. Nucleic Acids Res. *39*, 2834–2844. 10.1093/nar/gkq1188.

182. Stengl, B., Reuter, K., and Klebe, G. (2005). Mechanism and Substrate Specificity of tRNA–Guanine Transglycosylases (TGTs): tRNA-Modifying Enzymes from the Three Different Kingdoms of Life Share a Common Catalytic Mechanism. ChemBioChem *6*, 1926–1939. 10.1002/cbic.200500063.

183. Krissinel, E., and Henrick, K. (2007). Inference of macromolecular assemblies from crystalline state. J. Mol. Biol. *372*, 774–797. 10.1016/j.jmb.2007.05.022.

184. Beier, H., Barciszewska, M., and Sickinger, H.-D. (1984). The molecular basis for the differential translation of TMV RNA in tobacco protoplasts and wheat germ extracts. EMBO J. *3*, 1091–1096. 10.1002/j.1460-2075.1984.tb01934.x.

185. Biela, I., Tidten-Luksch, N., Immekus, F., Glinca, S., Nguyen, T.X.P., Gerber, H.-D., Heine, A., Klebe, G., and Reuter, K. (2013). Investigation of Specificity Determinants in Bacterial tRNA-Guanine Transglycosylase Reveals Queuine, the Substrate of Its Eucaryotic Counterpart, as Inhibitor. PLoS ONE *8*, e64240. 10.1371/journal.pone.0064240.

186. Guy, M.P., and Phizicky, E.M. (2014). Two-subunit enzymes involved in eukaryotic post-transcriptional tRNA modification. RNA Biol. *11*, 1608–1618. 10.1080/15476286.2015.1008360.

187. Land, M., Hauser, L., Jun, S.-R., Nookaew, I., Leuze, M.R., Ahn, T.-H., Karpinets, T., Lund, O., Kora, G., Wassenaar, T., et al. (2015). Insights from 20 years of bacterial genome sequencing. Funct. Integr. Genomics *15*, 141–161. 10.1007/s10142-015-0433-4.

188. Genome Information by Organsism Natl. Cent. Biotechnol. Inf. NCBI. https://www.ncbi.nlm.nih.gov/genome/browse/#!/overview/.

189. Nurk, S., Koren, S., Rhie, A., Rautiainen, M., Bzikadze, A.V., Mikheenko, A., Vollger, M.R., Altemose, N., Uralsky, L., Gershman, A., et al. (2022). The complete sequence of a human genome. Science *376*, 44–53. 10.1126/science.abj6987.

190. wwPDB consortium, Burley, S.K., Berman, H.M., Bhikadiya, C., Bi, C., Chen, L., Costanzo, L.D., Christie, C., Duarte, J.M., Dutta, S., et al. (2019). Protein Data Bank:

the single global archive for 3D macromolecular structure data. Nucleic Acids Res. *47*, D520–D528. 10.1093/nar/gky949.

191. Westhof, E., Dumas, P., and Moras, D. (1988). Restrained refinement of two crystalline forms of yeast aspartic acid and phenylalanine transfer RNA crystals. Acta Crystallogr. A *44 (Pt 2)*, 112–123.

STRUCTURE REFERENCES

The following table lists all structures referenced in this work and their protein data bank[190] accession codes.

PDB ID	Description	Reference
2TRA	*S. cerevisiae* tRNA$^{\text{Asp}}$	[191]
1C0A	*E. coli* tRNA$^{\text{Asp}}$ · Aa-TS	[55]
1EFW	*E. coli* tRNA$^{\text{Asp}}$ · *T. thermophilus* Aa-TS	[56]
1H3E	*T. thermophilus* RNA$^{\text{Tyr}}$ · Aa-TS	[59]
4RDX	*T. thermophilus* tRNA$^{\text{His}}$ · Aa-TS	[58]
4WJ4	*P. aeruginosa* tRNA$^{\text{Asn}}$ · Aa-TS	[61]
4WQ1	ribosome with Q34-tRNA$^{\text{Tyr}}$ at A-site (1$^{\text{st}}$ position mismatch)	[32]
4WZD	ribosome with Q34tRNA$^{\text{Tyr}}$ at P-site	[32]
1P0E	*Z. mobilis* TGT with preQ$_1$	[163]
1PUD	*Z. mobilis* TGT (apo)	[151]
1Q2R	*Z. mobilis* TGT with RNA (covalent intermediate)	[152]
1Q2S	*Z. mobilis* TGT with RNA (post-catalytic state)	[152]
2PWU	*Z. mobilis* TGT with guanine	[162]
1IQ8	*P. horikoshii* TGT (apo)	[159]
1IT7	*P. horikoshii* TGT with guanine	[159]
1IT8	*P. horikoshii* TGT with preQ$_0$	[159]
1J2B	*P. horikoshii* TGT with tRNA	[160]
6FV5	*M. musculus* QTRT2 (apo)	[157]
6H42	*H. sapiens* QTRT1 (apo)	[158]
6H45	*H. sapiens* QTRT1 with queuine	[158]
7NQ4	*H. sapiens* TGT with RNA (covalent intermediate)	this work
8OMR	*H. sapiens* TGT with tRNA	this work

ABBREVIATIONS

A	adenine or adenosine
Aa-TS	aminoacyl-tRNA-synthetase
ArcS	archaeosine synthase
arcTGT	archaeal tRNA guanine transglycosylase
bacTGT	bacterial tRNA guanine transglycosylase
BH4	tetrahydropterin
C	cytidine or cytosine
cryo-EM	cryogenic electron microscopy
Dnmt2	an RNA methyltransferase, abbreviation from "DNA methyltransferase"
ECF-type transporter	energy-coupling factor-type transporter
eukTGT	eukaryotic tRNA guanine transglycosylase
G	guanine or guanosine
G^+	archaeosine
GAC-QueC	functional equivalent of ArcS, abbreviation "glutamine amidotransferase class-II domain - QueC homolog"
galQ	galactosyl-queuosine
GCHI	GTP cyclohydrolase I
GTP	guanosine triphosphate
GUN-tRNA	tRNA with G34-U35-N36 anticodon
*hs*TGT	*Homo sapiens* TGT
I	inosine
LDH	lactate dehydrogenase

m^5C	5-methylcytidine
manQ	mannosyl-queuosine
ms^2i^6A	2-methylthio-N6-isopentenyladenosine
N	any nucleobase
NADPH/H+	nicotinamide adenine dinucleotide phosphate (reduced form)
*ph*TGT	*Pyrococcus horikoshii* TGT
Pmt1	pombe methyltransferase 1, a Dnmt2 ortholog
$preQ_0$	7-cyano-7-deazaguanine
$preQ_1$	7-aminomethyl-7-deazaguanine
PUA domain	pseudouridine synthase and archaeosine transglycosylase domain
Q	queuosine
q	queuine
QTRT1	eukaryotic tRNA guanine transglycosylase, catalytic subunit
QTRT2	eukaryotic tRNA guanine transglycosylase, non-catalytic subunit
QueA	S-adenosylmethionine:tRNA ribosyltransferase-isomerase
QueC	7-cyano-7-deazaguanine synthase
QueD	6-carboxy-5,6,7,8-tetrahydropterin synthase
QueE	7-carboxy-7-deazaguanine synthase
QueF	NADPH-dependent 7-cyano-7-deazaguanine reductase
QueF-L	functional equivalent of ArcS, abbreviation: "QueF-Like"
QueG	an epoxyqueuosine reductase, functional equivalent of QueH
QueH	an epoxyqueuosine reductase, functional equivalent of QueG
SAM	s-adenosylmethionine
T	thymine or thymidine

TGT	tRNA guanine transglycosylase
THF	tetrahydrofolate
tRNA	transfer RNA
U	uracil or uridine
yW	wybutosine
*zm*TGT	*Zymomonas mobilis* TGT
ψ	pseudouridine

ACKNOWLEDGEMENTS